KTH Land and Water Resources Engineering

MAPPING UNCERTAINTIES - A CASE STUDY ON A HYDRAULIC MODEL OF THE RIVER VOXNAN

Sara Andersson

August 2015

TRITA-LWR Degree Project 15:23
ISSN 1651-064X
ISRN KTH/LWR/Degree Project 15:23

Degree Project for Master's Program in Environmental Engineering and Sustainable Infrastructure

Department of Land and Water Resources Engineering

Royal Institute of Technology (KTH)

SE-100 44 STOCKHOLM, Sweden

Reference should be written as: Andersson, S. (2015) "Mapping Uncertainties – A case study on a hydraulic model of the river Voxnan" TRITA-LWR Degree Project 15:23 62 p.

SUMMARY

The European Commission's Flood Directive was adopted in 2007 after a decade where several severe flood events occurred in Europe. One of the implementation steps in the Flood Directive's first cycle was a requirement on the Member States to produce flood inundation maps for areas identified as having significant flood risk. One of these areas in Sweden was Edsbyn, having the river Voxnan flowing through the city.

Flood extent boundaries are often presented as crisp lines in flood inundation maps. However, there are many uncertainties underlying the process of creating these maps. It has therefore been argued that these crisp boundaries can be misleading. Due to this, the idea of probabilistic flood maps has been introduced. The probabilistic maps present the flood hazard as a probability rather than a crisp line, based on some type of uncertainty assessment.

The overarching aim of this thesis has been to investigate how different input and parameter uncertainties affect flood inundation models. These numerous uncertainties have been given an account for, as well as suitable assessment method for different types of uncertainties. A case study in form of an uncertainty assessment on the river Voxnan was also performed, in order to show how results from uncertainty analysis can be quantified and communicated visually in probabilistic flood inundation maps.

A one-dimensional MIKE 11 hydraulic model of a 62 km long part of Voxnan was used in the study, made available by MSB. The input uncertainty included in the case study was the magnitude of a 100-year flood in present climate as well as future climate conditions. The included parameter uncertainty was the spatially varying roughness coefficient, which implicitly describes momentum loss from various sources and thus affects the simulated water levels.

By combining a scenario analysis, GLUE calibration and Monte Carlo analysis, the different uncertainties with different natures could be assessed. As expected, significant uncertainties regarding the magnitude of a 100-year flood from frequency analysis was found. The largest contribution to the overall uncertainty is given by the variance between the nine included global climate models, emphasizing the importance of taking ensemble of projections into account in climate change studies.

The choice of greenhouse gas concentration scenario plays a significant role for how some of the individual global climate models projects the streamflow in Voxnan at the end of the century. Seen on the entire ensemble of global climate models, the importance of choice of greenhouse gas concentration scenario was marginal since the models compensate for each other's differences.

The spatially varying roughness coefficient in the hydraulic model gives a smaller contribution to the overall uncertainty, compared to the discharge uncertainty. The GLUE calibration method gave several roughness coefficient parameter sets that can all be argued to represent the system in an acceptable manner. These parameter sets yield water level variations of over three times the acceptance criterion of residual errors in the calibration points.

Furthermore, this study gives an example on how to present uncertainties visually in probabilistic flood inundation maps, working with the softwares MIKE 11, MATLAB and ArcMap. The conducted method of how to handle climate change scenario and model uncertainties in frequency analysis is also suggested to be a relevant result of the study.

Presenting flood inundation maps as probabilistic rather than deterministic is judged to be a more representative way, due to the many inherent uncertainties prevailing the maps. Important is however that the assumptions and potentially subjective decisions behind the uncertainty assessment are stated explicitly, for preventing further uncertainty contributions to an already uncertain-filled process.

SAMMANFATTNING

EU antog år 2007 ett direktiv för översvämningsrisker, efter ett decennium av flera svåra översvämningshändelser runtom Europa. En av faserna i direktivets första implementeringscykel var ett krav på medlemsländerna att upprätta översvämningskarteringar för identifierade områden med särskild översvämningsrisk idag eller i framtida förhållanden. Ett av dessa områden i Sverige var Edsbyn, med älven Voxnan flytande genom staden.

Gränsen för översvämningsplanet är ofta presenterad som en skarp linje i översvämningskarteringar. Det finns dock många underliggande osäkerheter i framtagningsprocessen av dessa kartor. Det har således hävdats att dessa skarpa linjer kan vara missvisande. Till följd av detta har idén om probabilistiska översvämningskartor blivit introducerad. De probabilistiska kartorna visar sannolikhet för översvämningshot istället för en skarp linje, baserat på någon form av osäkerhetsbedömning.

Det övergripande målet med detta examensarbete har varit att undersöka hur olika typer av indata- och parameterosäkerheter inverkar på översvämningsmodeller. Åtskilliga av dessa osäkerheter har redogjorts för, samt vilka olika osäkerhetsbedömningsmetoder som är lämpliga för olika typer av osäkerheter. Även en fallstudie i form av osäkerhetsanalys på älven Voxnan har genomförts, för att påvisa hur resultat från en osäkerhetsanalys kan kvantifieras och kommuniceras visuellt i probabilistiska översämningskartor.

En endimensionell hydraulisk modell i programvaran MIKE 11 användes i fallstudien. Modellen gjordes tillgänglig av MSB och studien inkluderade en 62 kilometer lång sträcka av Voxnan. Indataosäkerheten inkluderad i studien var storleken på ett hundraårsflöde, i dagens klimat såväl som ett framtida klimat. Den inkluderade parameterosäkerheten var den rumsligt varierande skrovlighetsparametern, vilken implicit beskriver rörelsemängdsförluster från olika källor och därmed påverkar den simulerade vattennivån. Det är ofta denna parameter som varieras då endimensionella hydrauliska modeller kalibreras mot historiska översvämningshändelser.

De olika osäkerheterna av skilda natur kunde utvärderas genom att kombinera en scenarioanalys, GLUE-kalibrering och Monte Carlo-analys. Som väntat, signifikanta osäkerheter gällande storleken på ett hundraårsflöde från frekvensanalys kunde fastställas. Det största bidraget till den övergripande osäkerheten visades komma från variansen mellan de nio inkluderade globala klimatmodellerna. Detta understryker vikten av att inkludera projektioner från ett flertal modeller i klimatförändringsstudier.

Valet av scenario för en framtida växthusgaskoncentration spelar en viktig roll för hur vissa av de individuella klimatmodellerna projicerar vattenföringen i Voxnan i slutet av århundrandet. Sett över hela ensemblen av klimatmodeller spelade valet av scenarioval mindre roll, eftersom vissa av klimatmodellerna kompenserade för varandras olikheter.

Osäkerheten i den rumsligt varierande skrovlighetsparametern gav i fallstudien en mindre inverkan på den övergripande osäkerheten än flödesosäkerheten. GLUE-kalibreringen resulterade i flera parameteruppsättningar som alla kan argumenteras representera systemet på ett acceptabelt sätt. Dessa parameteruppsättningar ger vattennivåskillnader på över tre gånger acceptanskriteriet för residualfel i kalibreringspunkterna.

Denna studie ger utöver detta ett metodologiskt exempel för hur osäkerheter kan presenteras visuellt i probabilistiska översämningskartor, med hjälp av programvarorna MIKE 11, MATLAB och ArcMap. Den genomförda metoden för hur klimatförändringsosäkerheterna, scenarion och modeller, hanterades i frekvensanalysen föreslås också vara ett relevant resultat av studien.

Att presentera översvämningshot i form av sannolikheter bedöms vara ett mer representativt sätt för detta presentera detta osäkra subjekt. Viktigt är dock att alla antaganden och eventuellt subjektiva val bakom osäkerhetsbedömningen anges explicit då resultaten presenters, eftersom resultaten som bäst är villkorliga på dessa. Detta för att förhindra ytterligare osäkerhetsbidrag till en redan osäkerhetsfylld process.

ACKNOWLEDGEMENTS

I would like to show my deepest gratitude to Christoffer Carstens at Länsstyrelsen Gävleborg and Ola Nordblom at DHI Sverige AB for excellent supervision throughout the entire project. Christoffer initiated the project idea and have been very helpful throughout the entire process, both with practicalities and with sharing knowledge regarding scientific methodologies and environmental modelling. Ola supplemented this with his great technical knowledge regarding the hydraulic model and MIKE software whenever needed. Ola was especially of great help in building the software system that made the Monte Carlo runs with MIKE 11 possible.

I would also like to thank my examiner Vladimir Cvetkovic for connecting me to this project in the first place - and also for being enthusiastic and encouraging throughout the process. I also wish to extend this to everyone at the LWR Department at KTH; for knowledge sharing and contributions to a welcoming atmosphere with many inspirational conversations throughout the entire master program.

I also wish to acknowledge the data providers; MSB for the hydraulic model, DHI for the MIKE Zero license, SMHI for the climate change projections, Ovanåkers Kommun for calibration data and Lantmäteriet for the maps and digital elevation model.

Finally, I would especially like to thank MSB for providing the funds the project needed in order to be realized.

Stockholm, August 2015

Sara Andersson

TABLE OF CONTENTS

ABBREVIATIONS

AEP	Annual Exceedance Probability
AMS	Annual Maximum Series
CDF	Cumulative Distribution Function
DBS	Distribution Based Scaling
DTM	Digital Terrain Model
DEM	Digital Elevation Model
GCM	Global Circulation Model
GLUE	Generalized Likelihood Uncertainty Estimation
GHG	Greenhouse Gas
LOA	Limits of Acceptability
MSB	Swedish Civil Contingencies Agency (Myndigheten för samhällsskydd och beredskap)
PDF	Probability Density Function
POT	Peak Over Threshold
RCM	Regional Climate Model
RCP	Representative Concentration Pathway
RMSE	Root Mean Square Error
TIN	Triangular Irregular Network

ABSTRACT

This master thesis gives an account for the numerous uncertainties that prevail one-dimensional hydraulic models and flood inundation maps, as well as suitable assessment methods for different types of uncertainties. A conducted uncertainty assessment on the river Voxnan in Sweden has been performed. The case study included the calibration uncertainty in the spatially varying roughness coefficient and the boundary condition uncertainty in the magnitude of a 100-year flood, in present and future climate conditions.

By combining a scenario analysis, GLUE calibration method and Monte Carlo analysis, the included uncertainties with different natures could be assessed. Significant uncertainties regarding the magnitude of a 100-year flood from frequency analysis was found. The largest contribution to the overall uncertainty was given by the variance between the nine global climate models, emphasizing the importance of including projections from an ensemble of models in climate change studies.

Furthermore, the study gives a methodological example on how to present uncertainty estimates visually in probabilistic flood inundation maps. The conducted method of how the climate change uncertainties, scenarios and models, were handled in frequency analysis is also suggested to be a relevant result of the study.

Key words: Hydraulic modelling; Flood inundation map; Uncertainty assessment; Climate change; Frequency analysis; Calibration; MIKE 11; Voxnan

1. INTRODUCTION

This initial chapter calls the need of the study through a background description, followed by outlining the aim and objectives of the study.

1.1. Background

Floods are part of the natural variation in the hydrologic system. Floods bring benefits like sediment transport, refill of groundwater storage and ecological services, but the risks of damage from floods are also substantial. Today, this is the natural disaster type that causes the largest economic damage. The vulnerability of floods have increased with socio-economic factors like increased population, urbanisation in areas susceptible to floods, deforestation, loss of wetlands and natural floodplain storage. Climate change is also projected to increase the intensity and frequency of floods in many areas. (EEA, 2010a; EEA, 2010b)

The European Commission's Flood Directive was adopted in 2007 after a decade where several severe flood events occurred in Europe. Between 1998 and 2009, the European floods resulted in more than 1100 fatalities, affecting over 3 million people and brought direct economic losses of over EUR 60 billion. Floods can also pose environmental risks, for example if the flood inundation reaches a developed area (EEA, 2010b; EC, 2015).

One of the implementation steps in the Flood Directive's first cycle was a requirement on the Member States to produce flood hazard maps for areas identified for having significant flood risk, toady or in the future (EC, 2007). The city of Edsbyn in Sweden was one of these identified areas, having the river Voxnan flowing through it (MSB, 2011).

Flood hazard maps, also known as flood inundation maps, define the area covered by water from a certain flood event. Even though the flood extent boundaries are often presented as crisp lines in flood hazard maps, there are many uncertainties underlying the process of creating these maps. Choice of hydraulic model, geometric description, estimation of design

flow magnitude and non-stationarity due to catchment change, climate change and variability are only a few of these. (Beven et al., 2011)

The idea of probabilistic flood maps has been introduced, see for example Smemoe et al. (2007), Merwade et al. (2008), Di Baldassarre et al. (2010) and Beven et al. (2011). It has been suggested that presenting the flood hazard as a probability, based on some type of uncertainty assessment, gives the subject a more correct representation due to the many underlying uncertainties. Furthermore, a need for clear methodologies and examples for this purpose has been expressed.

1.2. Aim and objectives of the study

The overarching aim of this thesis is to investigate how different input and parameter uncertainties affect flood inundation models. This will be made through an uncertainty analysis on a one-dimensional hydraulic model of the river Voxnan in Sweden, built in the software MIKE 11.

The input uncertainty included in the analysis is the magnitude of a 100-year flood in present climate as well as future climate conditions. The included parameter uncertainty is the spatially varying roughness coefficient, which implicitly describes momentum loss from various sources and thus affects the simulated water levels.

The aim of the thesis is to demonstrate how different types of uncertainties can be included in an uncertainty analysis. Furthermore, the study aims to show how the results from uncertainty analysis can be quantified and communicated visually in probabilistic flood inundation maps. Specific sub-objectives are:

- To quantify uncertainty estimates of the 100-year flood magnitudes in three scenarios; present climate and according to two greenhouse gas concentration scenarios in 2098; RCP 4.5 and RCP 8.5.
- To quantify an uncertainty estimate of the spatially varying roughness coefficient through a GLUE calibration of the model.
- To compile the numeric results of the uncertainty analysis and create probabilistic flood inundation maps in ArcMap.

2. FLOOD INUNDATION MAPS AND UNCERTAINTIES

This chapter aims at providing a theoretical overview and give an account for the state-of-the-art regarding the subjects handled in the thesis.

2.1. Floods and flood hazard maps

A 'flood' means that land that normally is not covered by water temporarily becomes so. How floods are categorized varies, but a general characterization is river and lake (fluvial) floods, overland (pluvial) floods in urban impervious areas due to heavy rain, coastal floods, groundwater floods and floods due to failure of artificial water systems. (EC, 2007; MSB, 2011; Jha et al., 2012)

Fluvial river floods occur when surface water runoff exceeds the capacity of the channel, causing river bank overflow and over-spill to nearby low-lying areas. Contributing factors to fluvial floods, except weather and hydrologic factors, are hence topography, land use, soil type, geomorphology, size of the catchment and the portion of lakes in the catchment. In Sweden, fluvial floods are typically occurring in spring due to snow melt, or during autumn due to heavy rain in combination with high soil moisture. (Bergström, 1994; MSB, 2011; Jha et al., 2012)

As mentioned in Chapter 1.1, one of the European Flood Directive's implementation steps is that it requires that the Member States produce flood hazard maps for areas identified as having potential significant flood risk,

either today or if it is considered likely to occur in the future. The Directive requires that the flood extent, water depth and, if appropriate, flow velocities are included on these maps. The required flood events are extreme event scenarios, medium probability scenarios (return interval of at least 100 years) and, if appropriate, high probability scenarios. (EC, 2007)

The flood hazard maps are then used for the subsequent steps in the Flood Directive implementation, in the process of producing flood risk maps and flood risk management plans. 'Flood risk' is defined as the combination of the probability of a flood event and its possible hostile consequences for human health, cultural heritage, economy and the environment. (EC, 2007)

In Sweden, the Swedish Civil Contingencies Agency (MSB) is responsible for identifying the areas with significant flood risk and for producing the flood hazard maps. It is only fluvial floods that have been taken into account in this first cycle. These maps underpins the flood risk maps and management plans in the subsequent implementation steps of the Directive, which are to be produced by the County Administrative Boards. Flood hazard maps are also used in municipal physical planning and for emergency services. (SFS, 2009; MSB, 2011; MSB, 2014a)

The computationally easiest way of producing a flood hazard map is by using a one-dimensional hydraulic model, from which simulated water levels and velocities are acquired. The process of setting up this type of model and producing flood hazard maps is summarized by Merwade et al. (2008) as:

1. Estimation of design flow, based on a hydrologic model or statistical frequency analysis.
2. Developing channel cross-sections, based on field surveys and/or digital terrain models (DTMs).
3. Running a hydraulic model with the design flow from Step 1 and cross-sections from Step 2. Other parameters in the model can be set through calibration of the model.
4. Interpolation of the cross-section's water levels to a georeferenced water surface. The interpolation method is often with a triangular irregular network (TIN).
5. The water depth is calculated by subtracting the DTM from the water surface. Hence, all positive water depth values give the flood inundation extent.

2.2. Uncertainties from a general point of view

A fundamental distinction of different natures of uncertainties can be drawn between aleatory versus epistemic uncertainties. Aleatory uncertainties are those that cannot be reduced since they are coming from the "natural variability" in the system behaviour. An example is the chaotic behaviour of the climate system. Therefore are the aleatory uncertainties treated as random uncertainties and are often represented as probabilities. (Beven et al., 2011; Capela Lourenço et al., 2014)

Epistemic uncertainties are on the contrary coming from a lack of knowledge and might therefore be possible to reduce through more research, better models or more knowledge. An example of an epistemic uncertainty is a model structure error. Even though epistemic uncertainties are reducible in theory, a model is by definition a simplification of reality and will therefore always bring epistemic uncertainty to some degree. (Beven et al., 2011)

It is generally unsuitable to represent an uncertainty with an epistemic nature as a quantified probability, since it can give an overconfident uncertainty estimate. Partly because the nature of the mechanisms behind the uncertainty is unknown and partly because these type of uncertainties are often non-stationary in time or space. The preferred representation methods can instead be based on possibilities, like using scenarios or giving weights to different possible outcomes, based on the so-called possibilistic Fuzzy Set theory. (Beven et al., 2011; Capela Lourenço et al., 2014)

Uncertainty can in many circumstances be a mixture of both aleatory and epistemic nature, making the distinction not always easily drawn. For example, there can exist epistemic uncertainties around the properties of an aleatory uncertainty. This might lead to confusion and it becomes important to express the assumptions behind a model uncertainty assessment to a decision maker. (Beven et al., 2011; Capela Lourenço et al., 2014)

2.3. **Frequency analysis**

The magnitude of an extreme hydrologic event is inversely related to its frequency of occurrence. Frequency analysis has a main objective of relating the magnitude of an extreme event to its frequency of occurrence, and vice versa. This is conducted by using hydrologic data to select a probability distribution function and fit the parameters to suit the available data. (Chow, 1988)

A probability distribution function represents the probability of occurrence of a random variable. Often, they are represented as Cumulative Distribution Functions (CDF) or Probability Density Functions (PDF). A CDF is a graph showing the probability that an outcome will be smaller than or equal a certain value. (Chow, 1988; Bedient, 2008)

2.3.1. ***Underlying assumptions***

Key assumptions in frequency analysis are that the hydrologic data is independent, identically distributed and that it originates from a stochastic and stationary (time-independent) hydrologic system. This would mean that the magnitude of one event does not depend on the magnitude of adjacent events, and that all data observations share the same statistical properties. (Bedient, 2008)

To comply with the independence assumption, a series of annual maximum discharge (AMS) is often chosen in flood frequency analysis - since the observation from one year to another can be expected to be independent (Chow, 1988). An alternate method is to use a Peaks-over-threshold (POT) series, including all discharge values over a set threshold limit. This can be useful when the series are not long enough, but introduces the difficulty of choosing the threshold value and assuring the independence of the data (Bezak et al., 2013). The homogeneity of the hydrologic data should be evaluated through time-series analysis prior to the frequency analysis, in order to detect eventual periodicities or non-stationary patterns (Bedient, 2008).

2.3.2. ***Concept of return period***

The most common way of indicating the probability of a flood of a given magnitude is to assign it a return period, which equals the inverse of its probability of occurrence. For example, a 100-year flood has an annual exceedance probability (AEP) of 0.01. This means that it is equalled or exceeded once, on average, every 100 years. Note that the term 'return period' can be misleading, since it can be interpreted of saying something about the actual time sequence of an event. (Maidment, 1993; Bedient, 2008; Beven et al., 2011)

Table 1. Probability that a flood with a certain return period will occur at least one during a certain period of years.

Return period [years]	Probability [%]		
	10 year period	50 year period	100 year period
10	65	99	100
100	9.6	39	63
1000	1	4.9	9.5
10 000	0.1	0.5	1

A 100-year flood does not mean that it will only happen once every 100 years, but rather that there is a 1 % risk of it to occur every year. An alternative way of addressing a 100-year flood is therefore to call it a 0.01 AEP flood. (Bedient, 2008; Beven et al., 2011)

Eq. 1 gives the probability of a flood with a return period of T years to occur at least once during a period of N years (Chow, 1988). Hence, a 100-year flood has a 63 % probability of occurring during a 100 year period of time (Table 1).

$$P(X \geq x_T \text{ at least once in N years}) = 1 - \left(1 - \frac{1}{T}\right)^N \qquad \text{Eq. 1}$$

2.3.3. *Choice of probability distribution function*

There are a number of different theoretical distribution functions that can be chosen from to fit the observations to. There are at least ten different distribution functions that have been applied to flood frequency analyses (Table 2). The normal distribution is typically not used in flood frequency analysis, since it is non-skewed and unbound while extreme values like observations in an AMS tends to be skewed and are nonnegative. (Bedient, 2008)

The most common probability distribution functions in flood estimation applications are according to Harlin (1992) the Gumbel, Log-Pearson Type III and lognormal distributions. The two-parameter distributions Gumbel, lognormal or Gamma are typically used for Swedish conditions (Svensk Energi et al., 2007). The standard distribution for frequency analysis of annual maximum floods in the United States is the three parameter Log-Pearson Type III distribution (Chow, 1988). Extreme value distributions form the basis of the standardized method for flood frequency analysis in Great Britain (Chow, 1988).

2.3.4. *Uncertainties in flood frequency analysis*

There are several sources of uncertainty connected to the frequency analysis. Merz and Thieken (2005) summarized these in seven source categories (Table 3). The choice of time period for the data is one, where a shorter series is increasing the uncertainty since the tales of the distribution (for finding the magnitude of floods with high return intervals) needs to be extrapolated. Bergström (1994) recommends to use a time series of at least half the length of the return interval that is to be calculated.

However, a longer time series increases the risk of it being non-stationary and inhomogeneous (Dahmen and Hall, 1990). Examples of potential changes in the system are urbanization, deforestation and climate change (Merz and Thieken, 2005). Furthermore, the stationarity assumption behind the frequency analysis might be invalid if the river is strongly affected by regulations (Svensk Energi et al., 2007).

Table 2. A selection of the most common probability distribution functions used in hydrology. $\overline{x}$ =mean of sample data, s_x = standard deviation of sample data, C_s = coefficient of skewness. (Chow, 1988)

Probability distribution function	PDF	Range of x and definition of parameters
Pearson Type III a.k.a. 3-parameter gamma	$f(x)=\frac{\lambda^{\beta}(x-\varepsilon)^{\beta-1}e^{-\lambda(x-\varepsilon)}}{\Gamma(\beta)}$ where $\Gamma(\beta)=\text{gamma func.}=\int_0^{\infty}\mu^{\beta-1}e^{-u}du$	$x\geq\varepsilon$ $\beta=\left(\frac{2}{C_s}\right)^2$ $\lambda=\frac{s_x}{\sqrt{\beta}}$ $\varepsilon=\overline{x}-s_x\sqrt{\beta}$
Log-Pearson Type III	$f(x)=\frac{\lambda^{\beta}(y-\varepsilon)^{\beta-1}e^{-\lambda(y-\varepsilon)}}{x\Gamma(\beta)}$ where $y=\log x$ $\Gamma=\text{gamma func.}$	$\log x\geq\varepsilon$ $\lambda=\frac{s_y}{\sqrt{\beta}}$ $\beta=\left[\frac{2}{C_s(y)}\right]^2$ $\varepsilon=\overline{y}-s_y\sqrt{\beta}$ Assuming $C_s(y)\geq 0$
Lognormal Special case of Log-Pearson Type III, when symmetric about its mean.	$f(x)=\frac{1}{x\sigma\sqrt{2\pi}}\exp\left(-\frac{(y-\mu_y)^2}{2\sigma_y^2}\right)$ where $y=\log x$	$x>0$ $\mu_y=\overline{y}$ $\sigma_y=s_y$
2-parameter gamma	$f(x)=\frac{\lambda^{\beta}x^{\beta-1}e^{-\lambda x}}{\Gamma(\beta)}$ where $\Gamma=\text{gamma func.}$	$x\geq 0$ $\lambda=\frac{\overline{x}}{s_x^2}$ $\beta=\frac{\overline{x}^2}{s_x^2}=\frac{1}{CV^2}$
Gumbel a.k.a. Extreme Value Type I. Special case of the General Extreme Value distribution	$f(x)=\frac{1}{\alpha}\exp\left[-\frac{x-u}{\alpha}-\exp\left(-\frac{x-u}{\alpha}\right)\right]$	$-\infty<x<\infty$ $\alpha=\frac{\sqrt{6}s_x}{\pi}$ $u=\overline{x}-0.5772\alpha$

Table 3. Summary of uncertainty sources in flood frequency analysis (Merz and Thieken, 2005).

Uncertainty source	Examples
Measurement errors	Water level measurement errors, rating curve error
Plotting position formula	Weibull, Hazen, Gringorten
Assumptions	Independence, stationarity, randomness, homogeneity
Sample selection	Representativeness of the observation period, using AMS or POT series.
Choice of distribution function	Lognormal, Log-Pearson Type III, Gumbel
Parameter estimation method	Method of moments, method of maximum likelihood
Sampling uncertainty	Time series length

Rating curves are used for relating a measured water level with a discharge value, based on relationships set up from previous measurements. The rating curve errors are generally the largest for extreme floods, which is unfortunate since these floods that are typically the ones used in flood frequency analysis. (Merz and Thieken, 2005)

The question of which theoretical probability distribution function to choose can be challenging since individual rivers vary in their optimal distribution (Bedient, 2008). It is therefore suitable to test more than one distribution when performing a frequency analysis (Svensk Energi et al., 2007). The different fits can be tested with quantitative measures, for example with the so called Kolmogorov-Smirnov test or by graphically comparing the fitted CDF with plotted measured observations by using a selected probability paper and plotting position (Bedient, 2008).

However, the measured values will often fit all distributions quite well, while the largest differences between the distributions show in the extreme values. Hence, the choice of distribution function is a large source of uncertainty when it comes to events with high return periods. (Merz and Thieken, 2005)

Another method for dealing with this distribution choice uncertainty is to fit the observations to a handful of selected distribution functions. A Maximum Likelihood measure can then be used to assign weights to the individual distribution functions, based on how well they represent the data set. From this, a composite distribution function can be constructed. It is then possible to observe which of the individual distribution functions that the composite probability distribution function is most similar to. For examples of this methodology, see Apel et al. (2004), (2006) or (2008).

The frequency analysis can be complemented with a confidence analysis to get a picture of the sample uncertainty in the calculations (Svensk Energi et al., 2007). For example, Beven et al. (2011) used a 95 % confidence interval of the 100-year flood magnitude from a General Extreme Value distribution to quantify the uncertainty in the design flood event. The computation method of confidence limits varies for different probability distribution functions (Bedient, 2008).

Table 4. The radiative forcing levels take into account the net effect of all anthropogenic greenhouse gas emissions and other forcing agents. The levels are defined as ± 5% of the stated level, relative to the pre-industrial levels. (van Vuuren et al., 2011)

GHG concentration scenario	Description	Radiative forcing level [W/m^2]	CO_2 equivalents [ppm]
RCP8.5	Rising radiative forcing pathway.	8.5	~ 1370
RCP6	Stabilization without overshoot pathway, stabilizing by 2100.	6	~ 850
RCP4.5	Stabilization without overshoot pathway, stabilizing by 2100.	4.5	~ 650
RCP2.6	Declining pathway after peak before 2100.	2.6 (peak at 3)	~ 490

2.4. Climate change and hydrologic projections

This section gives a theoretic introduction to climate change projections and how scenarios and models are turned into input data for flood inundation models.

2.4.1. *The Representative Concentration Pathways*

The development of the future climate is correlated with the development of the world, in terms of socio-economic change, technical change, emissions of greenhouse gases, air pollutants, etc. This is a clear epistemic uncertainty and it is impossible to foresee this development today. Due to this, the climate modelling community is using a range of climate outcomes as inputs to the global climate models. (van Vuuren et al., 2011)

A set of four Representative Concentration Pathways (RCPs) (Table 4) was developed for the Fifth Assessment Report by the Intergovernmental Panel on Climate Change (IPCC, 2013). The RCPs are greenhouse gas concentration trajectories, named after their radiative forcing levels by the year 2100 relative to the pre-industrial level: 2.6, 4.5, 6 and 8.5 W/m^2. (van Vuuren et al., 2011)

Each RCP is representing a large number of future scenarios, since each concentration level can be reached by a variety of combinations of economic, political, technological and demographic future developments. No RCP is meant to be appraised as more likely than the other, rather are they developed to describe the uncertainty that exists with regards to future climate outcomes. (Persson et al., 2015)

2.4.2. *From a global scale to a local hydrologic scale*

The RCPs are forming an important basis for inputs to Global Circulation Models (GCM), often called Global Climate Models (Fig. 1). These models simulate the climate on a global scale, which makes the computation grid of these models to be relatively coarse. A typical grid box size is 200-300 km in width, with varying heights. (Persson et al., 2015)

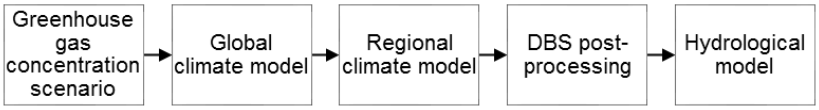

Fig. 1. Schematic overview of the process of turning global climate change projections to a local hydrologic scale.

It is necessary to downscale the results from a GCM with a Regional Climate Model (RCM) if they are needed on a local or regional scale. The RCM typically used for Sweden comes from the Rossby Centre, SMHI's climate modelling research unit. This process is called dynamical downscaling, and can for example result in a 50 km wide computation grid. (Persson et al., 2015)

Further statistical downscaling, through a Distribution-based scaling (DBS) method, enables the results from an RCM to be used as inputs in a hydrological model. The results from an RCM often includes systematic errors that needs to be corrected before using the results in a hydrological climate change assessment. The DBS fit simulated values with observed values to perform this bias correction. The DBS also scales the results to a higher resolution, typically 4 km wide. (Sjökvist, 2015)

The statistically downscaled and corrected projections can be used as input in hydrological models for hydrologic climate change studies. The two models HBV and HYPE are typical hydrological models used in Sweden. This can for example result in simulated streamflow time series, possible to use in climate change flood forecasting studies. (Sjökvist, 2015)

2.4.3. *Uncertainties in climate change projections and ensemble analysis*

The major uncertainty sources related to climate change impacts on hydrologic variables have here been summarized in four categories (Table 5), based on e.g. van der Linden and Mitchell (2009), Persson et al. (2015) and Shrestha et al. (2015).

The inherent natural variability within the climate system is a factor that needs to be taken into account when interpreting climate change projection results. The shorter the time horizon, the harder it can be to differentiate the internal variability from the long-term climate change patterns. Furthermore, the climate models are programmed to reflect this natural variability, but cannot be expected to be in synchronisation with the observations. The results from a climate model should be evaluated from a long-term statistical point of view (change in average amplitude, variability) rather than predicting how hot a certain year will be. (Persson et al., 2015)

There have been studies showing that the relative importance of uncertainties regarding downscaling methods and hydrologic parameters are small compared to the uncertainties regarding climate models and GHG concentration scenarios. The relative importance of the GHG concentration scenario is also depending on the time horizon of the study, the spread between different scenarios increases with a longer time span. (Shrestha et al., 2015)

Table 5. Summary of the major uncertainties in climate change projections on hydrologic variables.

Uncertainty category	Description/Examples
Natural variability	The inherent annual and decadal variability of the climate, e.g. due to NAO, El Niño, etc.
Model uncertainties	Choice of GCM, RCM and impact hydrological model, model structure errors, model parameters, initial model state
GHG concentration scenario	Feedback mechanisms, translating GHG emissions to radiative forcing, socio-economic development
Downscaling method	From GCM to RCM, from RCM to impact model

The chosen time horizon of the study also matters for the relative importance of variance represented by GCM versus RCM. Generally, a stronger climate signal increases the importance of the spread from different GCMs. This means that it becomes important to take the variability between different GCMs into account for an end-of-the-century study, while the choice of RCM becomes more relevant for studies closer to the present. (van der Linden and Mitchell, 2009)

The relative contribution to the overall uncertainty also differs between regions, simulation seasons and model variables. In Scandinavia it has been shown that the relative contribution to the variability in temperature and precipitation is somewhat stronger by the GCMs during winter months and by the RCMs during the summer months. (van der Linden and Mitchell, 2009)

Capela Lourenço et al. (2014) investigated how uncertainty generally is addressed in national climate change adaption planning and found that most countries included in the study consider different GHG concentration scenarios and different GCMs. Statistics are generally calculated across all GCM and RCM combinations for one GHG concentration scenario at a time.

This multi-model and multi-scenario approach is a common method for dealing with the most important uncertainties connected to climate change projections. The variability between model structures is sampled by using an ensemble of models, producing more reliable results. It is not possible to point out one GCM that best captures the entire climate system, but response trends observed in an ensemble of climate models are valued to be more likely since the same result have been achieved from different conditions. (van der Linden and Mitchell, 2009; Persson et al., 2015; Shrestha et al., 2015)

2.5. One-dimensional hydraulic models

The theory of one-dimensional hydraulic models will here be presented through a description of the used software MIKE 11. For an overview of other types of hydraulic models (zero-, two- or three-dimension hydraulic models), and other available software programs see for example Bedient (2008) or Asselman (2009).

2.5.1. *MIKE 11, Saint-Venant equations and solution scheme*

MIKE 11 is a one-dimensional modelling system developed by DHI. It can be used to simulate water flows, water quality and sediment transport in rivers, channels, estuaries and other water bodies. Its one-dimensionality implies that it is suitable for situations where there is one clearly dominating flow direction. (DHI, 2014a)

MIKE 11 is based on the partial differential equations Saint-Venant equations for one-dimensional flow, which allow the flow rate and water level to be computed as a function of time and space. By making the following assumptions, the Saint-Venant equations used in MIKE 11 can be derived from the conservation of mass and conservation of momentum equations (see e.g. Chow (1988) for a detailed presentation of that derivation).

- The simulated flow is one-dimensional, which means that the water level and velocity only vary in the longitudinal channel direction. Hence, the velocity is constant and water level is horizontal along any perpendicular axis (cross-section) to the longitudinal river channel.
- The water is incompressible and homogeneous, meaning that its density can be assumed constant.

- The slope of the river bottom is small, meaning that the cosine of its angle with the vertical can be assumed to equal the value one.
- The wave length is large compared to the water depth, meaning that the flow is assumed to be parallel with the bottom. This in turn enables the vertical acceleration to be assumed zero and a vertical hydrostatic pressure can be assumed valid.
- The flow is within the subcritical flow regime (often described as tranquil or streaming), meaning that there is a possibility for a gravity wave to propagate upstream.
- Resistance coefficients for steady uniform turbulent flow can be used, so that for example Manning's equation is applicable for describing the resistance effects.

(Chow, 1959; Chow, 1988; DHI, 2014a)

Applying these assumptions for flow between two cross-sections with the distance *dx*, the equations of mass and momentum conservation yields the one-dimensional Saint Venant equations as:

Conservation of mass

$$\frac{\partial Q}{\partial x}+\frac{\partial A}{\partial t}-q=0 \qquad \text{Eq. 2}$$

Conservation of momentum

$$\underbrace{\frac{\partial Q}{\partial t}}_{\text{Local acceleration}}+\underbrace{\frac{\partial}{\partial x}\left(\frac{\alpha Q^2}{A}\right)}_{\text{Convective acceleration}}+\underbrace{gA\frac{\partial h}{\partial x}}_{\text{Pressure force}}+\underbrace{\frac{gQ|Q|}{M^2AR^{4/3}}}_{\text{Friction force}}=0 \qquad \text{Eq. 3}$$

where

Q = discharge [L^3T^{-1}]

A = flow area [L^2]

q = lateral inflow per unit length [L^2T^{-1}]

a = momentum distribution coefficient [-]

g = gravitational acceleration constant [LT^{-2}]

h = water surface elevation [L]

M = Manning's coefficient [$L^{1/3}T^{-1}$]

R = hydraulic radius or resistance radius [L]

Eq. (3) is a dynamic wave description, meaning that the flow is unsteady and non-uniform. Eq. (2) and Eq. (3) do not have an exact analytical solution, MIKE 11 solves them numerically by using an implicit finite difference scheme called the Centred 6-point Abbott scheme. An implicit method means that it solves for the unknowns at all points for the current time step simultaneously. This means that it is more numerically stable and hence allows longer time-steps than an explicit solution scheme would. The results are water depth and average velocity at every cross-section. (Chow, 1988; Bedient, 2008; DHI, 2014a)

2.5.2. *Cross-sections*

MIKE 11 is discretising the river reach into a number of irregularly spaced cross-sections, placed perpendicular to the river flow direction for which the water level and main velocity are assumed to be constant. The topographical description of the area is hence made through the specified cross-sections. (DHI, 2014a)

The number of required cross-sections is therefore depending on the area, where a meandering channel or a varied topography in the channel and/or floodplain requires more cross-sections to capture these variations. Furthermore, the cross-sections need to be wide enough to cover the entire flood-plain that might become flooded. It is also important that the cross-sections cover possible new flow paths that the water can take in the particular flood event. (DHI, 2014a; MSB, 2014b)

2.5.3. *Boundary conditions and initial conditions*

All external model boundaries need a defined boundary condition. This can either be a constant or a specified time series of discharge or water level values. Discharge (constant or time-varying) is typically used for the upstream boundary conditions, while water level (constant, time-varying or rating curve, which is the known relationship between discharge and water level) is typically used for the downstream boundary conditions.

Initial conditions for all computation points in form of discharge or water level must also be specified. A global estimate is applied throughout the model, unless the user has defined local values. (DHI, 2014a)

2.5.4. *Bed resistance description*

The friction force term in Eq. (3) is showing the Manning description, which needs the user to specify a value of the roughness coefficient Manning's number *M*. This parameter is also known as the Strickler coefficient, and equals the inverse of the more conventionally used Manning's number *n*. Surface roughness, channel vegetation and channel irregularities are only a few of the factors that affect the roughness coefficient, which in turn affects the flow velocity. It is therefore a model parameter that can vary both spatially and temporally (e.g. through seasonal variations in vegetation). In MIKE 11, a global value of the roughness coefficient is applied for the entire model unless the user has defined local values. (DHI, 2014a)

Where possible, the roughness coefficient values should be decided from a calibration of the model. Otherwise, typical values of Manning coefficient for different types of channels can for example be found in Chow (1959). The values of *M* goes between 10 and 100 in SI base units, where a lower value indicates a rougher surface. (Chow, 1959, DHI, 2014a)

To a certain extent, the simplifications of flow physics and additional energy losses can be compensated through a calibration of the roughness coefficient. Hence, the shape of the river channel also affects the value of the roughness parameter. (Asselman, 2009)

2.5.5. *MIKE and the user interface*

The user interface in MIKE 11 is built around different editors, for which the Simulation editor integrate the others (Fig. 2). The Network editor allows editing of the river network and physical structures in the river (e.g. culverts and bridges), while also giving an overview of the model information. The information on all cross-sections are stored in the Cross-section editor. Boundary conditions are specified in the Boundary editor, as constant values or connected to time-series. The Parameter editor controls other supplementary information used in the simulation, like initial condition values and roughness coefficient values. (DHI, 2014b)

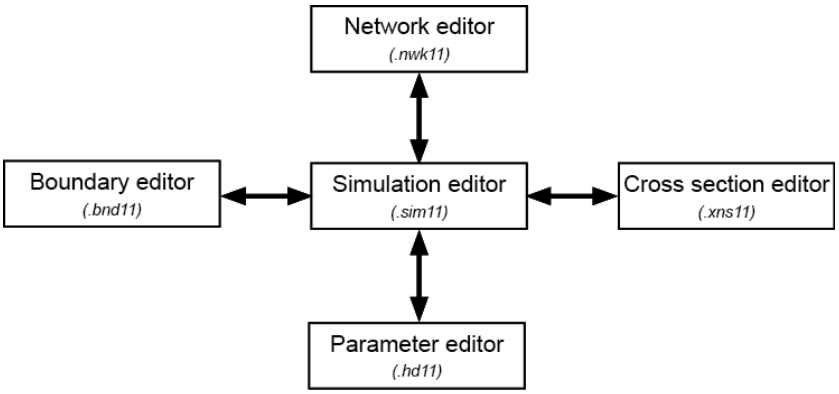

Fig. 2. Overview of the different editors connected to MIKE 11 and how they are integrated through the Simulation editor.

The settings in the Boundary editor are saved as a text file with the extension *.bnd11*. The parameter settings in the Parameter editor are in a corresponding manner saved as a text file with the extension *.hd11*. The integration to the Simulation editor is configured by specifying these files with the specified settings. The set-up in the Simulation editor is saved as a file with the extension *.sim11*. (DHI, 2014b)

Within the MIKE user interface there is also a Batch Simulation editor (Fig. 3). This allows the user to define a number of simulations that will be performed automatically on a base simulation file. The user can in the Batch Simulation editor define what parameters that should be varied in the batch simulation, and define the inputs for each simulation. For example, if five simulations with different roughness parameter values are to be made – five different *.hd11* files with the different parameter values are specified in the Batch Simulation editor. (DHI, 2014b)

2.5.6. *Uncertainties in one-dimensional hydraulic models*

When it comes to one-dimensional hydraulic models, they suffer from the disadvantages of not being able to capture the lateral spreading of the flood wave and the topography is not continuously defined but instead through a number of subjectively located cross-sections. (Asselman, 2009)

Besides the choice of model, the geometric description and the channel roughness parameter also have significant impacts on the overall uncertainty (Table 6). The geometric description is the most important aspect in the contribution of the hydraulic model to the overall uncertainty, which

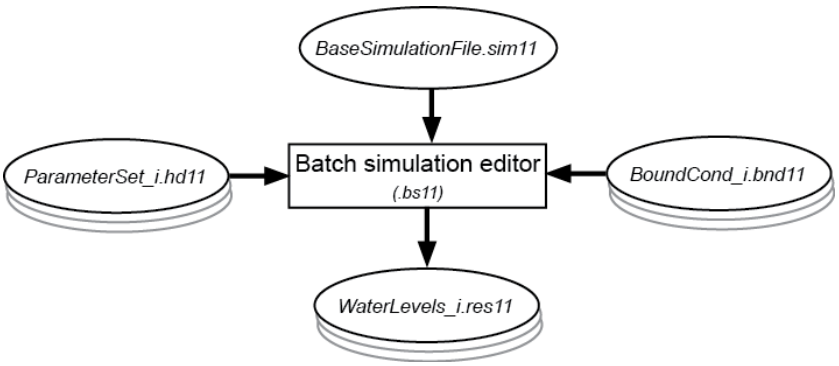

Fig. 3. Example of a set-up with the Batch Simulation editor where parameter values and boundary conditions are varied for three simulations.

Table 6. Summary of the major uncertainty categories from hydraulic models.

Uncertainty category	Examples
Model dimension	Simplification of the hydrodynamic processes
Geometric description	Underlying terrain data
	Configuration of cross-sections (how many, where they are located)
	Hydraulic structure representation (bridges, culverts, embankments)
Channel roughness parameter	Manning's number *M*
	Spatial and temporal variation

depends upon the quality on the underlying topographic data as well as how the modeller configures the cross-sections. (Merwade et al., 2008)

There have been studies showing one-dimensional models performing equally well as two-dimensional when it comes to simulating flood inundation extents, given uncertainties in inflow, topography and validation data (Asselman, 2009). But again, the suitability of the one-dimensional assumption is depending on the area of study.

2.6. Flood extent delineation through geospatial analysis

As mentioned in Chapter 2.5.2, cross-sections for the hydraulic model are extracted from a terrain data set. Terrain data is thereafter used again in the flood inundation map creation process when the one-dimensional water level simulations are turned into horizontal flood inundation extents. The quality of the terrain data used for the mapping step plays a significant role in the overall process. (Merwade et al., 2008)

All conversions and interpolation methods will introduce uncertainty to a varying degree. One example is the interpolation of the raw terrain data to a surface, which can be done with various techniques and give various results. The overall variations might be small, but can be significant for the hydraulic modelling result if the terrain is very heterogeneous. However, a flat terrain means larger uncertainties in the horizontal flood delineation extent, since a small height error can lead to a large horizontal extent variation. (Merwade et al., 2008; Brandt, 2009)

The cross-section water levels are often first interpolated to a TIN surface and then to a raster water surface, in order to perform raster operations and delineate the flood extent. These interpolations are however not very significant, since the water surface is assumed to be linear. But naturally, a coarser raster introduce a higher uncertainty since each pixel is only given one height value. (Merwade et al., 2008)

Depending on the purpose of the flood inundation mapping, a digital terrain resolution of three to four meters is suggested to be sufficient for most cases. If the terrain is very flat or if there are high demands on the maps reliability, a resolution of less than one meter should be used. (Brandt, 2009)

2.7. Uncertainty estimation methods in modelling

There exists a wide range of techniques for uncertainty estimation in environmental modelling. Long, there have been a lack of a "code of practice" as a guide in uncertainty analysis in hydraulic modelling (Merwade et al., 2008). However, there have been contributions to this in recent years.

Beven et al. (2011) provided a framework for assessing uncertainty in fluvial flood risk mapping and Hall and Solomatine (2008) provided a framework for uncertainty analysis in flood risk management decisions.

The uncertainty estimation methods and related topics judged to be relevant for this project are described below. See e.g. Beven (2008) or Hall (2008) for more complete overviews.

2.7.1. *Forward uncertainty analysis and sensitivity analysis*

So called forward uncertainty analysis is performed on models that are required to make predictions without available data for calibration. Reasons for this can for example be lack of historical data or that predictions on an uncertain future are to be made. In these cases, the model results and the uncertainty estimates are completely depending on the assumptions made by the modeller. (Beven, 2008)

Sensitivity analysis is connected to forward uncertainty analysis in the sense that both explore the model space. In order for the modeller to concentrate the effort on the assumptions of the most significant parameters, a sensitivity analysis is particularly useful for models without historical data. Sensitivity analysis is an assessment how sensitive the results are to individual parameters and/or parameter combinations. (Beven, 2008)

Monte Carlo

Monte Carlo analysis is a method for sampling the parameter space through a repetitive model evaluation. By assigning posterior distributions for selected model parameters, the model can be run for each random parameter sample set and a correlating distributions of the model results can be found (Fig. 4). Hence, this method is typically performed on uncertainties that can be expressed as probabilities. (Juston, 2012)

When sampling the variables, co-variation of parameters should be included if possible. Choices around the parameter ranges and distributions can be subjective and should be made explicit. If no information on the distribution is known, a uniform distribution within the assumed range is often used. For high dimensional parameter spaces, the number of required iterations can become very high, which can be computationally demanding. (Hall, 2008)

Scenario analysis

One way of dealing with uncertainties that cannot be expressed as chance, odds or probabilities is to perform scenario modelling. Use of scenarios of these types of boundary conditions is a common feature of both forward uncertainty analysis and sensitivity analysis. The modelling results are

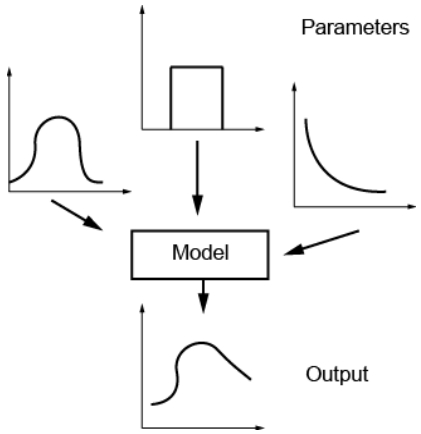

Fig. 4. Sketch of a typical Monte Carlo set-up. The probability density functions for three parameters are used to draw samples from, the model is run many times and a probability density function of the output is obtained.

in these cases entirely conditional on the choice of scenarios, so again it becomes crucial to state the assumptions when presenting the results. (Beven, 2008)

2.7.2. *Inverse uncertainty analysis and calibration*

Inverse uncertainty estimation techniques are possible to perform when historical data is available. Model calibration through historic observations can be used to add faith to the model predictions while also constrain the uncertainty estimates. In hydraulic model calibrations, it is often the roughness coefficient parameter that is adjusted to historic water level and discharge measurements. (Beven, 2008; Asselman, 2009)

Residual errors and likelihood functions

A residual error (Eq. 4) is the net difference between an observed and simulated model response, deviating from observation error and/or simulation error (Juston, 2012).

$$\varepsilon_i = O_i - M_i\left(\Theta, I\right) \quad \text{Eq. 4}$$

where

ε = set of residuals for i observations

O_i = data observations

M_i = model output with model parameters Θ and input data I

It can be difficult, if not impossible, to find the relative contributions from different model errors, uncertainties, inadequacies of data to this lone error indicator. A likelihood function in environmental modelling use the information in a residual error series in guiding model parameter estimations. (Juston, 2012)

Likelihood functions can be characterised as formal or informal, with the difference that a formal function is based on an assumed statistical error model whereas informal functions are not. A statistical error model might for example assume the residuals to be independent and normally distributed. These type of assumptions of the nature of the errors have however been suggested to not typically be justifiable in hydrologic modelling. Root Mean Square Error (RMSE) is an example of a simple informal function that is often used for evaluating models in calibration. (Liu et al., 2009; Juston, 2012)

$$RMSE = \sqrt{\frac{\sum_{i=1}^{n}(\varepsilon_i)^2}{n}} \quad \text{Eq. 5}$$

where

n = total number of observations i

(Juston, 2012)

Limits of acceptability

Informal likelihood functions have been criticised in some modelling applications of being too subjective, in the sense of using some informal likelihood measure and subjectively choosing a threshold for when the model is considered to be acceptable or not. A Limits of Acceptability (LOA) approach have been proposed with the aim to mitigate this. (Juston, 2012)

The LOA approach suggests that the acceptable range for residuals should be set by analysing uncertainties in observation and input data. It then becomes clear if the model output is at least within the observational accuracy range, which is suggested to be a good starting point for evaluating whether or not a model is behavioural or not. The LOA approach was introduced by Beven (2006) in the equifinality thesis manifesto. (Beven, 2006; Liu et al., 2009)

Overparametrisation

When trying to calibrate parameter values on more parameters than can be supported by the available calibration data, the problem of overparametrisation occurs. As the models have become more complex, this is a common issue since the models have a high degree of freedom, and although it is possible to find one good fit to the observations after a calibration, the overparametrisation means that it is not certain that this is the only model that would give a good fit. When dealing with this, the aim is often to try to decrease the dimensionality of the model space, while at the same time capture the local characteristics of the system. (Beven, 2008)

Equifinality and GLUE

The equifinality thesis acknowledges the possibility that there may exist multiple models (model structures and/or parameter sets) that all are able to represent the modelled system in an acceptable manner, as opposed to the optimality approach when one optimal model is searched. Equifinality is the base of the Generalized Likelihood Uncertainty Estimation (GLUE) method, an extension from the Monte Carlo calibration method that integrates uncertainty estimation. The method was first suggested by Beven and Binley (1992) and aims providing a more reasonable and robust representation of the system by keeping all models judged to be behavioural for consideration. (Beven, 2006)

Based on how the different models performs during the calibration, they will be given a likelihood score based on a chosen likelihood measure. The models considered to be non-behavioural are hence given a likelihood of zero. The set of models can then represent the uncertainty through posterior parameter densities and output prediction bounds. More or less subjective decisions regarding

- likelihood measure choice
- acceptance criteria
- choice of parameter and/or input data to be considered as uncertain
- sampling ranges

need to be taken and should be made explicit. (Beven and Binley, 1992; Beven, 2006)

2.8. Towards a probabilistic flood map approach

As mentioned in Chapter 1.1, the idea of probabilistic flood inundation maps have been introduced (e.g. Pappenberger et al. (2005), Smemoe et al. (2007), Merwade et al. (2008), Di Baldassarre et al. (2010), Beven et al. (2011)). The basic idea is that the probabilistic maps present the flood hazard as a probability of inundation instead of one crisp inundation line. This enables visualisation of how the assessed uncertainties propagate to the flood inundation extent. One-dimensional hydraulic models are typically used in the process of creating probabilistic flood inundation maps, since the simulation running time needs to be relatively short.

It has been argued that the presentation of flood hazards as probabilities are a more suitable representation for the subject than deterministic maps,

since a crisp line can give a misleading impression of certainty. As Di Baldassarre et al. (2010) concludes, for deterministic maps to be scientifically justified, they should be based on the most physically-realistic models available. However, these types of complex models (e.g. two-dimensional or even three-dimensional hydraulic models) require more calibration data than is often available. And in those cases where data is available, uncertainties like the magnitude of a 100-year flood will still prevail. Hence is has been concluded that probabilistic flood inundation maps would be more appropriate, and there is a need for formation and development of clear methodologies and applications. (Di Baldassarre et al., 2010)

3. STUDY AREA, DATA, MODELS AND TOOLS

The following chapter describes the area under study, available models and data.

3.1. Area description

Voxnan is a 190 km long river in central Sweden. Belonging to the catchment Ljusnan, it starts from the lake Siksjön in Härjedalen and falls into the lake Varpen in Hälsingland. Being the largest tributary flow to the river Ljusnan, Voxnan has an average discharge of 39 m^3/s at its outlet point. The drainage area of Voxnan is about 3710 km^2 and its main land use and soil type is forest and glacial till respectively. With 85 dams registered it has a degree of regulation of 14 %, with the largest hydro power plant Alfta KRV (32.4 MW, 110 GWh/year). (Vattenregleringsföretagen, 2003; SMHI, 2015)

A 120 km long meandering part of upper Voxnan is a nature reserve, holding important nature values including a species-rich biota and recreational values connected to outdoor activities. This part of the river is almost completely unaffected by river regulations, making it the longest unregulated river reach in the county of Gävleborg. (Länsstyrelsen Gävleborg, 1990)

The upper study boundary is the part of Voxnan where the nature reserve ends, near Voxnabruk at the stream discharge gauge station Nybro (Fig. 5). The river turns east downstream of Nybro and flows through the cities of Edsbyn and Alfta. The lower study boundary was set to be the dam in Runemo, downstream of Alfta and the lake Norrsjön. Hence, a 62 km long part of Voxnan is included in this study.

Voxnan is relatively narrow and shallow, and in combination with being relatively un-regulated in its upstream part, it is easily flooded in periods

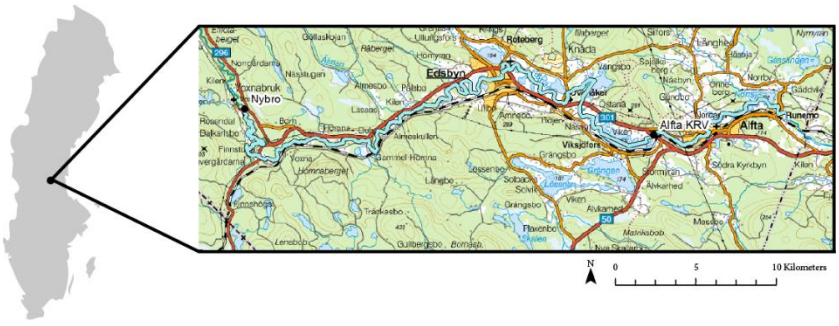

Fig. 5. Location of the study area in Sweden. The thick blue line represents the reach of Voxnan included in the study; from Nybro, past Edsbyn and Alfta, ending at Runemo dam.

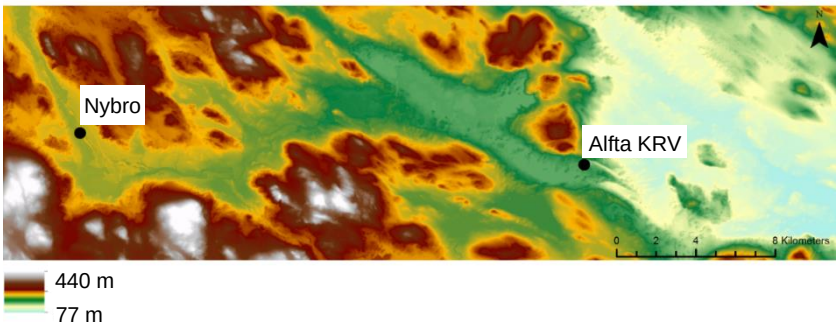

Fig. 6. Digital terrain model Grid2+ of the study area. The measuring stations Nybro and Alfta KRV for the streamflow data are marked. (Lantmäteriet, 2009)

of high precipitation and/or snowmelt. Historically there has occurred approximately one flood event every fifth year. The most severe flood event in modern times occurred in September 1985, when water bearing reached a value of ten times the annual average and the water level at the island in Edsbyn was three meters higher than normal. (Bergström, 1994; Ovanåkers kommun, 2014)

Edsbyn is one of the 18 geographical areas in Sweden that in 2011 was identified by MSB as having significant flood risk, during the first implementation step of the European Commission's Flood Directive. It was reported that 435 habitants and 487 employees were situated within the area for a 100-year flood. It was also concluded that a flood could potentially reach areas of environmentally hazardous nature and a Natura 2000 nature protection area (MSB, 2011).

3.2. **Digital Terrain Model**

The elevation data used is the GSD-Elevation data, Grid 2+ from Lantmäteriet (Fig. 6). The elevation grid is based on the elevation points from aerial laser scanning that has been classified as ground and water. The grid has a resolution of 2 meters and is reported to have an average absolute elevation accuracy of 0.05 meters for open, hard and level surfaces. For steeply sloping terrain, the elevation accuracy is generally lower. Overall, the average elevation error is reported to be smaller than 0.5 meters. (Lantmäteriet, 2015)

The terrain grid was based on and delivered in the official national coordinate systems SWEREF99 TM in plane and RH2000 in height (Lantmäteriet, 2015). These coordinate systems are used throughout this project as well.

3.3. **Tools and maps**

The used software versions with references are listed in below.

- ArcMap 10.1 (ESRI, 2012) with license from KTH Royal Institute of Technology.
- MATLAB R2014b (The MathWorks, 2014) with license from KTH Royal Institute of Technology.
- MIKE Zero 2014, for running MIKE 11 (DHI, 2014c) with license from DHI Sverige AB.

Lantmäteriet has copyright of all the background maps used in this report.

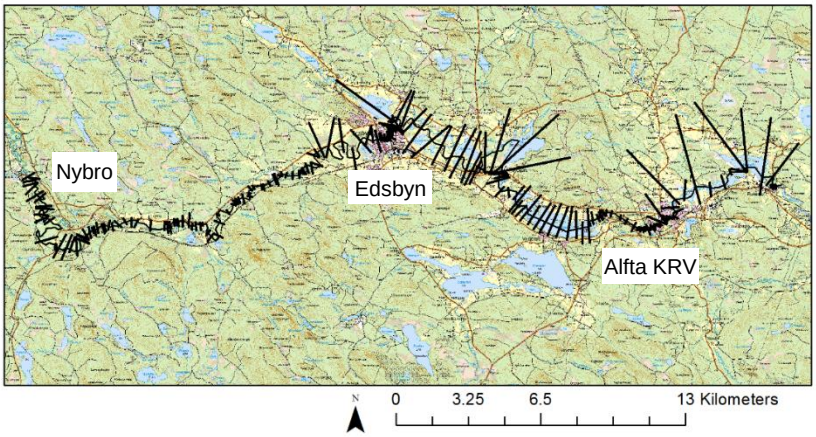

Fig. 7. Cross-section configuration of the hydraulic model.

3.4. Hydraulic model

A one-dimensional MIKE 11 hydraulic model of the chosen part of Voxnan was made available from MSB. The delivered model from 2013 originally covers a 97 km long part of Voxnan and was an update of a previous hydraulic model from 1999 to the new National Elevation Model. The update was performed by DHI Sverige AB upon request from MSB. (MSB, 2013)

The 62 km long part of the hydraulic model included in this study consists of 208 cross-sections (Fig. 7). The geometric description of the cross-sections have been based on the National Elevation Model with 2 meters resolution described in Chapter 3.2. The bathymetry for the river is based on the estimations made for the 1999 hydraulic model. The estimations are reported to have been based on the average water surface profile from a national waterfall record. Some bottom profile information was also given by bridge blue prints and a municipal measurements around Edsbyn in 2013. A number of physical structures in form of dams, culverts, bridges and weirs are also included in the model. (Räddningsverket, 1999; MSB, 2013)

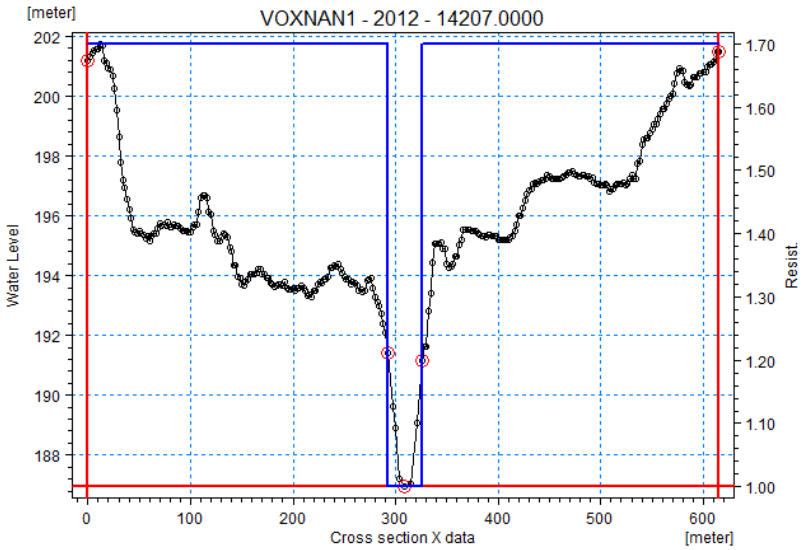

Fig. 8. The most upstream cross-section in the model. The black line is showing the geometric description, plotted against the left y-axis. The blue line is showing the resistance distribution, plotted against the right y-axis.

Table 7. Metadata on the historic daily streamflow records. MHW means the mean of the yearly maximum values.

	Nybro	Alfta KRV
SMHI station number	740	1890
Coordinates in SWEREF 99	X 528142, Y 6803319	X 553514, Y 6801703
Catchment area	2250.9 km^2	3130.4 km^2
Sample mean	25.6 m^3/s	32.4 m^3/s
Sample max	305 m^3/s	361 m^3/s
Type	Regulated discharge	Regulated discharge
Measured regulated MHQ/Calculated natural MHQ	93/106	120/133

The resistance description is according to Manning's formula. A factor of 1.7 had been set to describe the relative resistance between the river bed and flood plain (Fig. 8) in every cross-section, manually marked at every cross-section. This means that the resistance in the flood plain is constantly 70 % higher than the defined roughness coefficient *M* for the river bed.

The hydraulic calculations are based on a fully dynamic wave approximation. Important assumptions are that no dam or bridge failures occur, the water is clean and no discharge goes to the power turbines at the hydroelectric power plants. No consideration of the effect of wind or waves have been taken into account. (MSB, 2013)

3.5. Historic streamflow data

Measured daily streamflow data for Nybro and Alfta KRV (Table 7) from 1 January 1960 to 31 December 2013 was used, provided by SMHI (2015). The measuring station in Nybro is a water level gauge and Alfta is a hydropower dam station. Discharge is estimated from water level measurements through a rating curve, giving the relation between discharge and water level. (Chow, 1988; SMHI, 2015)

Both stations are measuring a regulated streamflow, which can affect the magnitude of the streamflow in the event of high discharge. Based on calculations by SMHI, the highest flows are estimated to be 14 % higher for Nybro and 11 % higher for Alfta in natural state compared to the regulated measurements (Table 7).

3.6. Climate change projections of streamflow

Climate change projections for annual maximum streamflow at Nybro and Alfta KRV was provided by SMHI (Table 8, Fig. 9). The used data was projections from 2059 to 2098. The climate data consists of projections from nine GCMs and the two GHG concentration scenarios RCP 4.5 and RCP 8.5. All projections are based on the RCM RCA4, the DBS method and the hydrological model HBV-Sverige. (Sjökvist, 2015)

Projections have shown a warmer climate in Gävleborg County is expected to lead to earlier and smaller spring floods, due to less snow cover. The discharge is expected to increase during winter and stay approximately the same during summer and autumn. Due to this, the magnitude of 100-year flood is expected to stay the same or even decrease. (SGI, 2010; Sjökvist, 2015)

Table 8. Statistics on the annual maximum series from the historic streamflow records (1960-2013) and the climate projections for two GHG concentration scenarios (2059-2098).

	Nybro			Alfta KRV		
	Historic	**RCP 4.5**	**RCP 8.5**	**Historic**	**RCP 4.5**	**RCP 8.5**
Minimum [m³/s]	29	28	36	41	35	46
Maximum [m³/s]	305	227	215	361	296	318
Mean [m³/s]	94	90	90	118	118	117
Standard deviation [m³/s]	55	32	30	68	43	40

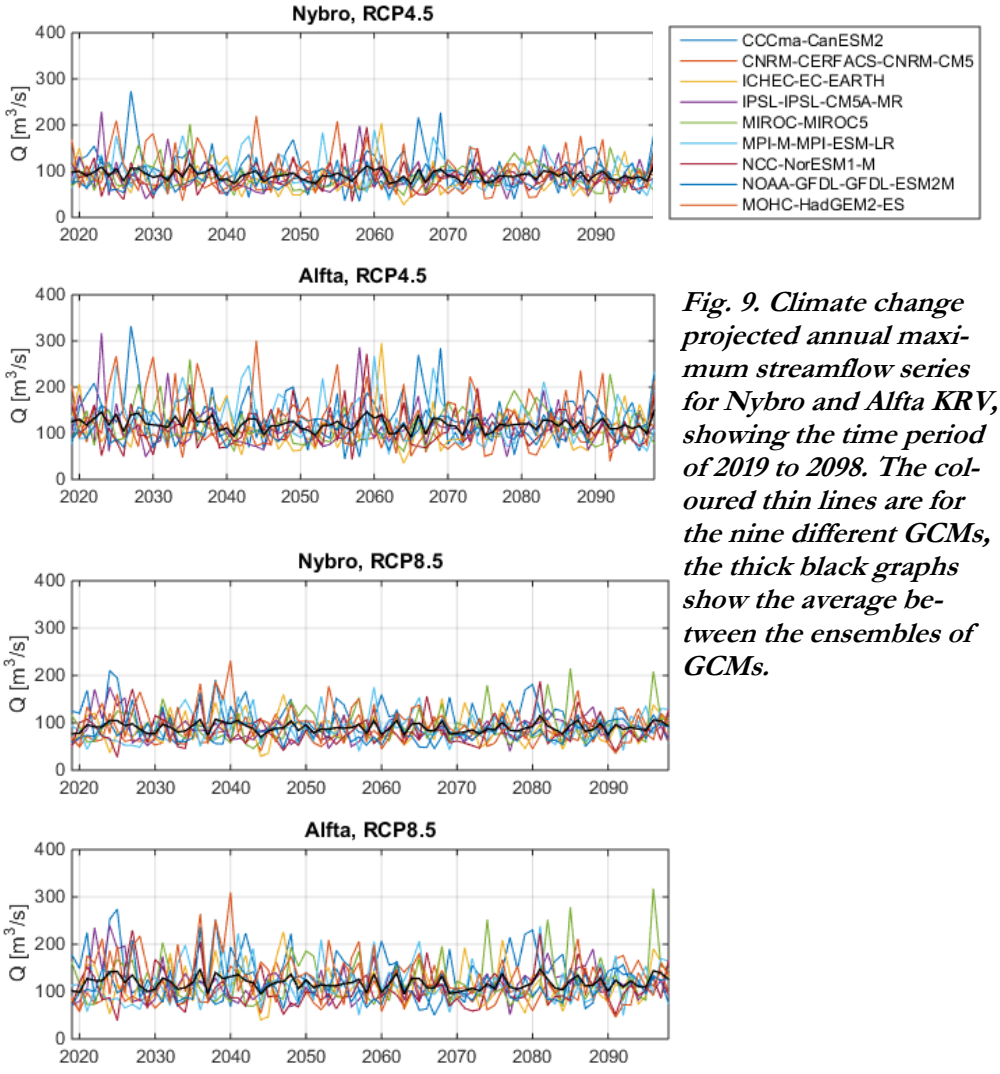

Fig. 9. Climate change projected annual maximum streamflow series for Nybro and Alfta KRV, showing the time period of 2019 to 2098. The coloured thin lines are for the nine different GCMs, the thick black graphs show the average between the ensembles of GCMs.

Table 9. Measured water levels from the flood event September 1985 (Ovanåkers kommun, 2015, DHI Sverige AB, 2015). The locations of the different calibration points can be seen in Fig. 10.

Calibration point number, *i*	Location description	Measured water level [m]
1	Lake Viksjön	155.85
2	Ovanåker	156.45
3	Ovanåker	156.55
4	Ullungen (Edsbyn)	157.55
5	Bridge over stream Lillån (Edsbyn)	157.59
6	Gårdstjärn (Edsbyn)	166.99
7	Nybro	195

3.7. Calibration data

Calibration data was given by Ovanåker municipality and DHI Sverige AB for the flood event September 1985. Water level measurements at seven locations (Table 9, Fig. 10) were given, covering different locations between Nybro and the lake Viksjön. An aerial photography over the lake Norrsjön, downstream of Alfta, was also used (Fig. 11).

Streamflow data for the flood event was available from the historic streamflow records described in Chapter 3.5; 305 m^3/s at Nybro (1985-09-10) and 360 m^3/s at Alfta KRV (1985-09-11). (Ovanåkers kommun, 2014; DHI Sverige AB, 2015; Ovanåkers kommun, 2015; SMHI, 2015)

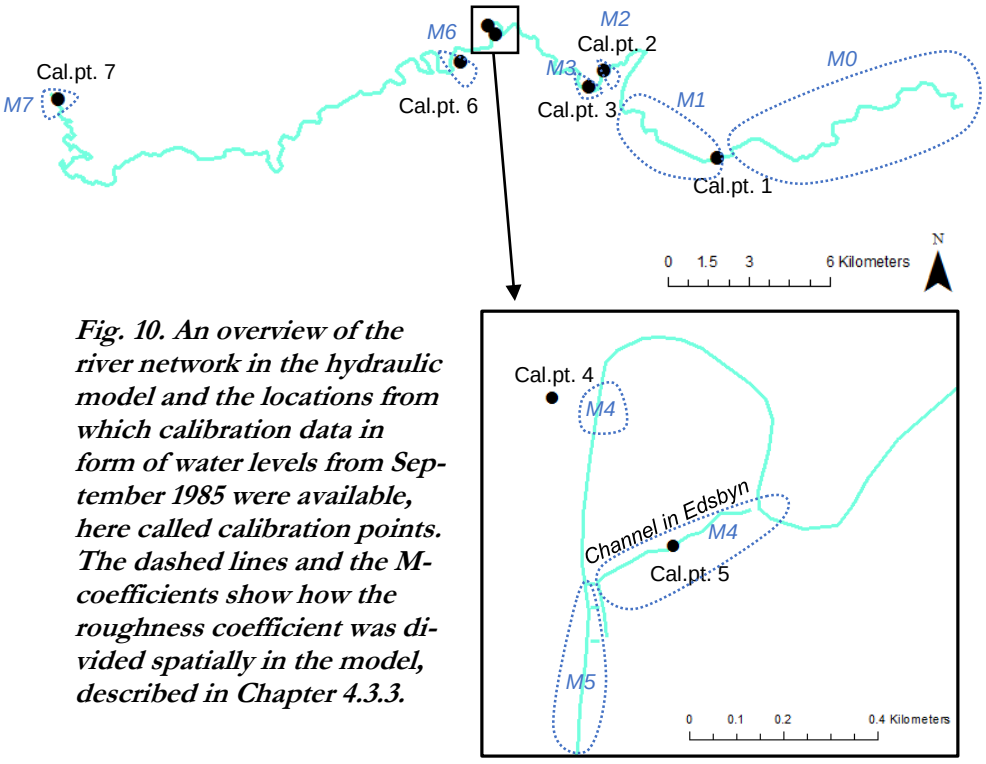

Fig. 10. An overview of the river network in the hydraulic model and the locations from which calibration data in form of water levels from September 1985 were available, here called calibration points. The dashed lines and the M-coefficients show how the roughness coefficient was divided spatially in the model, described in Chapter 4.3.3.

Fig. 11. Aerial photography over Norrsjön Runemo from the flood event September 1985 (Ovanåkers kommun, 2014). The arrows indicate the area from comparison with the digital terrain model could give an estimate of the water level.

4. METHODOLOGY

This chapter aims at giving an account for the methodologies used for the different steps throughout the project.

4.1. Choice of uncertainties and uncertainty assessment methods

The first chosen variable to include in this uncertainty assessment was the magnitude of a 100-year flood in present climate and future climate. The reason for this choice was that uncertainty from frequency analysis has shown to play a large part for the overall uncertainty (Apel et al., 2008; Beven et al., 2011). This choice also allowed for taking the climate change aspect in consideration. The choice of return period 100 years was made on the fact that this is a common return period in flood inundation maps and in physical planning. It was also judged to be appropriate with consideration of the length of available time series for the frequency analysis.

The quite extensive available calibration data provided the right circumstances for also including calibration uncertainty estimation method in the analysis. This lead to the choice of also including the uncertainty of the spatially varying roughness coefficient Manning's number *M*. This choice was based on that it is most often this parameter that is calibrated when a hydraulic model is to be set up before a flood inundation mapping. It is also consistent with how the hydraulic model had been calibrated by MSB (2013).

The choices of uncertainty assessment methods were based on a decision tree (Fig. 12) given by Beven (2008). Quantitative calibration data of measured water levels was available for model evaluation, which lead to a choice of GLUE method calibration for the estimation of the roughness coefficient uncertainty.

Data for model evaluation was however not available for the 100-year flood uncertainty. The uncertainty from frequency analysis could be defined statistically, which lead to a choice of Monte Carlo method. This also gave the opportunity to combine the accepted models (parameter sets) from the GLUE calibration. Furthermore, this would give an opportunity to perform Monte Carlo analysis with MIKE 11 as well as producing probabilistic flood inundation maps with ArcMap.

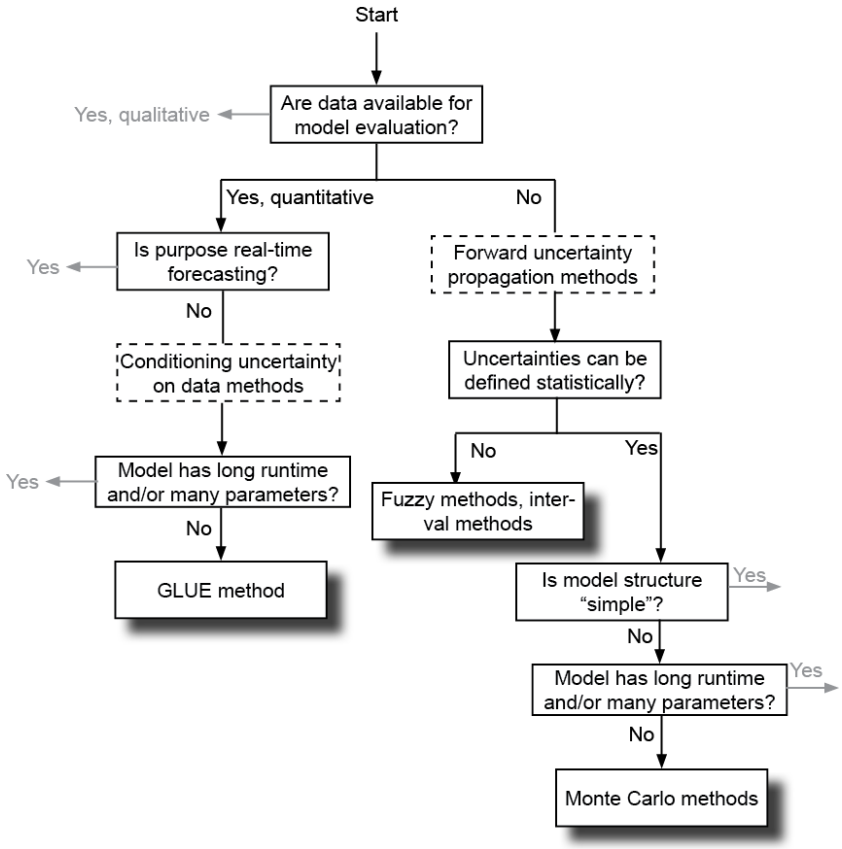

Fig. 12. Decision tree for choosing uncertainty estimation method provided by Beven (2008). Only the parts of the decision tree for this project are included.

The uncertainty regarding the different scenarios and GCMs could not be defined statistically, leading to a Scenario analysis method. The common multi-model (ensemble of projections from different GCMs) and multi-scenario (different GHG concentration scenarios) approach for representing climate change uncertainty was therefore judged to be applicable also in this case.

4.2. **Methodological overview**

The uncertainty assessment was decided to, with Monte Carlo analysis, result in probability distributions of water levels at all cross-sections as well as a probabilistic flood inundation map (Fig. 13). This was to be combined with a scenario analysis, by performing the Monte Carlo analysis for five different scenarios (Table 10).

Scenario A, Scenario B and Scenario C include uncertainty of discharge and roughness coefficient for different discharge conditions: in present climate, future RCP 4.5 climate and future RCP 8.5 climate respectively. Scenario I only includes the discharge uncertainty and Scenario II only includes the roughness coefficient uncertainty.

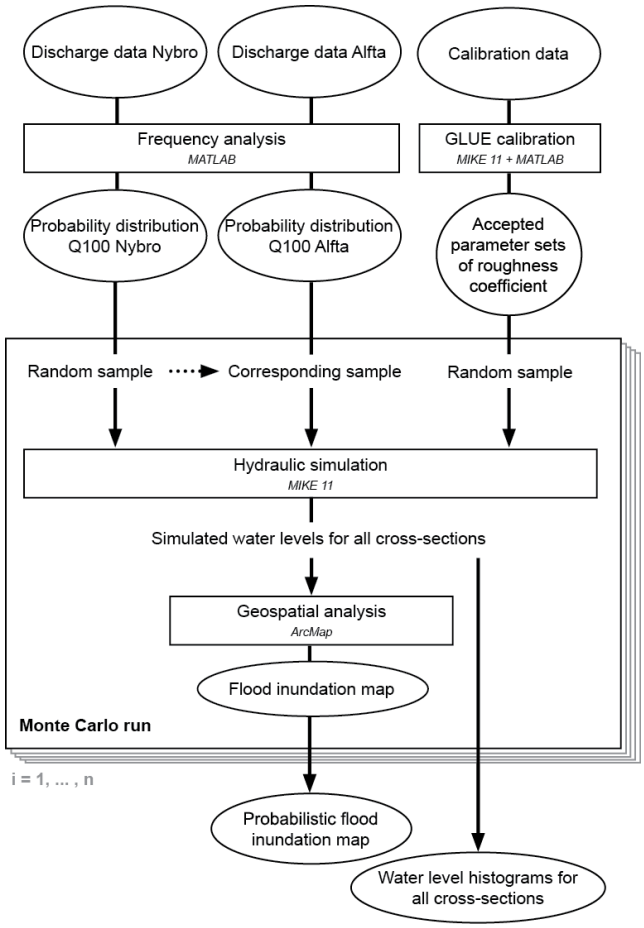

Fig. 13. Overview of the uncertainty estimation process conducted for each scenario.

Table 10. Overview of the five scenarios used in the Monte Carlo analyses after estimations of uncertainty quantifications had been conducted.

	Discharge		Roughness coefficient	
	Varied/ constant	**Description**	**Varied/ constant**	**Description**
Scenario A	Varied.	Samples from **present climate** frequency analysis.	Varied.	Sampled models from GLUE calibration
Scenario B	Varied.	Samples from future climate frequency analysis, **RCP 4.5**.	Varied.	Sampled models from GLUE calibration
Scenario C	Varied.	Samples from future climate frequency analysis, **RCP 8.5**.	Varied.	Sampled models from GLUE calibration
Scenario I	Varied.	Samples from present climate frequency analysis.	Constant	Manually calibrated model
Scenario II	Constant	Q100 in 2098 according to MSB (2013).	Varied.	Sampled models from GLUE calibration

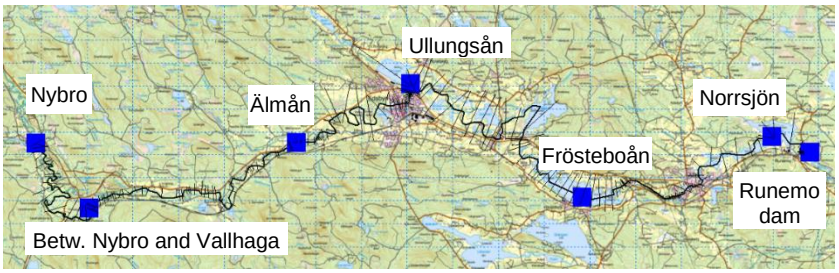

Fig. 14. Locations of the boundary conditions in the hydraulic model.

4.3. Hydraulic model adjustments

The adjustments made on the hydraulic model provided by MSB is described in this section.

4.3.1. *Boundary conditions*

Seven boundary conditions were specified for the hydraulic model (Fig. 14, Table 11). The upper boundary condition was the 100-year flood sample for Nybro. The four joining tributary flows between Nybro and Alfta KRV were area-scaled so that the simulated hydrologic load at Alfta KRV would equal the sampled magnitude of the 100-year flood at Alfta KRV (Eq. 6).

$$Q_i = qA_i = \left(\frac{\Delta Q100}{\Delta A}\right)A_i \qquad \text{Eq. 6}$$

where

Q_i = area-scaled tributary flow [L^3T^{-1}]

q = specific discharge [LT^{-1}]

A_i = area of sub-catchment of tributary flow [L^2]

$\Delta Q100$ = difference between samples of 100-year flood in Nybro and Alfta KRV [L^3T^{-1}]

ΔA = area difference between catchment at Nybro and catchment at Alfta KRV [L^2]

Hence, it was assumed that the specific discharge was the same for all sub-catchments. The locations of the four tributary flow boundary conditions were kept as it was in the delivered hydraulic model by MSB (2013). The areas for the different sub-catchments were provided by SMHI (2015).

Table 11. Boundary conditions of the hydraulic model. The flow boundary conditions were all scaled according to the sampled values for Nybro and Alfta KRV. The water level was kept constant for all runs.

Location	Type	Value
Nybro	Upper boundary condition, open	$Q100_{Nybro}$
Between Nybro and Vallhaga	Distributed source	10.7 % of ΔQ100
Älmån	Point source	7.5 % of ΔQ100
Ullungsån	Point source	22.5 % of ΔQ100
Frösteбån	Point source	59.3 % of ΔQ100
Norrsjön	Point source	10 % of $Q100_{Nybro}$
Downstream of Runemo dam	Lower boundary condition, open	+ 89.4 m

The tributary flow in Norrsjön was scaled with relation to the magnitude of the sampled value at Alfta KRV. For finding a suitable scaling factor, a simulation was performed with the same hydrologic load as was measured from calibration flood event 1985. The simulated water level for Norrsjön was then compared with the estimated calibration water level from comparing the aerial photography (Fig. 11) with the digital terrain model. The scaling factor of 10 % could be estimated from this type of "pre-calibration". This value also agreed with the relative catchment sizes between Alfta KRV and Runemo dam.

The river reach right downstream of Runemo dam was chosen to be the downstream boundary of the model. This enabled the downstream boundary condition of the model to be described as a constant water level, with the dam decreasing the risk of affecting the water level upstream. The water level boundary condition was estimated from the digital terrain model and chosen so that it did not affect the upstream water levels.

The discharge boundary conditions were all set to be constant, in contrast to using time varying hydrographs. This was chosen since it was not the temporal variation of the flood wave that was of interest here, but rather the steady state solutions from many different runs. The use of hydrographs versus constant values is an uncertainty in itself, beyond the scope of this project. See e.g. Thurin (2011) for a comparison between these two types of boundary conditions.

4.3.2. *Simulation period and initial conditions*

The simulation period was set to six days and the simulation time step to 30 seconds. This was sufficient for guaranteeing a steady state solution of the water levels as well as numerical stability. The computation time was approximately ten seconds per simulation, which was judged to be acceptable for the Monte Carlo runs.

The initial conditions of the water levels at all computation points were set to be based on a so-called hot start-file, which is a result file containing water levels from a previous simulation. A steady state solution is typically reached faster if the initial conditions are lower water levels than the steady state levels, why a simulation with a hydrologic load just below the lowest Monte Carlo samples was performed to acquire a suitable hot start-file.

4.3.3. *Spatial variation of the roughness coefficient parameter*

The roughness coefficient Manning's number *M* was varied spatially by specifying eight different parameter values (Table 12). The set-up was mainly based on the availability of calibration data of measured water levels (Fig. 10). The aim was to only vary the parameter values between the points where calibration data was available, keeping the degree of freedom low. The nature of the river reach was also taken into consideration.

The parameter *M0* was not included in the Monte Carlo runs, since the dams at Alfta KRV prevents it from having any effect the water levels at any of the calibration points. *M1* was set to apply for the entire lake Viksjön and *M5* was applied for the entire blocky part between Österforsen dam and lake Ullungen.

The rest of the parameter values (*M2*, *M3*, *M4*, *M6* and *M7*) was specified pointwise at calibration points. MIKE 11 linearly interpolates the roughness coefficient values between the user-specified values.

Table 12. The spatial variation of Manning's number M. The location of the different calibration points can be seen in Fig. 10.

	Description
M0	The entire part of the hydraulic model downstream of Alfta KRV. Does not affect any of the calibration points and are excluded from the Monte Carlo analyses. Value kept to be 20, which was the same as was given by MSB (2013).
M1	Entire Viksjön, for calibration of cal.pt. 1.
M2	Located at cal.pt 2, for calibration of cal.pt 2.
M3	Located at cal.pt 3, for calibration of cal.pt.3.
M4	Located at cal.pt.4, for calibration of cal.pt.4. Also affects cal.pt. 5. The entire channel running from the energy plant is also given the value *M4*.
M5	Blocky part downstream of Österforsen dam and upstream of lake Ullungen. Has a small influence on cal.pt. 5 and cal.pt.4.

4.4. Performing Monte Carlo analysis with MIKE 11

The Monte Carlo analyses with MIKE 11 could be conducted by using MATLAB's ability to read, write and save text files (Fig. 15). Based on a template from Ola Nordblom at DHI Sverige AB, a MATLAB script file was constructed that could save boundary condition files and parameter files for every Monte Carlo sample. The script in MATLAB also connected all these boundary condition files and parameter files to a batch file.

The batch file was thereafter run within the Batch Simulation editor in MIKE 11, carrying out the specified number of iterations of hydraulic simulations. The steady state solution from every iteration was then exported from the binary result files. A MS-DOS program *res11read.exe* was provided by DHI for converting all binary result files to text files. The text files were finally imported to one table for each scenario, with one row for each cross-section and one column for each iteration.

4.5. Frequency analysis

4.5.1. *Data screening*

The daily streamflow records for Alfta and Nybro[1] from 1960 to 2013 were turned into Annual Maximum Series with 54 records. The AMSs were screened according to the basic procedure by Dahmen and Hall (1990), in order to verify their stationarity, consistency and homogeneity prior to the frequency analysis. This includes:

- Plot the data for a visual inspection, so that obvious trends or discontinuities can be detected (Fig. 16).
- Test the absence of trend with Spearman's rank-correlation method.
- Test the stability of variance with the F-test.
- Test the stability of mean with the t-test.

[1] From Nybro there are measured streamflow data available for 1913-1925 and 1940-2013, but an AMS including all these years did not hold the stability of variance test. Furthermore, it was decided that an equally long time series as the one from Alfta KRV would result in more similar confidence intervals for the two stations (since the standard error of estimate does depend on the number of observations, meaning that a shorter time series leads to a wider confidence interval). Using the whole time series for Nybro would lead to a confidence interval of roughly half the size of Alfta, which could be problematic since the matching of the sampled values are through the cumulative distribution probability from the confidence interval.

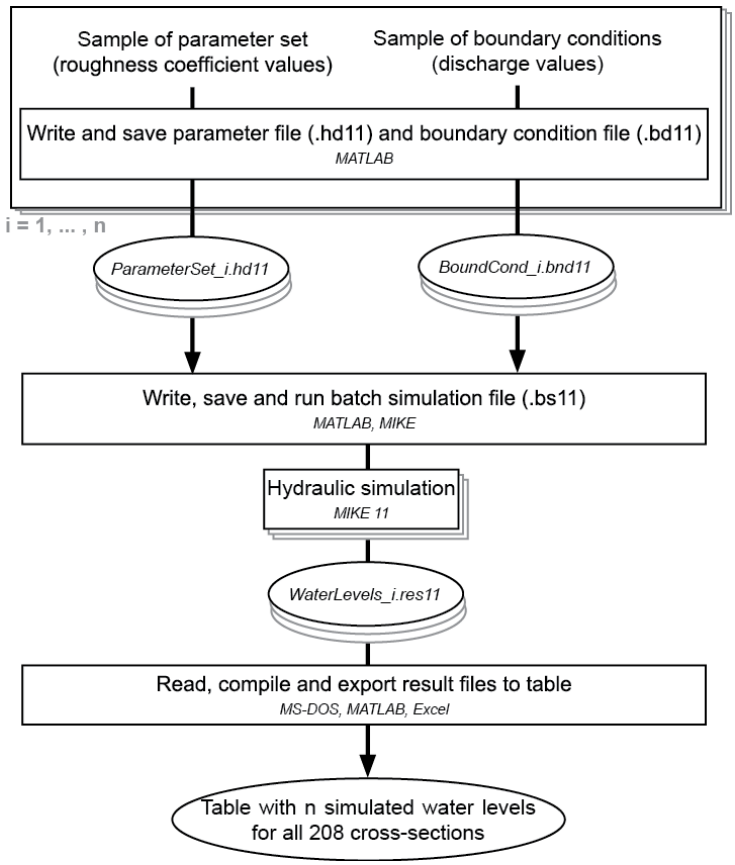

Fig. 15. Overview of how the Monte Carlo runs were conducted, with the input of samples of selected parameters and boundary conditions. The output table could then be imported to ArcMap for geospatial analysis.

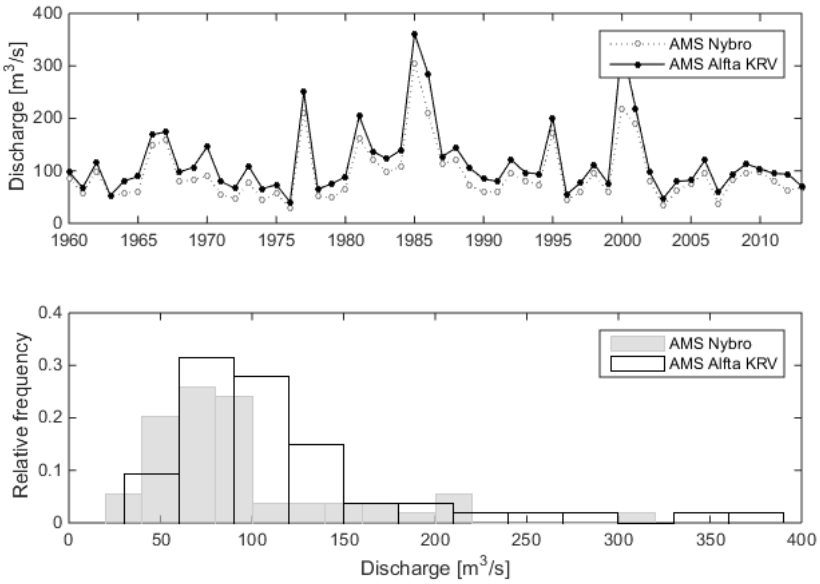

Fig. 16. Hydrographs and histograms of the two annual maximum series for Nybro and Alfta KRV 1960 – 2013. No evident signs of linear trend, periodic trend, change in variance or change in average can be detected visually from the hydrograph. The histograms show that the data is positively skewed.

Table 13. Statistics on the 54-year Annual Maximum Series for Nybro and Alfta KRV between the years 1960 to 2013, from SMHI (2015). The confidence interval used for the Student's t-distribution and Fisher's F-distribution is the customary value of 95 % (Dahmen and Hall, 1990).

	Nybro	Alfta KRV
Minimum [m^3/s]	29.0	40.6
Maximum [m^3/s]	305	361
Mean [m^3/s]	93.5	117.6
Standard deviation [m^3/s]	54.5	67.6
Skewness	1.82	2.02
Absence of trend test statistic, t_t ($-2.0 < t_t < 2.0$)	-0.51	0.10
Stability of variance test statistic, F_t ($0.441 < F_t < 2.27$)	2.15	1.61
Stability of mean test statistic, t_t ($-2.0 < t_t < 2.0$)	0.67	0.75

The AMSs were judged to pass the tests since the test statistics were located within their corresponding confidence intervals, with the customary significance level of two-tailed 5 % (Table 13). The time series were therefore judged to be valid to use in the frequency analysis. For more details on these data screening procedures, see Dahmen and Hall (1990).

4.5.2. *Calculation of 100-year flood with confidence intervals*

The AMSs for Nybro and Alfta KRV was fitted to the three probability distribution functions Gumbel, lognormal and Log-Pearson Type III. Methods of fit were with help of frequency factors for Gumbel and Log-Pearson Type III, while methods of moments was used for the lognormal distribution.

The magnitude of the 100-year flood was calculated for the three distributions, with corresponding 95 % confidence intervals (Table 14). The standard error of estimate was used for finding the confidence intervals for Gumbel and Log-Pearson Type III and the calculation for lognormal distribution followed a standard routine suggested by U.S. Water Resources Council Method. These methodology choices was based on equations and recommendations given by Chow (1988). The equations for Gumbel calculations are given below.

Magnitude of 100-year flood:

$$K_T = -\frac{\sqrt{6}}{\pi}\left\{0.5772 + \ln\left[\ln\left(\frac{T}{T-1}\right)\right]\right\} \quad \text{Eq. 7}$$

$$x_T = \bar{x} + K_T s \quad \text{Eq. 8}$$

where

x_T = magnitude of event with return period T

K_T = frequency factor for return period T

s = standard deviation of the AMS

$\bar{x}$ = arithmetic mean of the AMS

Table 14. Overview of how the 100-year flood magnitudes and their respective confidence intervals were calculated. The method choices are based on recommendations by Chow (1988).

Probability distribution function	Method of fit	Method of finding confidence interval
Gumbel	Frequency factors	Standard error of estimate
Lognormal	Method of moments	According to Bulletin 17B, Appendix 9
Log-Pearson Type III	Frequency factors	According to Bulletin 17B, Appendix 9

Confidence interval:

$$s_e = \left[\frac{1}{n}(1+1.1396K_T+1.1000K_T{}^2)\right]^{1/2} s \qquad \text{Eq. 9}$$

$$\text{Interval} = x_T \pm s_e z_a \qquad \text{Eq. 10}$$

where

s_e = standard error of estimate

n = size of series

z_a = standard normal variable for significance level a (1.96 for a 95 % confidence interval)

The magnitude of the 100-year flood with its 95 % confidence interval from the Gumbel distribution was chosen to be used in the rest of the uncertainty assessment. Partly because it gave a similar magnitude of the 100-year flood as that MSB had used, and partly because it is also the type that SMHI use.

The observations in the AMSs were also probability plotted according to an empirical plotting position first proposed by Gringorten. This was done to compare the observations with the fitted cumulative probability distributions. The magnitude of each observation was plotted against their return period as:

$$T = \frac{n+1-2a}{m-a} \qquad \text{Eq. 11}$$

where

n = size of series

m = descending rank of the observation in the series

a = distribution dependant parameter

(Bedient, 2008)

The value for the distribution dependant parameter was given the suggested value of 0.4 for when the exact distribution is not known (whereas 0.375 is for lognormal and 0.44 is for Gumbel) (Bedient, 2008).

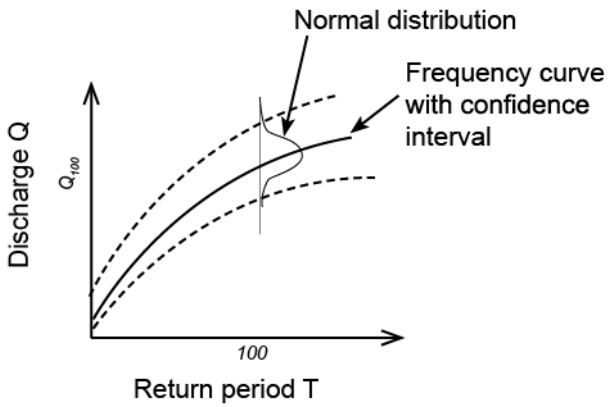

Fig. 17. Sketch of how the confidence limits for the 100-year flood was used to find a normal distribution from which the Monte Carlo samples were drawn.

4.5.3. *Generating discharge samples for the scenarios*

Present climate (Scenario A and Scenario I)

A normal probability distribution was fitted to the 95 % confidence interval (Fig. 17) of the Gumbel type 100-year flood. The confidence interval was divided by four to get the standard deviation parameter, since about 95 % of the values drawn from a normal distribution lies within the interval of the average plus minus two standard deviations. The magnitude of the 100-year flood gave the mean parameter for the normal distribution.

This normal probability distribution was hence the distribution from which random samples were to be drawn for the Monte Carlo analysis. 1000 samples were considered sufficient and reasonable for the computation time of running the hydraulic model.

The sampling was performed in MATLAB. Prior to the random sampling, the normal distribution were truncated at the 95 % confidence interval, guaranteeing that the samples would stay within these limits (as suggested by e.g. Beven (2008)). In order to simulate plausible situations, the samples for Alfta KRV were chosen to match the same cumulative probability value as the corresponding Nybro value had.

Future climate (Scenario B and Scenario C)

The sampling procedure for the future climate projections followed the same procedure as for the present climate. Each GHG concentration scenario had nine time series of projections from nine GCM models, which were kept separated in this process. In other words, for each GHG concentration scenario and location, there were nine AMSs for which nine different 100-year floods with confidence intervals were calculated. 100 samples were then drawn from each normal distribution corresponding to these confidence intervals.

The samples for Nybro and Alfta KRV were also matched in a corresponding way as described above. This resulted in, for each GHG concentration scenario, 900 random samples for both Nybro and Alfta KRV, representing the ensemble of GCMs. By performing the sampling procedure for one GCM series at a time, the differences between the GCMs could be identified.

4.6. Calibration

Initially, a manual calibration using a simple "trial and error" method was performed. An optimal model was searched by adjusting *M1* to *M7* with the aim of minimising the absolute residual errors. By adjusting one parameter value at a time, starting furthest downstream with *M1* and then going gradually upstream, was the risk of influencing already adjusted values decreased.

The manual calibration was performed for both the range 10-50 and the range 15-35 for the Manning's number *M*. The narrower interval of Manning is more representable to the values often used in flood inundation models (Chow, 1959), and is decreasing the risk of over- and underestimating water levels on the locations where there are long distances to calibration points.

After the manual calibration, a Monte Carlo calibration following the GLUE methodology was performed. 4000 parameter sets (combinations of *M1* to *M7*) were sampled from a uniform distribution of the chosen parameter range 10 to 50. The samples were used in 4000 simulations of the hydraulic model. The acceptable models (combinations of *M1* to *M7*) were chosen according to defined acceptance criteria's. The GLUE calibration procedure was thereafter repeated with the narrower parameter range 15 to 35.

4.6.1. *Generating roughness parameter samples for the scenarios*

The roughness coefficient values were not to be varied in Scenario I, for which the manually calibrated model with the narrower range of 15 to 35 of the Manning's number was used.

For the other scenarios, the accepted models from the GLUE calibration with the narrower range (15 to 35) was used, fulfilling the acceptance criteria of all residual errors being less than 0.4 meters. The choice of acceptance criteria is subjective. This particular acceptance criteria was chosen, for the sake of comparison, as it was the same as MSB used in their flood inundation mapping (MSB, 2013).

The residual errors for this acceptance criteria was also within the accuracy of the least precise water level measurement, which was the value for Nybro of having no decimal places. The acceptance criterion was hence within the observational accuracy to some extent, like suggested by the LOA approach.

4.7. Geospatial analysis

The flood inundation extent maps were produced with a series of geo-processing steps in ArcMap. The shape of the cross-sections could be exported as a shape file from the Cross-section editor in MIKE 11. One shape file per scenario was created. The tables holding the water levels from all simulations was joined to their corresponding shape file, georeferenced by unique cross-section IDs.

The geo-processing steps for producing the maps were set up in ModelBuilder in order to automatize the process, using the "for"-iterator (Fig. 18). For each simulation, the water levels of the cross-sections were interpolated to a TIN and then linearly interpolated to a water surface raster with the same resolution as the DEM. The flood extent could then be found with the raster calculator, by choosing all pixels with a water level higher than the DEM level. River connectivity was then assured by conversion of the flood extent raster to polygons. The polygons intersecting with the river network was selected and converted back to a raster flood inundation map.

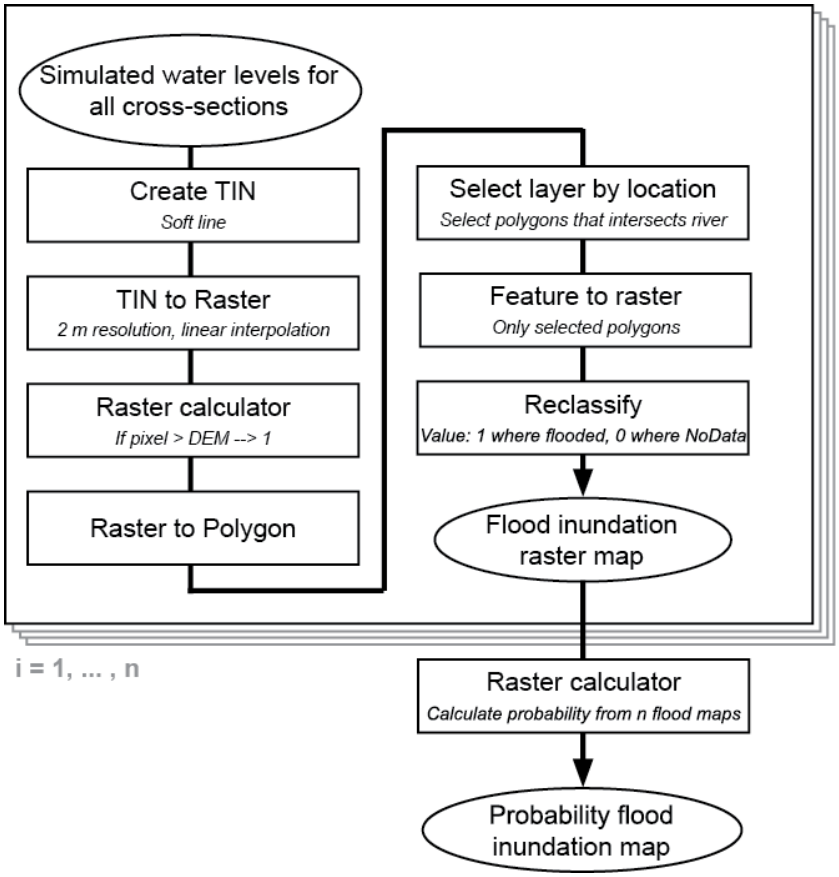

Fig. 18. The geo-processing steps taken in ArcMap to produce the flood inundation maps. The iterative process is performed in ModelBuilder. The model was run for one scenario at a time.

Prior to the model runs for the different scenarios, a first flood inundation map was created to compare with the flood inundation maps produced by MSB (2013), in order to detect eventual mapping flaws. As is often needed when flood inundation maps are produced, modifications of a few cross-sections were required. The reach of theses cross-sections were extended, so that they covered the whole inundated area (Fig. 19).

The cross-section modifications was performed at lake Vägnan in Ovanåker and at Alfta and lake Norrsjön. Other than this, the produced flood inundation map was estimated to be reasonable, so no further modifications (e.g. adding dikes or modifying the DEM) were judged to be necessary for the scope of this project.

After the model in ModelBuilder had been run, for each scenario separately, the resulting flood inundation maps were used for creating the probabilistic flood inundation maps according to:

$$P = \frac{\sum_{i=1}^{n} f_i}{n} \qquad \text{Eq. 12}$$

where

P = probability that the pixel will be flooded according to the simulations

$$f_i = \begin{cases} 1 \text{ if flooded} \\ 0 \text{ if not flooded} \end{cases}$$

n = total number of simulations in the scenario

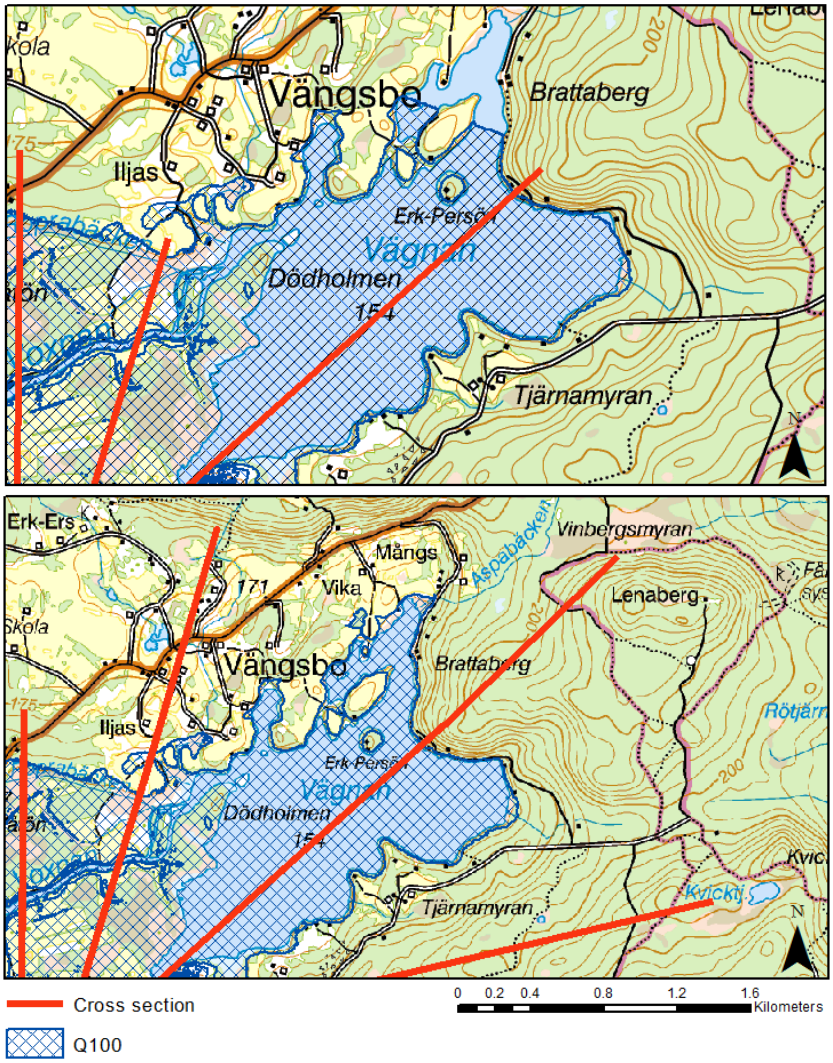

Fig. 19. The cross-sections imported from MIKE 11 at the lake Vägnan in Ovanåker needed to be extended to prevent an incorrect cut in the simulated flood inundation extent.

5. RESULTS

This chapter presents the results of the study, divided into four sub-chapters. The probabilistic flood inundation maps of Scenario A, Scenario B and Scenario C can be found in Appendix II.

5.1. Frequency analysis, present and future climate

The three probability distribution functions Gumbel, lognormal and Log-Pearson Type III are plotted with the probability plots of the records in the AMSs (Fig. 20). Differences between the three distribution functions are increasing with return period, especially for Log-Pearson Type III compared to the other two. The probability plotted observed records are within the 95 % confidence interval for the Gumbel distribution, although the form of the plotting position does not match any of the distribution functions entirely.

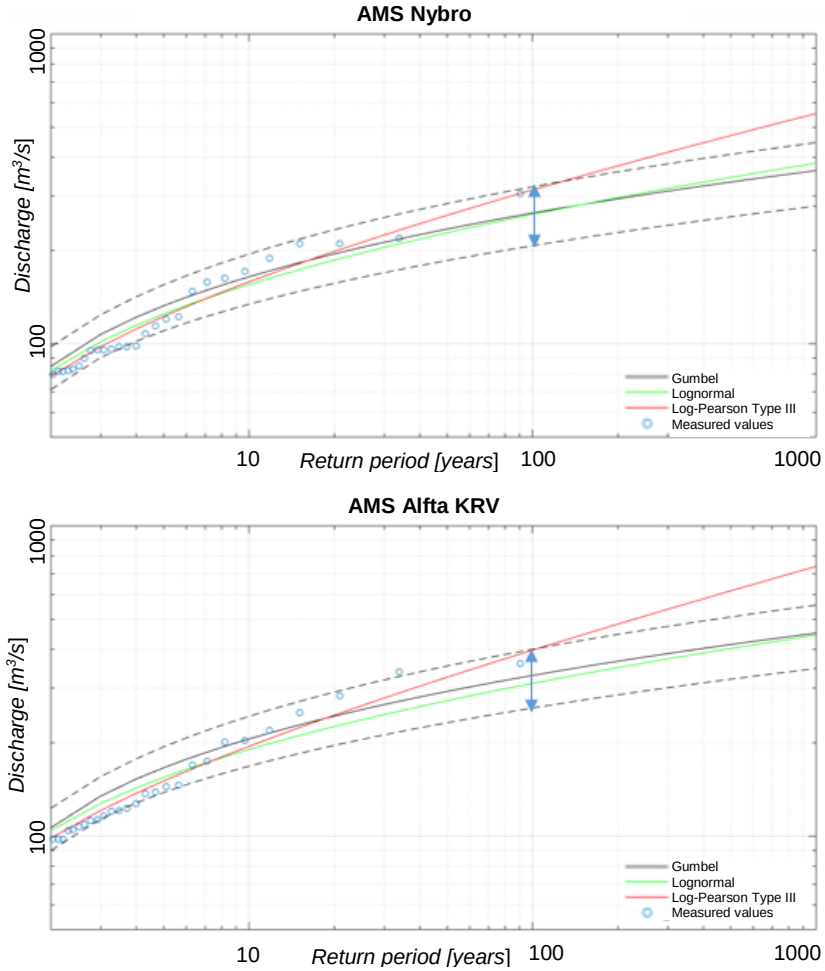

Fig. 20. Loglog plots of the CDFs of Gumbel, lognormal and Log-Pearson Type III. The dots are measured values according to the plotting position. The dashed lines are the 95 percent confidence interval from the Gumbel distribution. The blue arrows indicate the confidence interval of the 100-year flood for which the normal distributions were fitted.

The magnitude for 100-year flood with corresponding 95 % confidence interval was calculated for Nybro (Table 15) and Alfta KRV (Table 16) with frequency analysis based on historic measurements (Scenario A) as well as future climate change projections (Scenario B and Scenario C). For Scenario A, this has been calculated for Gumbel, lognormal and Log-Pearson III. Gumbel and lognormal give quite similar magnitudes of the 100-year flood, lognormal giving a bit wider confidence interval. Log-Pearson Type III is significantly larger, both in magnitude and width of confidence interval.

The variance between the different GCMs projections is clearly showing when comparing the magnitude of 100-year floods and the confidence intervals (Fig. 21, Fig. 22). The GCMs have different biases and also respond to GHG concentration in various ways. For example, the model *GCM MOHC-HadGEM2-ES* goes from giving the largest magnitudes relative to the other GCMs in RCP 4.5 to a much lower position in RCP 8.5. The opposite applies for the model *MIROC-MIROC5*. It is also evident that no confidence interval for a single GCM would cover the whole ensemble span of calculated 100-year floods for all scenarios.

Table 15. Magnitudes of the 100-year flood for Nybro, with corresponding confidence intervals.

From historic measurements from 1960-2013				
Probability distribution function	**Q100 [m3/s]**		**95 % confidence interval of Q100**	
Gumbel (used in Scenario A)	264		[207, 321]	
Lognormal	262		[209, 357]	
Log-Pearson Type III	314		[245, 444]	
From climate change projections for 2059-2098				
Global Climate Model	**Scenario B, RCP 4.5 (all Gumbel)**		**Scenario C, RCP 8.5 (all Gumbel)**	
	Q100 [m^3/s]	**95 % confidence interval of Q100**	**Q100 [m3/s]**	**95 % confidence interval of Q100**
CCCma-CanESM2	236	[185, 286]	206	[166, 246]
CNRM-CERFACS-CNRM-CM5	155	[128, 183]	155	[128, 182]
ICHEC-EC-EARTH	184	[145, 223]	173	[139, 208]
IPSL-IPSL-CM5A-MR	166	[135, 197]	154	[129, 179]
MIROC-MIROC5	169	[138, 200]	221	[172, 270]
MPI-M-MPI-ESM-LR	207	[164, 249]	199	[159, 239]
NCC-NorESM1-M	174	[140, 208]	181	[143, 219]
NOAA-GFDL-GFDL-ESM2M	155	[128, 182]	143	[119, 166]
MOHC-HadGEM2-ES	224	[174, 274]	184	[148, 220]

5.2. **Calibration**

The manual calibration attempts with the "trial and error" method give a large span of effective roughness coefficient values (Table 17). *M3* give no sign of having an upper limit when trying to reduce the residual error in Calibration Point 3. The calibrated values of *M2* and *M4* also had to be decreased when decreasing the parameter range, resulting in a higher RMSE value for this calibration attempt (Table 18).

The calibrations following the GLUE method with 4000 simulations for each parameter range give slightly higher RMSE values than the manual calibration attempts (Table 19). The acceptance limit for the acceptance criteria (all absolute residual errors being smaller than a certain limit) was adjusted, finding that the number of accepted models decreased accordingly. The ten accepted parameter sets from the GLUE calibration with a narrower parameter range acceptance criteria of all residual errors being smaller than 0.4 meter was chosen to be used for the scenario Monte Carlo analyses.

Table 16. Magnitudes of the 100-year flood for Alfta KRV, with corresponding confidence intervals.

From historic measurements from 1960-2013				
Probability distribution function	**Q100 [m3/s]**		**95 % confidence interval of Q100**	
Gumbel (used in Scenario A)	330		[259, 400]	
Lognormal	311		[252, 416]	
Log-Pearson Type III	397		[311, 559]	
From climate change projections for 2059-2098				
Global Climate Model	**Scenario B, RCP 4.5 (all Gumbel)**		**Scenario C, RCP 8.5 (all Gumbel)**	
	Q100 [m^3/s]	**95 % confidence interval of Q100**	**Q100 [m3/s]**	**95 % confidence interval of Q100**
CCCma-CanESM2	300	[236, 364]	269	[215, 322]
CNRM-CERFACS-CNRM-CM5	206	[168, 245]	210	[173, 248]
ICHEC-EC-EARTH	252	[197, 306]	237	[189, 286]
IPSL-IPSL-CM5A-MR	213	[174, 252]	209	[174, 244]
MIROC-MIROC5	240	[194, 287]	311	[240, 382]
MPI-M-MPI-ESM-LR	280	[220, 340]	253	[202, 305]
NCC-NorESM1-M	242	[193, 292]	219	[175, 264]
NOAA-GFDL-GFDL-ESM2M	209	[173, 245]	192	[160, 224]
MOHC-HadGEM2-ES	300	[231, 369]	235	[189, 281]

During the manual calibrations, *M1* was adjusted to decrease the residual error in Calibration Point 1, then *M2* was adjusted to decrease the residual error in Calibration Point 2, etc. Dotty plots (Fig. 23, Fig. 24) from the GLUE calibrations show how these residual errors depend on the individual calibration points. The form of the dotty plots give indication of how strong each *M* value affects its calibration point. Accepted versus rejected models indicate if there seems to be "one optimum" value of *M* or not for calibration in this set-up. It is also visualized how e.g. *M3* seems to have its optimum beyond the parameter range, as indicated from the manual calibration.

Dotty plots from the GLUE calibrations of the individual *M* values against the total RMSE values (Fig. 25, Fig. 26) show how strongly each *M* value affects the RMSE of the entire model. *M7* has the strongest individual effect of the overall RMSE, showing that outside the "optimum" low point, the RMSE increases linearly with the value of *M7*.

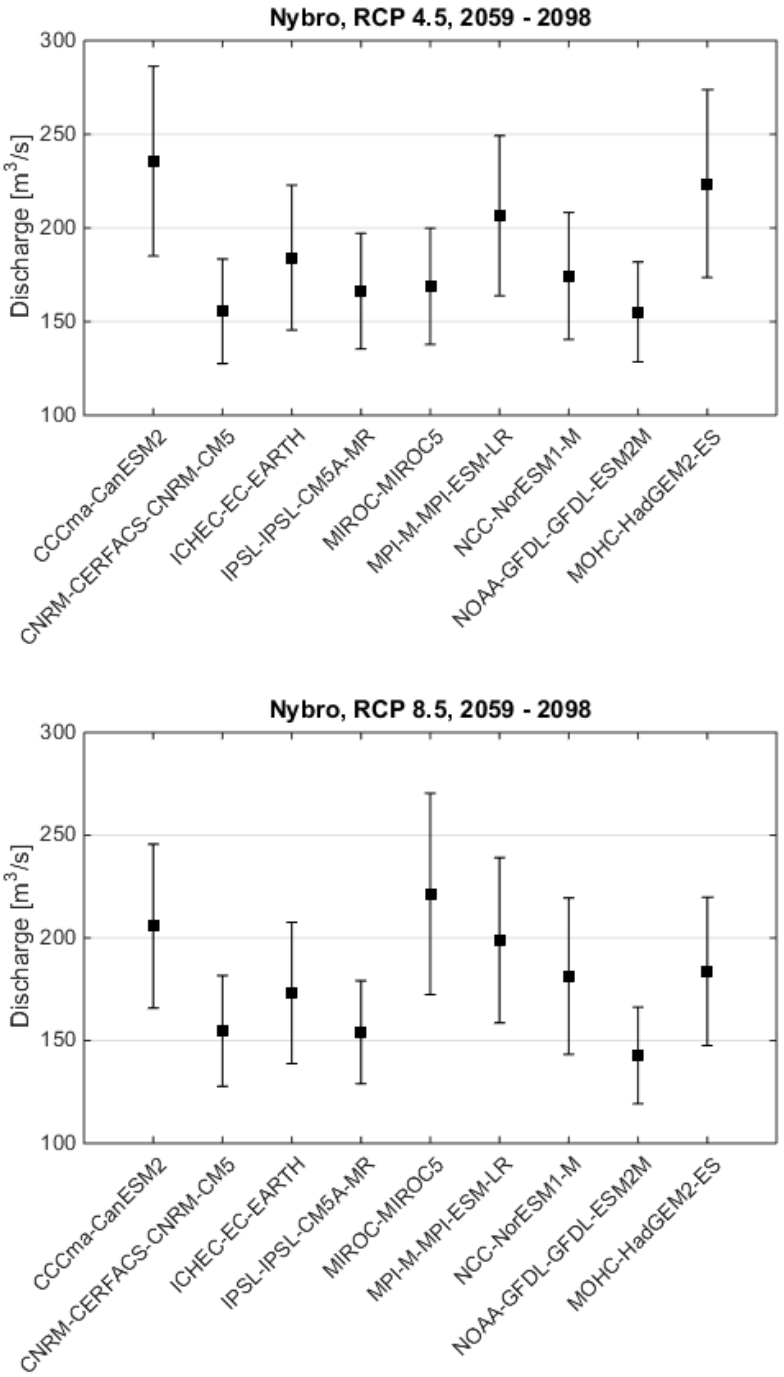

Fig. 21. Calculated 100-year flows for Nybro with corresponding 95 % confidence intervals, for the individual global climate models.

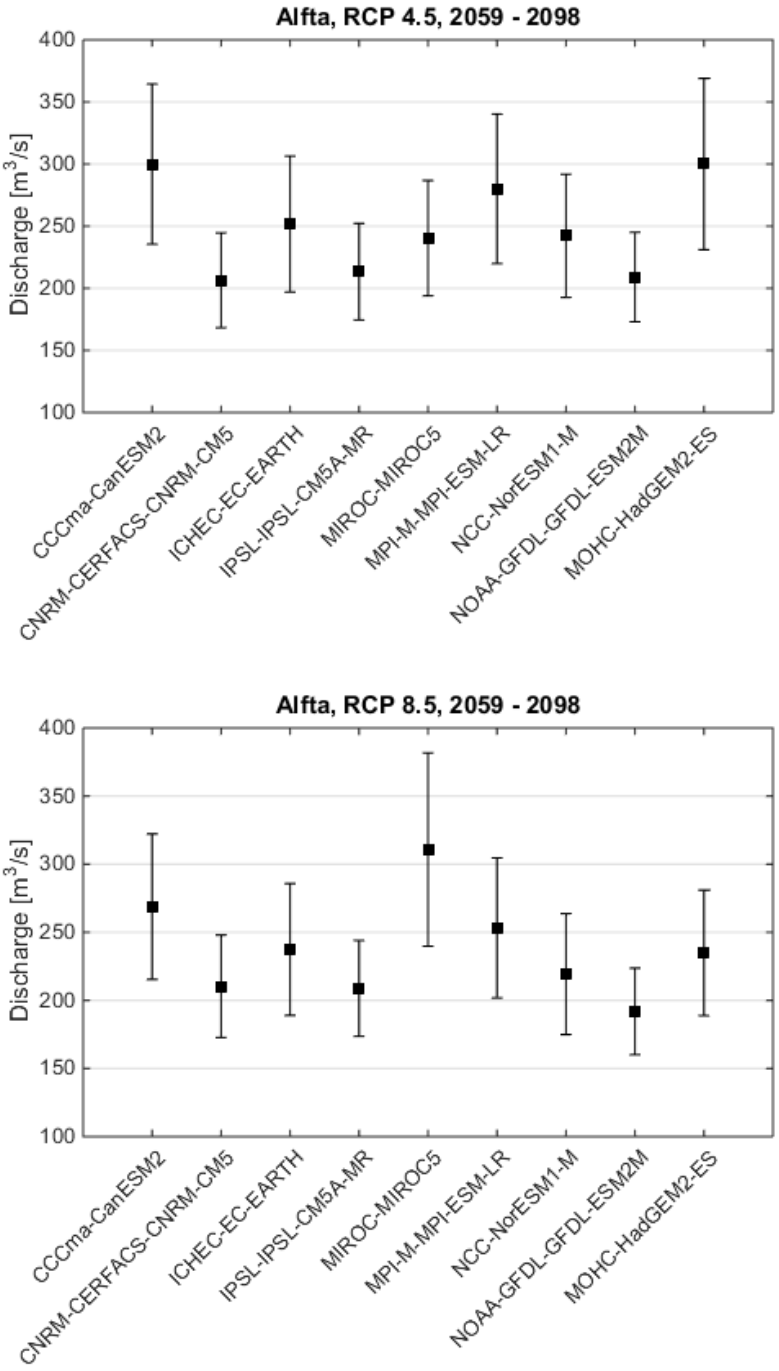

Fig. 22. Calculated 100-year flows for Alfta KRV with corresponding 95 % confidence intervals, for the individual global climate models.

Table 17. Roughness coefficient values from the manual "trial and error" calibrations, keeping within two different parameter ranges.

	Description	Calibration with parameter range 10-50	Calibration with parameter range 15-35
M1	Entire Viksjön (from Kalvnäs upstream of Viksjön to Alfta KRV), for calibration of cal.pt. 1.	20.7	20.7
M2	Located at cal.pt 2, for calibration of cal.pt 2.	38.7	35
M3	Located at cal.pt 3, for calibration of cal.pt.3.	50	35
M4	Located at cal.pt.4, for calibration of cal.pt.4. Also affects cal.pt. 5. The entire channel running from the energy plant is also given the value *M4*.	46	35
M5	Blocky part downstream of Österforsen dam and upstream of lake Ullungen. Showed to have a small influence on cal.pt. 5 (and 4).	25	25
M6	Located at Österforsen dam, for calibration of cal.pt.6.	20	20
M7	Located at Nybro, for calibration of cal.pt. 7	20	20

Table 18. Observed and simulated water levels from the manual calibration attempts.

i	Location calibration point	Measured water level [m]	Parameter range [10, 50]		Parameter range [15, 35]	
			Simulated water level [m]	$\lvert\varepsilon_i\rvert$ [m]	Simulated water level [m]	$\lvert\varepsilon_i\rvert$ [m]
1	Lake Viksjön	155.85	155.851	0.001	155.851	0.001
2	Ovanåker	156.45	156.451	0.001	156.451	0.001
3	Ovanåker	156.55	156.722	0.172	156.782	0.232
4	Ullungen (Edsbyn)	157.553	157.553	0.000	157.788	0.235
5	Bridge over stream Lillån (Edsbyn)	157.59	157.584	0.006	157.809	0.219
6	Gårdstjärn (Edsbyn)	166.993	166.994	0.001	166.994	0.001
7	Nybro	195	194.884	0.116	194.84	0.116
***RMSE* [m]**			0.078		0.156	

Table 19. Calibration attempts with GLUE calibration method, using the informal likelihood function RMSE.

Parameter range	Samples of parameter sets [#]	Acceptance criteria	Accepted parameter sets [#]	RMSE range for accepted parameter sets
[10, 50]	4000	$\left\|\varepsilon_i\right\|_{i=1\ldots7} < 0.5$	214	[0.12, 0.38]
		$\left\|\varepsilon_i\right\|_{i=1\ldots7} < 0.4$	87	[0.12, 0.31]
		$\left\|\varepsilon_i\right\|_{i=1\ldots7} < 0.3$	19	[0.12, 0.24]
		$\left\|\varepsilon_i\right\|_{i=1\ldots7} < 0.2$	0	-
[15, 35]	4000	$\left\|\varepsilon_i\right\|_{i=1\ldots7} < 0.5$	116	[0.24, 0.38]
		$\left\|\varepsilon_i\right\|_{i=1\ldots7} < 0.4$	10	[0.24, 0.29]
		$\left\|\varepsilon_i\right\|_{i=1\ldots7} < 0.3$	0	-

5.3. **Monte Carlo samples for the scenarios**

The number of simulations for each scenario was a result based on the frequency analysis and GLUE calibration (Table 20). Scenario A was run 1000 times with 1000 different discharge samples and ten different sets of roughness parameter values. Scenario B and Scenario C was run 900 times each, with the same roughness parameter sets as Scenario A and with 100 discharge samples from each of the nine GCMs.

Scenario I was run 1000 times for the same discharge samples as Scenario A, but keeping the roughness coefficient constant, according to the manually calibrated parameter set. Scenario II was run ten times for the accepted roughness parameter sets, keeping the discharge boundary conditions constant.

For Scenario A, 1000 random samples were drawn from the normal distributions (which had been fitted to the 95 % confidence intervals shown as blue arrows in Fig. 20). Histograms of the 1000 samples for Nybro and Alfta KRV respectively follows the shape of the sampling distributions well, staying within the 95 % confidence intervals (Fig. 27).

Discharge samples for Scenario B and Scenario C are 900 samples that come from the ensemble of GCMs (100 samples per GCM), resulting in positively skewed histograms (Fig. 28). The difference between the two GHG concentration scenarios is not particularly big, given the samples from the entire ensemble of GCMs.

The ten accepted parameter sets (Fig. 29) from the GLUE calibration was used an equal number of times in the Monte Carlo analysis. It can be seen again that *M1*, *M5* and *M6* have wide ranges of accepted *M* values, in some ways compensating for each other. A high value in *M5* and a low value in *M6* is an accepted combination in the same way that a low value in *M5* and a high value in *M6* is an accepted combination.

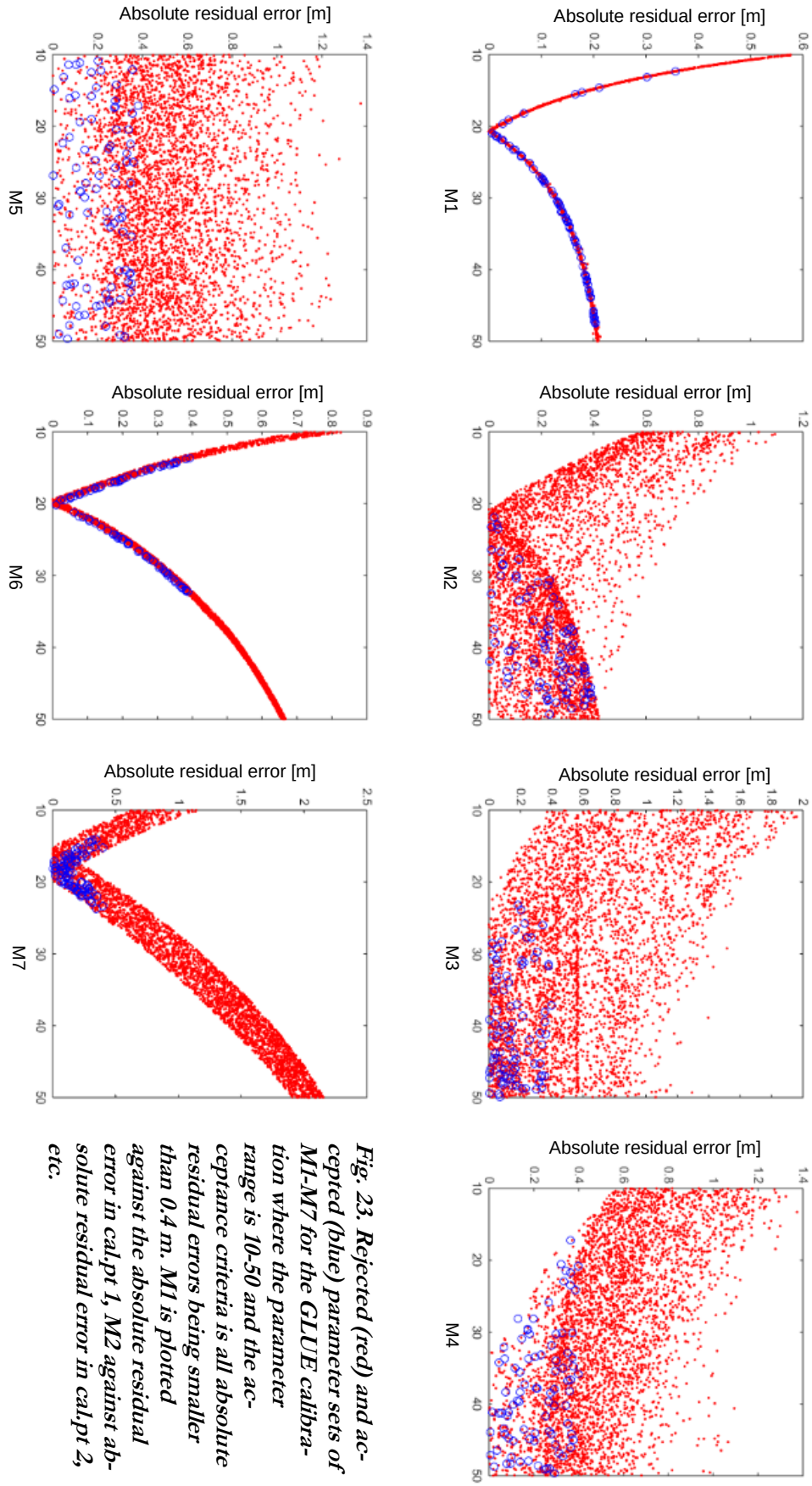

Fig. 23. Rejected (red) and accepted (blue) parameter sets of M1-M7 for the GLUE calibration where the parameter range is 10-50 and the acceptance criteria is all absolute residual errors being smaller than 0.4 m. M1 is plotted against the absolute residual error in cal.pt 1, M2 against absolute residual error in cal.pt 2, etc.

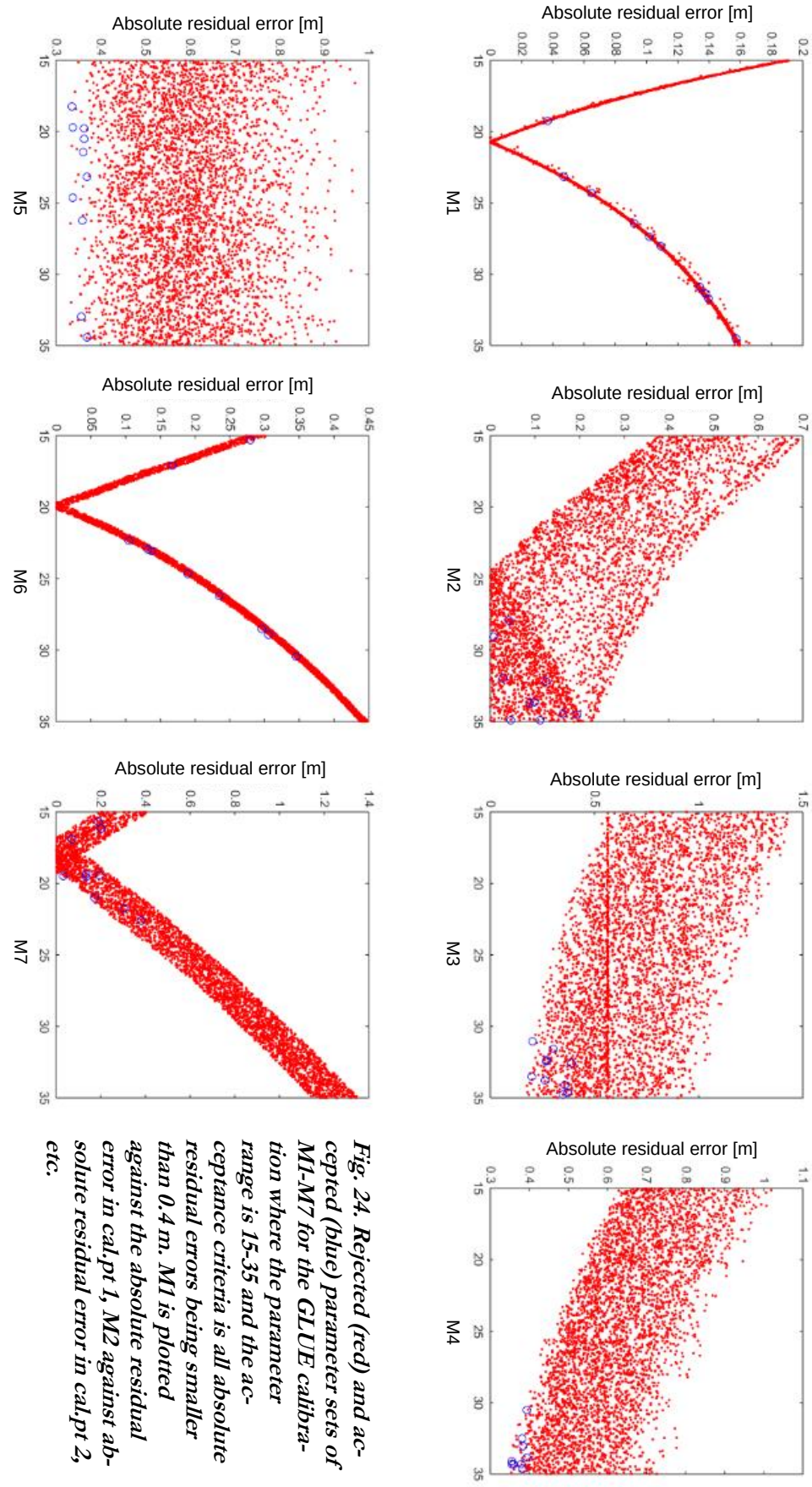

Fig. 24. Rejected (red) and accepted (blue) parameter sets of M1-M7 for the GLUE calibration where the parameter range is 15-35 and the acceptance criteria is all absolute residual errors being smaller than 0.4 m. M1 is plotted against the absolute residual error in cal.pt 1, M2 against absolute residual error in cal.pt 2, etc.

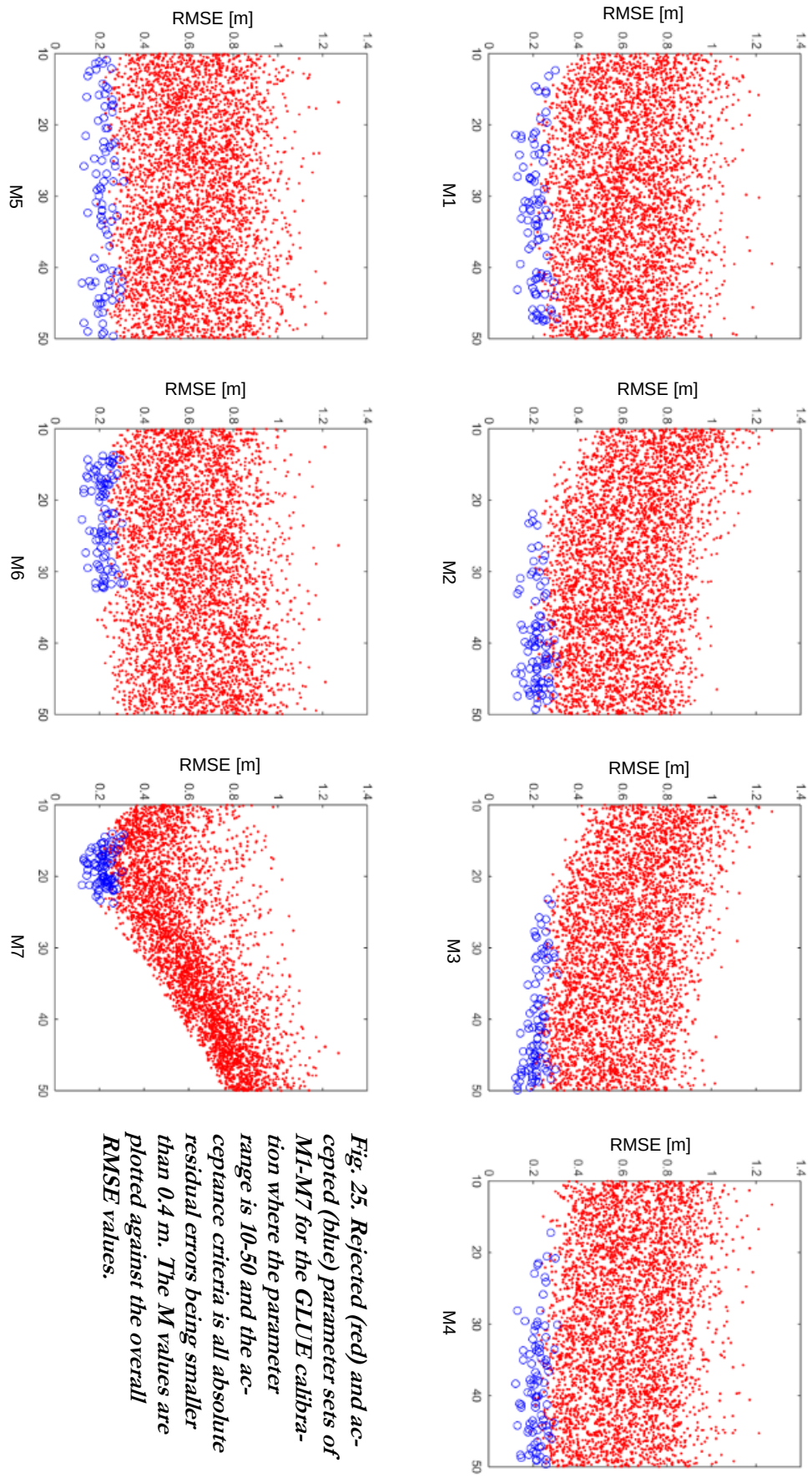

Fig. 25. Rejected (red) and accepted (blue) parameter sets of M1-M7 for the GLUE calibration where the parameter range is 10-50 and the acceptance criteria is all absolute residual errors being smaller than 0.4 m. The M values are plotted against the overall RMSE values.

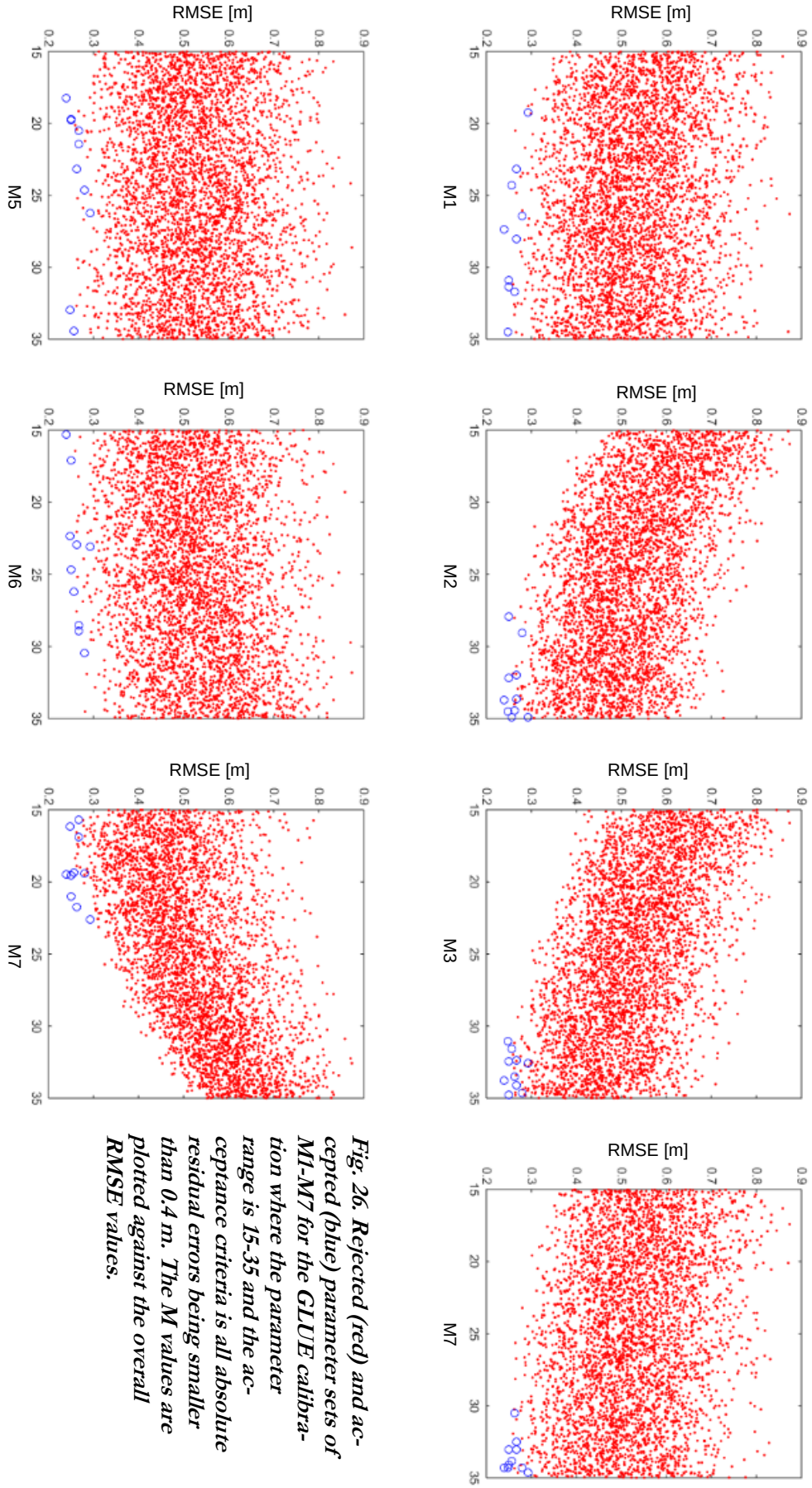

Fig. 26. Rejected (red) and accepted (blue) parameter sets of M1-M7 for the GLUE calibration where the parameter range is 15-35 and the acceptance criteria is all absolute residual errors being smaller than 0.4 m. The M values are plotted against the overall RMSE values.

Table 20. Overview of the five scenarios used in the Monte Carlo analyses after estimations of uncertainty quantifications had been conducted.

	Discharge	Roughness coefficient
Scenario A (present climate)	Varied. 1000 samples.	Varied. 10 samples from GLUE cal. with *M* 15-35.
Scenario B (RCP 4.5)	Varied. 900 samples (100 per GCM).	Varied. 10 samples from GLUE cal. with *M* 15-35.
Scenario C (RCP 8.5)	Varied. 900 samples (100 per GCM).	Varied. 10 samples from GLUE cal. with *M* 15-35.
Scenario I	Varied. 1000 samples (same as Scenario A)	Constant. From manual cal. with *M* 15-35.
Scenario II	Constant. 261 m^3/s for Nybro and 323 m^3/s for Alfta KRV, which were the Q100 values according to MSB (2013).	Varied. 10 samples from GLUE cal. with *M* 15-35.

5.4. Simulated water levels and probabilistic maps

The histograms for simulated water levels varies in shape between different cross-sections and scenarios (Fig. 30, Fig. 31). For Scenario A are the simulated water levels colour coded according to the roughness coefficient parameter set used in the simulation, and for Scenario B and Scenario C are the GCMs colour coded. The bias of the different GCMs can be seen in the tendency to result in high or low water levels. The difference between the roughness parameter sets, seen in the graphs for Scenario A, give a smaller variation of simulated water levels than the different GCMs.

Large parts of the probabilistic flood inundation maps for Scenario A, Scenario B and Scenario C can be found in Appendix II. Scenario A and Scenario I give quite similar water levels and flood maps, since the variation of the roughness coefficient was found to be small in comparison to the relative contribution from the discharge uncertainty (Fig. 32). Hence, the uncertainty zone for Scenario II is small.

The resulting water level histograms and probability maps from Scenario B and Scenario C are fairly alike, since it is the results from the whole ensemble of GCMs (Fig. 32). The sizes of their horizontal flood extents are approximately the same as for the other scenarios, but with wider uncertainty zones due to greater ranges of simulated water levels.

Overall, Scenario C gives the largest water level variance between its simulations, closely followed by Scenario B (Table 21). Scenario II gives the least variance between its ten simulations. The variability in Scenario A almost corresponds to the individual variances in Scenario I and Scenario II.

Table 21. Differences between maximum and minimum water level for the cross-sections.

	Mean difference between each cross-section's max. and min. water level for all simulations [m]	Maximum difference between each cross-section's max. and min. water level for all simulations [m]
Scenario A	1.25	2.03
Scenario B	1.81	2.59
Scenario C	1.88	2.76
Scenario I	0.92	1.34
Scenario II	0.48	1.35

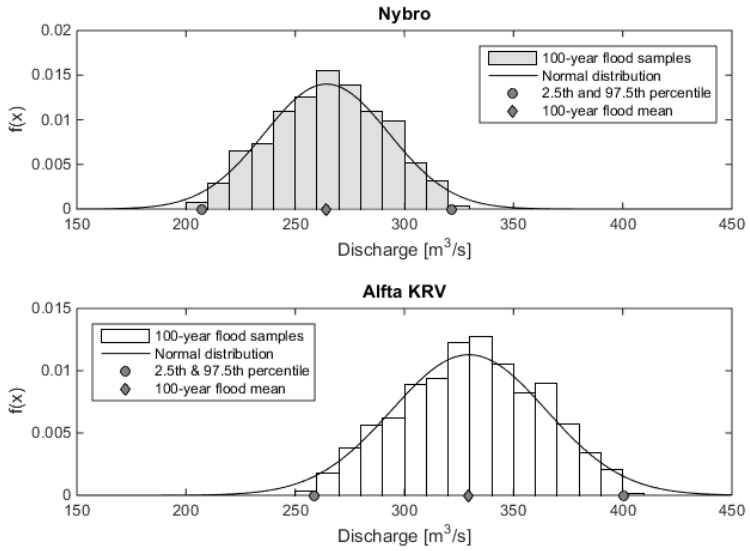

Fig. 27. Streamflow discharge inputs to Scenario A based on frequency analysis of historic measurements.

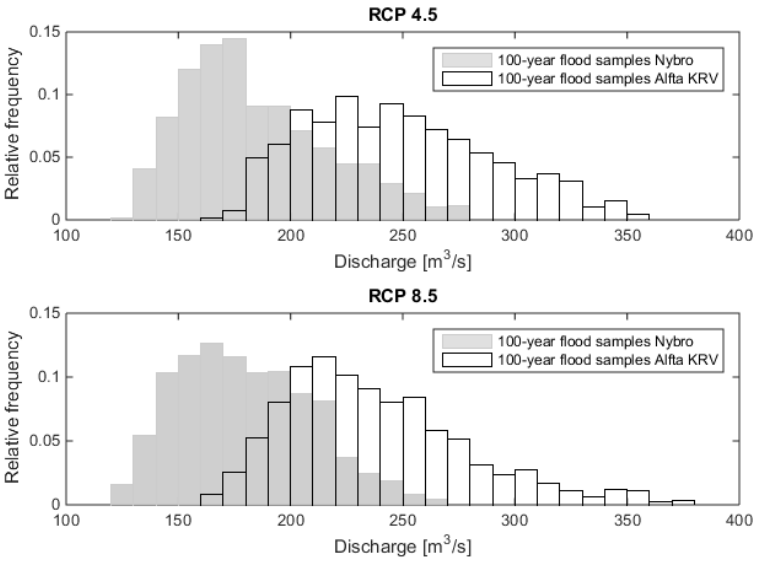

Fig. 28. Streamflow discharge inputs to future climate Scenario B (RCP 4.5) and Scenario C (RCP 8.5).

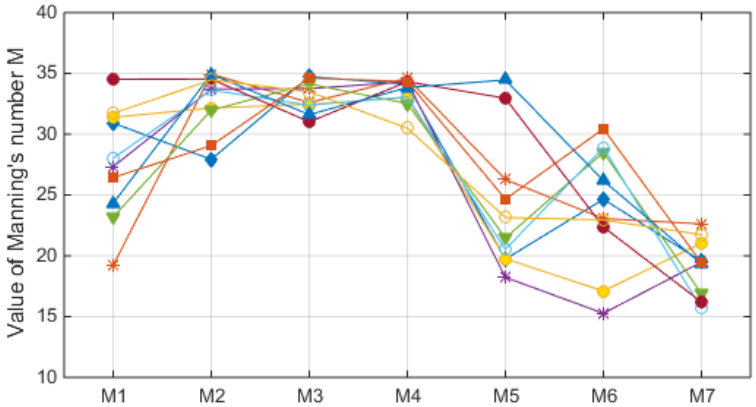

Fig. 29. Roughness coefficient values for the ten accepted models (parameter sets) used in all scenarios except Scenario I.

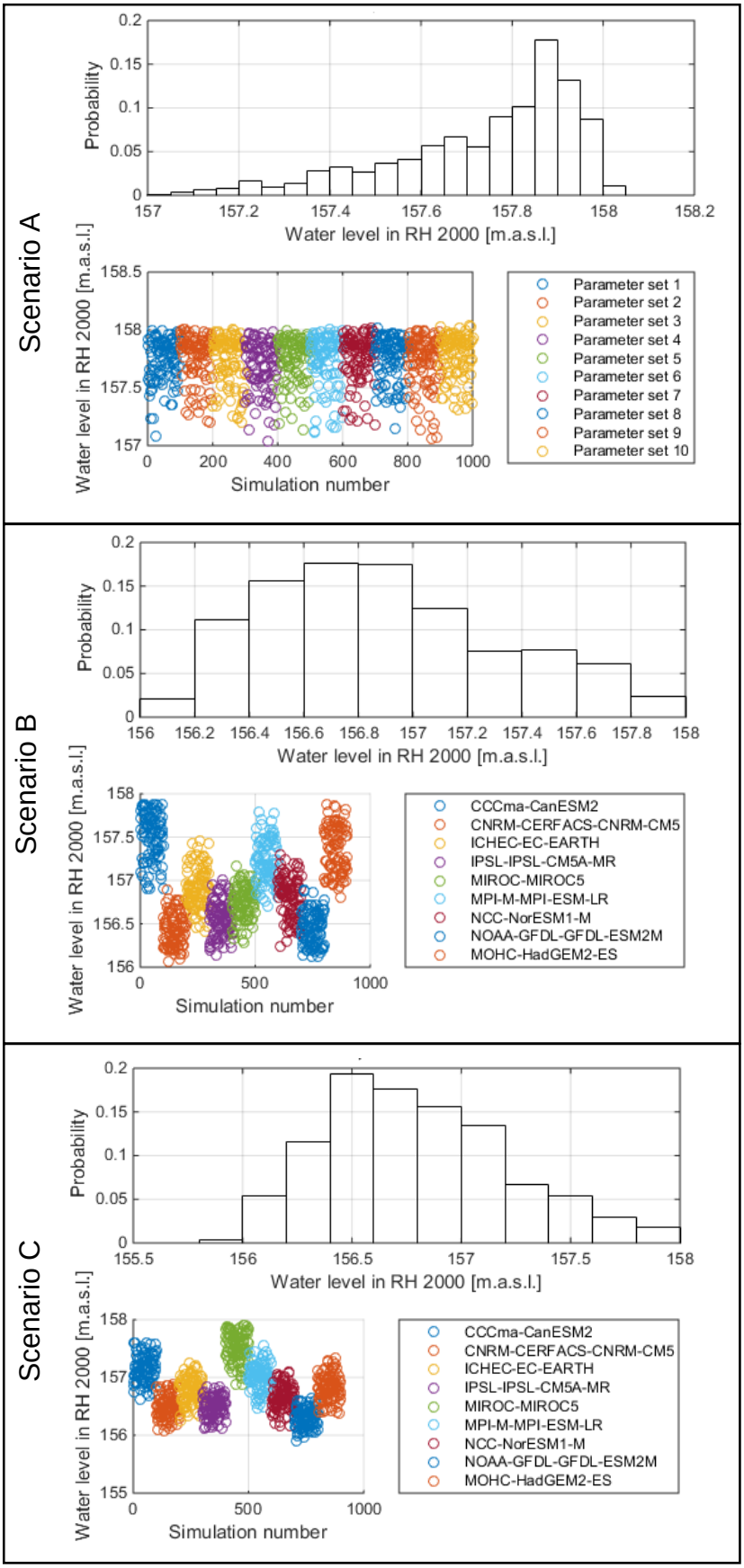

Fig. 30. Simulated water levels for Edsbyn at lake Ullungen. The water levels in Scenario A are colour coded according to the roughness coefficient parameter sets whereas Scenario B and Scenario C are colour coded according to the GCMs.

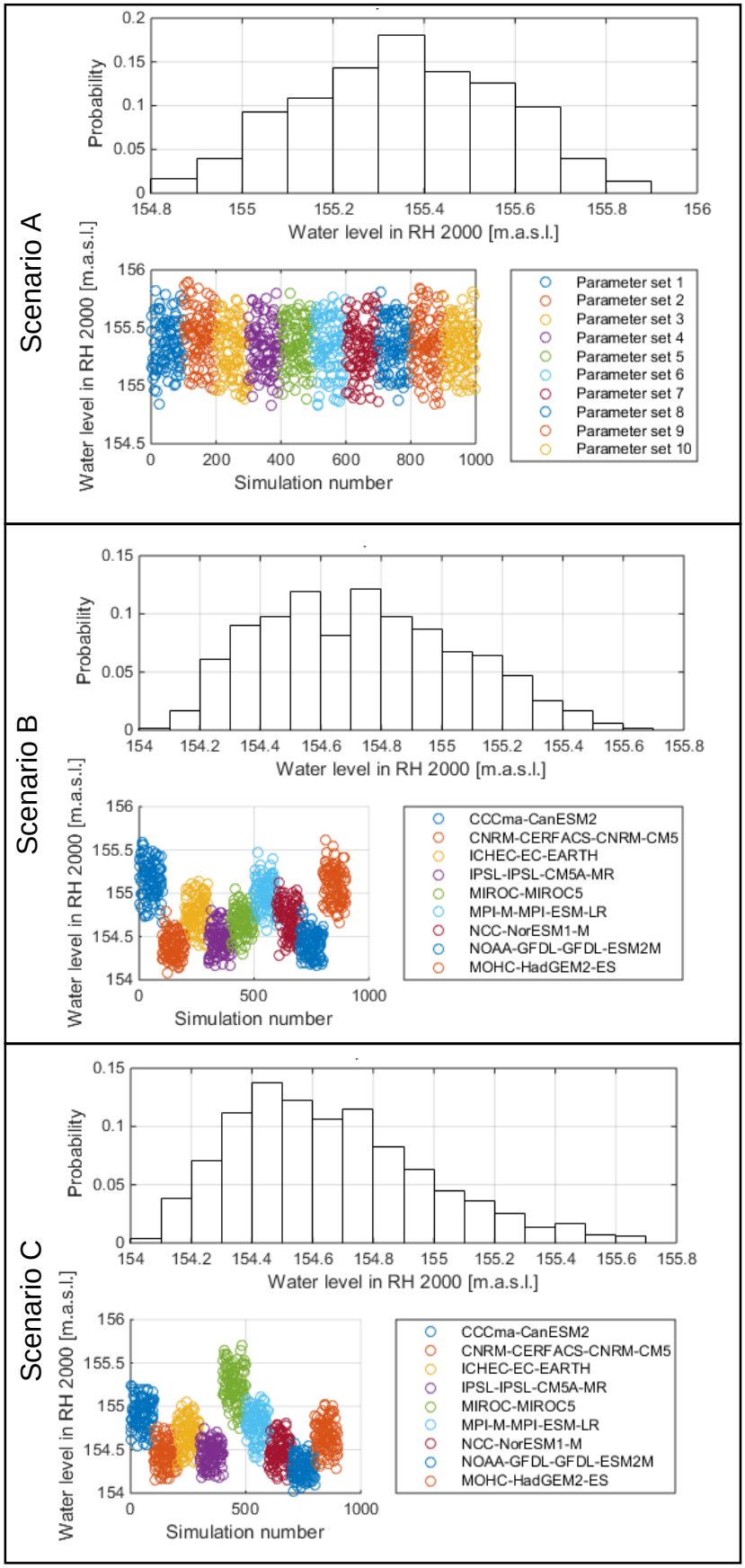

Fig. 31. Simulated water levels for Alfta KRV, upstream of the power plant. The water levels in Scenario A are colour coded according to the roughness coefficient parameter sets whereas Scenario B and Scenario C are colour coded according to the GCMs.

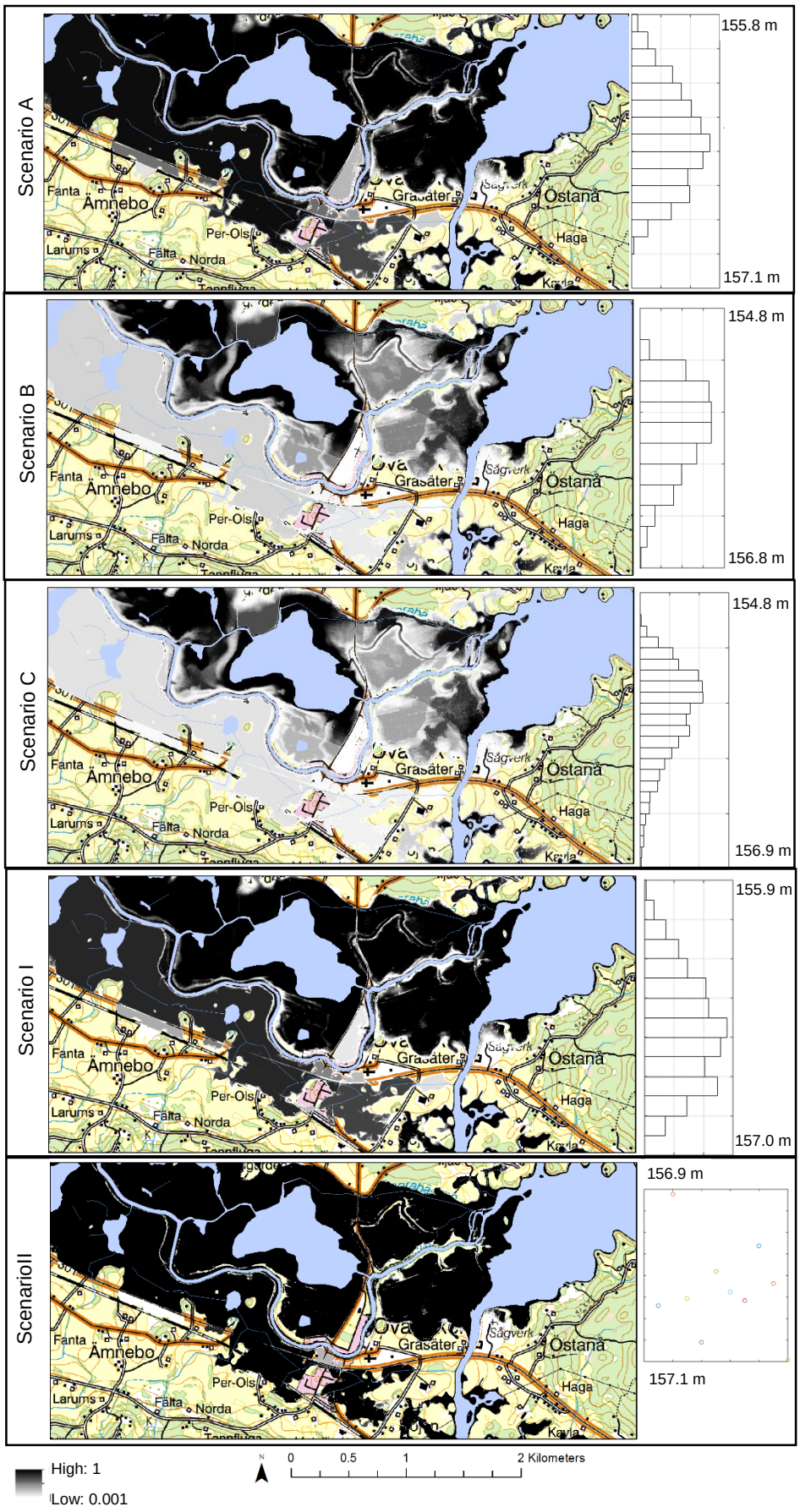

Fig. 32. Probabilistic flood inundation maps of Häxmyrtjärn in Ovanåker. The histograms show the distribution of the simulated water levels, between the maximum and minimum simulated water level.

6. DISCUSSION

The following chapter discusses selected aspects of the methodology and results. The discussion is divided into six main parts.

6.1. Frequency analysis

As the literature review had given a hint of, the results show that the statistical uncertainties related to the frequency analysis are significant. The choice of probability distribution function alone showed to give a large contribution to the overall uncertainty, where the Log-Pearson Type III function differed from the Gumbel and lognormal types (e.g. compare 314 m^3/s with 264 m^3/s for the 100-year flood in Nybro). This uncertainty seemed especially challenging to handle since different literature sources give different recommendations and methods. Furthermore, the confidence interval calculations are performed in various ways for different distribution functions.

Nonetheless, performing a frequency analysis where observations are adjusted to an ensemble of distribution functions can be a means of its own, even if the choice of distribution function is always more or less subjective. Then it has at least been made explicit that there exists large uncertainties around the magnitude of a 100-year flood, which otherwise commonly is represented by one specific number in deterministic flood mappings.

The conducted method of performing frequency analysis and sampling random values from an ensemble of climate projections from different GCMs is suggested to be a central result of this study. The choice of this method came from the aim of performing the frequency analysis as stringent as possible between the present climate and future climate scenarios. The method also allowed for keeping the GHG concentration scenarios and the relative contributions from the different GCMs separate throughout the entire process. The results could thus be presented both as ensembles (like the probabilistic maps and histograms in Fig. 32) as well as kept separate (like the colour coded plots in Fig. 30 and Fig. 31).

6.2. Calibration results

The calibration showed that a manual calibration according to "trial and error" gave a lower RSME than any of the runs from the GLUE method gave (Table 18, Table 19). This indicates that the GLUE calibration could have benefited from additional runs. Nonetheless, the 4000 GLUE calibration runs gave several parameter sets that can be argued to all represent the system in an acceptable manner and is therefore valued to make up a valid uncertainty estimate of the roughness coefficient parameter.

The dotty plots (Fig. 23, Fig. 24) from the GLUE calibrations proved to be a clear visualisation of how the water levels in the calibration points varied with changing the corresponding *M* value. The plots showed that for some points it can be valuable to spend time on searching for an optimum value, as manual "trial and error" calibration often do, while this seemed to be impractical for other calibration points.

Model set-up and local conditions seem to determine whether or not there seems to be an "optimum" *M* value for the individual points. The model structure and local conditions also determine how the individual *M* values affect the overall RMSE, also clearly visualised in dotty plots (Fig. 25, Fig. 26). The GLUE calibration is, once set up, automatized and can save manual work time.

It should be stressed that the choice of acceptance criterion of all absolute residual errors being smaller than 0.4 meters was subjective, as the literature review suggested it often is. The choice was mainly based on wanting

to use the same acceptance criterion as MSB had done for the model previously, to visualize how large uncertainties that particular choice would yield. However, a choice according to a LOA approach could be argued to be more "objective". A LOA approach would perhaps lead to using different acceptance criteria for different calibration points, based on the estimated accuracy of the calibration data. Inclusion of the uncertainty of the calibration discharge magnitude could also be included when choosing suitable acceptance criteria.

6.3. Simulation results

6.3.1. *Discharge uncertainty and roughness coefficient uncertainty*

The scenarios that include the discharge uncertainty all give significantly larger water level variability than Scenario II where only the roughness coefficient uncertainty is included (Table 21). This was expected, based on the different methods of estimating the two different uncertainties. The accepted roughness coefficient values were selected by choosing the parameter sets giving accepted water levels, why it can be considered likely that this estimate would yield a smaller variation of simulated water levels than the discharge uncertainty. The discharge uncertainty estimate was based on statistical analysis in the frequency analysis, independent from the simulated water levels.

The acceptance criterion, all residual errors being smaller than 0.4 meters for the calibration points, still resulted in a maximum variability of 1.35 meters for one of the cross-sections (Table 21). This is found to be an interesting reminder of the fact that intermediate water levels will still be in the risk of being over- or underestimated, even though the water levels in the calibration points give a considerably smaller variation. This would not have been possible to show with the manual calibration alone, and could be important to point out when presenting the expected accuracy of a performed calibration.

Furthermore, the simulations show that the relative contributions between the discharge variable (shown in Scenario I) and the roughness coefficient variable (shown in Scenario II) are almost additive when combined in Scenario A (Table 21), in contrast to compensating for each other. This method of comparing the individual uncertainty of different variables with their combined uncertainty could especially be rewarding in a study where additional uncertainties were included in the Monte Carlo analysis, whose interaction with each other was not well understood beforehand.

6.3.2. *Climate change uncertainty*

The simulation results visualize (Fig. 30, Fig. 31) what the frequency analysis also show (Fig. 21, Fig. 22), regarding the relative importance for the overall uncertainty of the GHG concentration scenario and the GCM choice. The GHG concentration scenario shows to play a crucial role for how some of the individual GCMs projected the 100-year flood at the end of the century. One GCM goes from a relatively high to a relatively low 100-year flood magnitude from RCP 4.5 to RCP 8.5, while another GCM does the opposite. This difference clearly shows the model uncertainty in climate change projections, how some models react to a certain climate signal in different ways.

Looking at the entire ensemble of GCMs, the choice of GHG concentration scenario plays a smaller role on the overall uncertainty, due to the GCMs different ways of respond and therefore compensating for each other. RCP 8.5 in Scenario C gives a slightly larger variability between the simulations than RCP 4.5 in Scenario B (Table 21) and therefore also a

generally larger uncertainty zone in the probabilistic flood inundation maps. This was also expected, since the literature review indicated that a stronger climate signal generally increases the importance of the spread from different GCMs.

The large variability between the GCMs (see e.g. the colour coded plots for Scenario B and Scenario C in Fig. 30 and Fig. 31) confirms how important it is to use projections from several models in climate change studies, due to their different bias and since none of the models can be said to be better than the other in representing the entire climate system. However, it is also the usage of ensemble projections that diminished the importance of the GHG concentration scenario choice, since the GCMs compensated for each other in this particular case study.

In Gävleborg County, the magnitude of a 100-year flood is expected to stay the same of even decrease at the end of the century (Table 15). As mentioned, the horizontal flood extent of the probabilistic maps is quite similar between the present climate and future climate, but with larger uncertainty zones for the future climate scenarios (Fig. 32). This is suggested to be a relevant information to physical planners, to avoid misinformed decisions being taken. This method of comparison would presumably even be more crucial for physical planners and decision makers in areas where the magnitude of the 100-year flood is expected to increase at the end of the century.

6.4. Methodology

The aim with this report has been to explain the methodology clear enough to be repeatable. The method of fitting a normal distribution to a confidence interval from which random discharge samples are drawn has been made in flood uncertainty studies before (e.g. Beven et al. (2011)). The performed method of handling the RCP scenarios and the ensemble of climate change projection series in frequency analysis was however not obvious prior to this work, why this particular method is suggested to be a relevant contribution on its own.

Quite some effort in this study was put into giving an account for important uncertainties behind the process of creating flood inundation maps and suitable uncertainty assessment methods available. Furthermore, the technical aspect of performing Monte Carlo simulations with MIKE 11 and integrating the results in ArcMap to produce the probabilistic maps was also a fundamental part of the endeavour. Once set up, this type of assessment is in many stages automatized, so repeating the procedure would not be nearly as time-demanding.

Performing this Monte Carlo analysis on a MIKE 11 model requires a bit of programming knowledge to implement. If a more user-friendly integrated software was to be built, it would ease the work process and hence also possibly making these type of uncertainty assessments more common. It could possibly also make the uncertainty assessment process more transparent, which could be beneficial when communicating the method and results to planners and decision makers.

The focus in this case study have been fluvial floods, but the method could be used for other types of floods as well. Additional uncertainties could also be included in this type of uncertainty assessment.

Worth mentioning is that all climate change projections in this study were based on the same RCM and hydrological model, meaning that the influence of these particular models and how they interact with the GCMs have not been investigated here. The uncertainties introduced by the methodological choices in this study has not been investigated either, for example

how the interpolation methods in GIS affect the resulting flood inundation maps.

6.5. Contribution of the uncertainty assessment

Even though uncertainty assessment can sometimes seem like an overwhelming task due to the relatively complex nature of uncertainties, it should be stressed that it is an important part of modelling. This is especially true for models used for decision making, to avoid misinformed decisions based on results that give the impression of being more certain than they really are.

How to use uncertainties in decision making have been excluded from the scope of this project. Worth noting is that decision makers can use the probabilistic maps just like the deterministic maps when making decisions if they wish. For example, they can choose to follow the 50th percentile of flood extent for most locations. If an area is particularly high-risk, a higher percentile can be chosen instead.

Probabilistic flood inundation maps have been argued to be a more fair representation of the subject than deterministic maps. They visualise how chosen uncertainties propagate through the flood inundation model in an effective way. Furthermore, they enable the possibility of including an ensemble of climate change projections, which has been shown to be important for climate change studies.

Even though it will never be possible to perform a completely objective and comprehensive uncertainty assessment, it should not be a reason for not performing these types of assessments at all. It should however be emphasized how important it becomes to make all assumptions available for the decision makers as well, since the uncertainty assessments at best can be conditional on these.

Making decisions based on probabilistic uncertainty assessments also require that it should be clear for the decision maker what the probabilities are showing. For example, the probabilities in the probabilistic flood inundation maps from Scenario B are in no way claiming to represent the probability of RCP 4.5 to be realised. The probabilities in the maps are only representing the outcome from these particular simulations. This is also important to communicate if probabilistic maps were to be published for the public.

In physical planning, it is common to use the simulated water level at the specific cross-section when making decisions. For this purpose, the histograms of the simulated water levels for the scenarios can be used (Fig. 30, Fig. 31, Fig. 32).

6.6. Suggestions on future work

From a long-term and general point of view, continuing to give examples of how to assess uncertainties in flood inundation studies is judged to be beneficial since it contributes to setting a "code of practice" on both how to methodologically perform the assessments, and also how to acknowledge uncertainties in decision making.

Regarding MIKE 11, it is suggested to be relevant to investigate how to vary the geometrical description (e.g. configuration of cross-sections) in a Monte Carlo analysis. The geometrical description was suggested to play a significant part for the overall uncertainty for one-dimensional models from the literature review, but was excluded in this study. Other uncertainties, like rating-curve uncertainty and dam failure events could also be further included in this type of Monte Carlo assessment.

Further developments of the software, making the process of conducting this type of Monte Carlo analysis with MIKE 11 easier and more user-friendly, would together with more examples on how to assess and handle uncertainties be useful steps in the direction towards turning probabilistic flood inundation maps to tradition rather than being an exception.

7. CONCLUSIONS

This thesis gives an account for the many uncertainties behind one-dimensional hydraulic models and flood inundation maps, as well as suitable uncertainty assessment methods for different types of uncertainties. The different types of uncertainties included in the case study of the flood inundation model of the river Voxnan could be assessed by combining a GLUE calibration, Monte Carlo analysis and scenario analysis.

As expected, significant uncertainties regarding the magnitude of a 100-year flood from frequency analysis was found. The largest contribution to the overall uncertainty is given by the variance between the nine global climate models, emphasizing the importance of taking ensemble of projections into account in climate change studies.

The choice of greenhouse gas concentration scenario plays a significant role for how some of the individual global climate models projects the streamflow in Voxnan at the end of the century. Seen on the entire ensemble of global climate models, the importance of choice of greenhouse gas concentration scenario is marginal since the models compensate for each other's differences.

The spatially varying roughness coefficient in the hydraulic model gives a smaller contribution to the overall uncertainty compared to the discharge uncertainty. The GLUE calibration method gave several roughness coefficient parameter sets that can all be argued to represent the system in an acceptable manner. These parameter sets yield water level variations of over three times the acceptance criterion of residual errors in the calibration points.

Furthermore, the study gives an example on how to present uncertainties visually in probabilistic flood inundation maps, from MIKE 11, MATLAB and ArcMap. The conducted method of how to handle climate change scenario and model uncertainties in frequency analysis is also suggested to be a relevant result of the study.

Presenting flood inundation maps as probabilistic rather than deterministic is judged to be a more representative way, due to the many inherent uncertainties prevailing the maps. Important is however that the assumptions and potentially subjective decisions behind the uncertainty assessment are stated explicitly, for preventing further uncertainty contributions to an already uncertain-filled process.

REFERENCES

Apel, H., Merz, B., Thieken, A. H. 2008. Quantification of uncertainties in flood risk assessments. *International Journal of River Basin Management* **6**: 149-162.

Apel, H., Thieken, A., Merz, B., Blöschl, G. 2006. A Probabilistic Modelling System for Assessing Flood Risks. *Natural Hazards* **38**: 79-100.

Apel, H., Thieken, A. H., Merz, B., Blöschl, G. 2004. Flood risk assessment and associated uncertainty. *Natural Hazards and Earth System Sciences* **4**: 295-308.

Asselman, N. 2009. Flood Inundation Modelling – Model Choice and Proper Application. *FLOODsite*. WL Delft Hydraulics. 142 p.

Bedient, P. B. 2008. Hydrology and floodplain analysis, Harlow, Prentice Hall. 795 p.

Bergström, S. 1994. Sveriges hydrologi: grundläggande hydrologiska förhållanden, Norrköping: Sveriges meteorologiska och hydrologiska institut SMHI; Uppsala: Svenska hydrologiska rådet. 138 p.

Beven, K. J. 2006. A manifesto for the equifinality thesis. *Journal of Hydrology* **320**: 18-36.

Beven, K. J., Binley, A. 1992. The future of distributed models: Model calibration and uncertainty prediction. *Hydrological Processes* **6**: 279-298.

Beven, K. J., Leedal, D., McCarthy, S. 2011. Framework for Assessing Uncertainty in Fluvial Flood Risk Mapping. *FRMRC Research Report SWP1.7*. 73 p.

Beven, K. 2008. Environmental Modelling: An Uncertain Future?, Independence, KY, USA, CRC Press. 328 p.

Bezak, N., Brilly, M., Sraj, M. 2013. Comparison between the peaks-over-threshold method and the annual maximum method for flood frequency analysis. *Hydrological Sciences Journal* **59**: 959-977.

Brandt, S. A. 2009. Betydelse av höjdmodellers kvalitet vid endimensionell översvämningsmodellering. Gävle: Högskolan i Gävle. 38 p.

Capela Lourenço, T., Rovisco, A., Groot, A., Nilsson, C., Füssel, H.-M., Van Bree, L., Street, R. B. 2014. Adapting to an Uncertain Climate: Lessons From Practice, Cham, Springer International Publishing: Cham. 182 p.

Chow, V. T. 1959. Open-channel hydraulics, Tokyo: McGraw-Hill. 680 p.

Chow, V. T. 1988. Applied hydrology, New York: McGraw-Hill. 572 p.

Dahmen, E. R., Hall, M. J. 1990. Screening of hydrological data: tests for stationarity and relative consistency. Wageningen, The Netherlands: International Institute for Land Reclamation and Improvement. 63 p.

DHI 2014a. MIKE 11 A Modelling System for Rivers and Channels Reference Manual. 524 p.

DHI 2014b. MIKE 11 A Modelling System for Rivers and Channels User Guide. 430 p.

DHI 2014c. MIKE Zero 2014. Hørsholm, Denmark: DHI.

DHI SVERIGE AB 2015. Personal communication through e-mail, 2015-04-10.

Di Baldassarre, G., Schumann, G., Bates, P. D., Freer, J. E., Beven, K. J. 2010, Flood-plain mapping: a critical discussion of deterministic and probabilistic approaches. *Hydrological Sciences Journal* **55**: 364-376.

EC. 2007. Directive 2007/60/EC of the European Parliament and of the Council of 23 October 2007 on the assessment and management of flood risks (Text with EEA relevance). *Official Journal of the European Union* **288**: 27–34.

EC. 2015. Flood Risk Management [Online]. Available: http://ec.europa.eu/environment/water/flood_risk/ [Accessed 26 May 2015].

EEA 2010a. The European Environment State and Outlook 2010 Water Resources: Quantity and Flows. *State of the environment report No 1/2010*. Luxembourg: Publications Office of the European Union. 32 p.

EEA 2010b. Mapping the impacts of natural hazards and technological accidents in Europe An overview of the last decade. *EEA Technical Report*. Luxembourg: Publications Office of the European Union. 144 p.

ESRI 2012. ArcMap 10.1. Redlands, California: ESRI.

Hall, J. 2008. Development of framework for the influence and impact of uncertainty. *FLOODsite*. University of Newcastle. 150 p.

Hall, J., Solomatine, D. 2008. A framework for uncertainty analysis in flood risk management decisions. *International Journal of River Basin Management* **6**: 85-98.

Harlin, J. 1992. Hydrological modelling of extreme floods in Sweden. Stockholm: Kungliga Tekniska Högskolan. 304 p.

IPCC 2013. Climate Change 2013: The Physical Science Basis. Contribution of Working Group I to the Fifth Assessment Report of the Intergovernmental Panel on Climate Change. Cambridge, United Kingdom and New York, NY, USA: Cambridge University Press. 1535 p.

Jha, A. K., Bloch, R., Lamond, J., 2012. Cities and Flooding: A Guide to Integrated Urban Flood Risk Management for the 21st Century, Herndon, VA, USA, World Bank Publications. 631 p.

Juston, J. M. 2012. Environmental Modelling: Learning from Uncertainty. Stockholm: KTH Royal Institute of Technology. 36 p.

Länsstyrelsen Gävleborg 1990. Voxnans Naturvårdsområde [Online]. Available: http://www.lansstyrelsen.se/gavleborg/SiteCollectionDocuments/Sv/djur-och-natur/skyddad-natur/naturreservat/ljusdal/Voxnan/beslut-voxnan-hylstrommen.pdf [Accessed 16 June 2015].

Lantmäteriet 2009. GSD-Elevation data, grid 2+.

Lantmäteriet 2015. Product description: GSD-Elevation data, Grid 2+. 12 p.

Liu, Y., Freer, J., Beven, K. J., Matgen, P. 2009. Towards a limits of acceptability approach to the calibration of hydrological models: Extending observation error. *Journal of Hydrology* **367**: 93-103.

Maidment, D. R. 1993. Handbook of hydrology, New York, NY, USA: McGraw-Hill. 1424 p.

Merwade, V., Olivera, F., Arabi, M., Edleman, S. 2008. Uncertainty in Flood Inundation Mapping: Current Issues and Future Directions. *Journal of Hydrologic Engineering* **13**: 608-620.

Merz, B., Thieken, A. H. 2005. Separating natural and epistemic uncertainty in flood frequency analysis. *Journal of Hydrology* **309**: 114-132.

MSB 2011. Identifiering av områden med betydande översvämningsrisk. MSB diarienr 2011-2996. 109 p.

MSB 2013. Översvämningskartering utmed Voxnan. MSB diarienr 2013-3000. 62 p.

MSB. 2014a. Översvämningskartering [Online]. Available: https://www.msb.se/sv/Forebyggande/Naturolyckor/Oversvamning/Oversiktlig-oversvamningskartering/ [Accessed 1 June 2015].

MSB. 2014b. Vägledning för översvämningskartering av vattendrag Fakta, inspirerande exempel och tips för en bra beställning. MSB publ.nr. MSB631. 43 p.

Ovanåkers Kommun 2014. Översvämningsportalen [Online]. Available: http://www.ovanaker.se/puffar/oversvamningsportalen.5.3538b25513d860958fa460.html [Accessed 16 June 2015].

Ovanåkers Kommun 2015. Personal communication through e-mail, 2015-04-21.

Pappenberger, F., Beven, K. J., Horritt, M., Blazkova, S. 2005. Uncertainty in the calibration of effective roughness parameters in HEC-RAS using inundation and downstream level observations. *Journal of Hydrology* **302**: 46-69.

Persson, G., Strandberg, G., Berg, P. 2015. Vägledning för användande av klimatscenarier. SMHI Klimatologi Nr 11. Norrköping: SMHI. 61 p.

Räddningsverket 1999. Översiktlig översvämningskartering längs Voxnan. SRD diarienr KD-11137-1-0. 11 p.

SFS 2009. Förordning (2009:956) om översvämningsrisker. SFS nr: SFS nr: 2009:956.

SGI 2010. Gävleborgs län. Översiktlig regional klimat- och sårbarhetsanalys - naturolyckor. SGI diarienr 2-0906-0452. 80 p.

Shrestha, S., Anal, A. K., Salam, P. A., Van Der Valk, M. 2015. Managing Water Resources under Climate Uncertainty: Examples from Asia, Europe, Latin America, and Australia, Cham, Springer International Publishing, Cham. 122 p.

Sjökvist, E., Axén Mårtensson, J., Dahné, J., Köplin, N., Björck, E., Nylén, L., Berglöv, G., Tengdelius Brunell, J., Nordborg, D., Hallberg, K., Södling, J., Berggreen Clausen, S. 2015. Klimatscenarier för Sverige - Bearbetning av RCP-scenarier för meteorologiska och hydrologiska effektstudier. SMHI diarienr 2014/1904/2.4. 36 p.

Smemoe, C. M., Nelson, E. J., Zundel, A. K., Miller, A. W. 2007. Demonstrating Floodplain Uncertainty Using Flood Probability Maps. *Journal of the American Water Resources Association* **43**: 359-371.

SMHI. 2015. Vattenwebb [Online]. Available: http://vattenwebb.smhi.se/ [Accessed 1 April 2015].

Svensk Energi, Svenska Kraftnät, SveMin 2007. Riktlinjer för bestämning av dimensionerande flöden för dammanläggningar - Nyutgåva 2007. 34 p.

The Mathworks 2014. MATLAB R2014b. United States: MathWorks.

Thurin, S. 2011. Översvämningsrisker längs Funboån. Uppsala: Uppsala Universitet. 59 p.

van der Linden, P., Mitchell, J. F. B. E. 2009. ENSEMBLES: Climate Change and its Impacts: Summary of research and results from the ENSEMBLES project. Met Office Hadley Centre, FitzRoy Road, Exeter EX1 3PB, UK. 160 p.

van Vuuren, D., Edmonds, J., Kainuma, M., Riahi, K., Thomson, A., Hibbard, K., Huritt, G., Kram, T., Krey, V., Lamarque, J. F., Masui, T.,

Meinshausen, M., Nakicenovic, N., Smith, S., Rose, S. 2011. The representative concentration pathways: an overview. *Climatic Change* **109**: 5-31.

Vattenregleringsföretagen 2003. Schematisk bild av Ljusnan [Online]. Available: http://www.ljusnanriver.se/Sch_kartor/LSVF%20schematiska%202003-03-27%20m%20info.pdf [Accessed 16 June 2015].

APPENDIX I – RESULTS DELIVERED IN DIGITAL FORMAT

The results are delivered in digital format in both maps and water levels.

Excel, MATLAB and image files, giving data on the simulation results for all cross-sections

File name	Description
Waterlevels.xls	Excel tables with all simulated water levels.
View_waterlevels.m	MATLAB program for visualising the simulated water levels for a chosen cross-section.
CS_numbers.png	Map of the unique cross-section IDs

ArcGIS shape files. The coordinate system in plane is SWEREF 99 and the height system is RH 2000

File name	Description
Netw	River network
CS_ScI	Cross-sections with water levels for Scenario I.
CS_ScII	Cross-sections with water levels for Scenario II.
CS_ScA	Cross-sections with water levels for Scenario A.
CS_ScB	Cross-sections with water levels for Scenario B.
CS_ScC	Cross-sections with water levels for Scenario C.

ArcGIS raster files. Resolution: 2 m. Value: Probability of flooding where the value 1 means that the pixel was flooded in all simulations for the specified scenario.

File name	Description
Probmap_ScI	Probabilistic flood inundation map for Scenario I, present climate discharge uncertainty.
Probmap_ScII	Probabilistic flood inundation map for Scenario II, roughness coefficient uncertainty.
Probmap_ScA	Probabilistic flood inundation map for Scenario A, present climate discharge and roughness coefficient uncertainties.
Probmap_ScB	Probabilistic flood inundation map for Scenario B, future climate discharge in emission scenario RCP 4.5 and roughness coefficient uncertainties.
Probmap_ScC	Probabilistic flood inundation map for Scenario C, future climate discharge in emission scenario RCP 8.5 and roughness coefficient uncertainties.

APPENDIX II – PROBABILISTIC FLOOD INUNDATION MAPS

The probabilistic flood inundation maps for Scenario A, Scenario B and Scenario C can be found for six chosen locations along the model reach. The probabilities are shown in a continuous gradient from black to white, where complete black means that the pixel was flooded for all simulations for that scenario. The blue on top of the probability layer indicates where there normally is water.

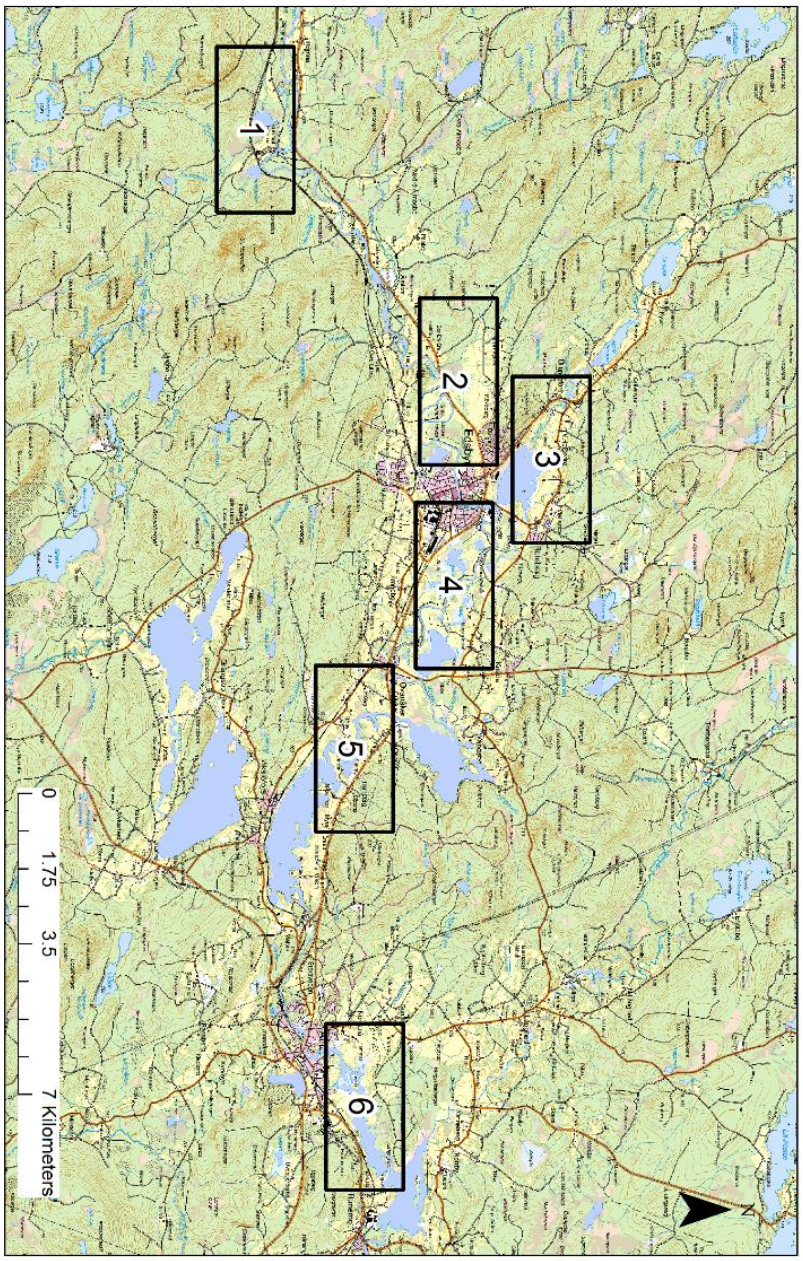

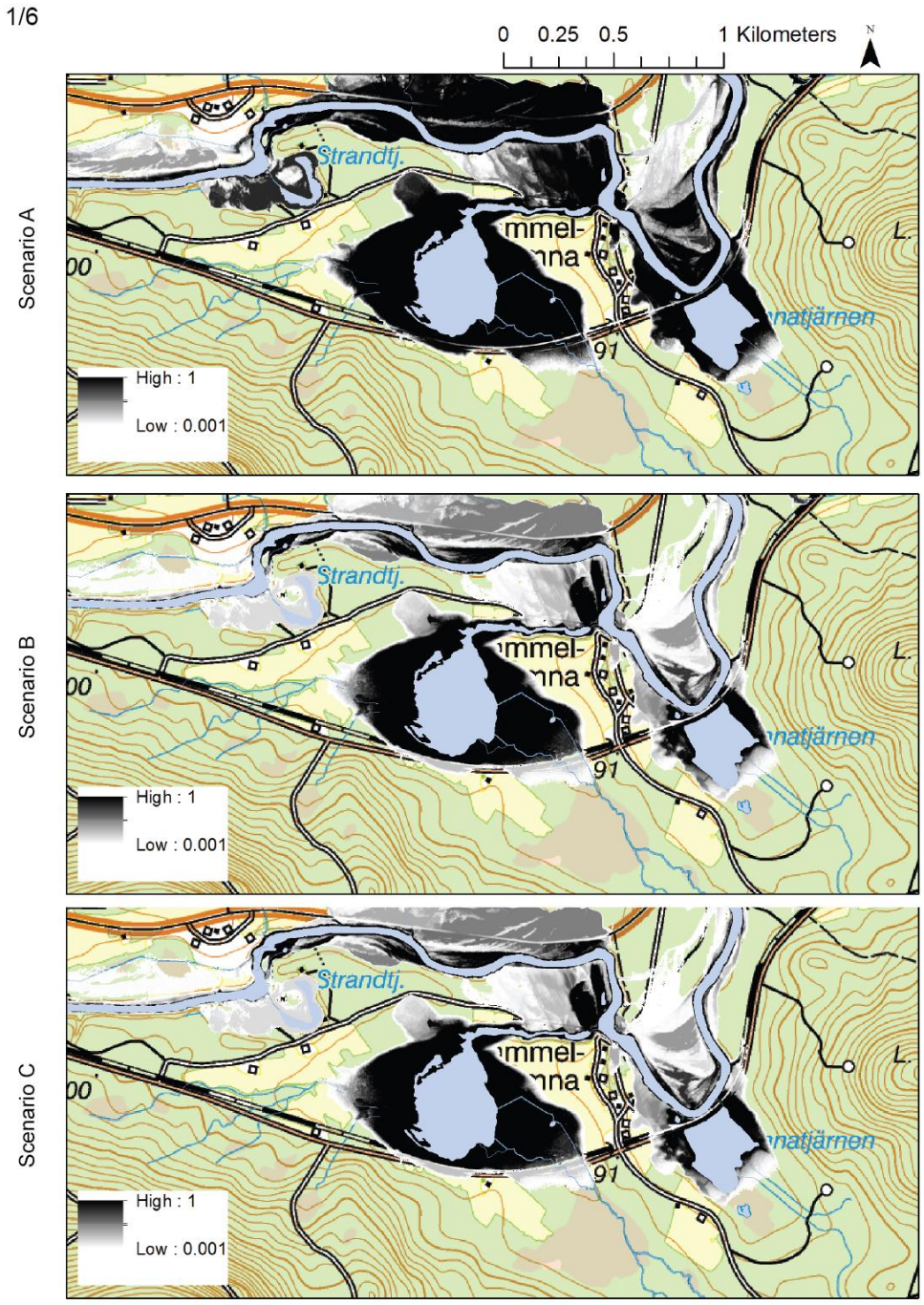
1/6
0 0.25 0.5 1 Kilometers
N
Scenario A
Scenario B
Scenario C
Strandtj.
High : 1
Low : 0.001

2/6

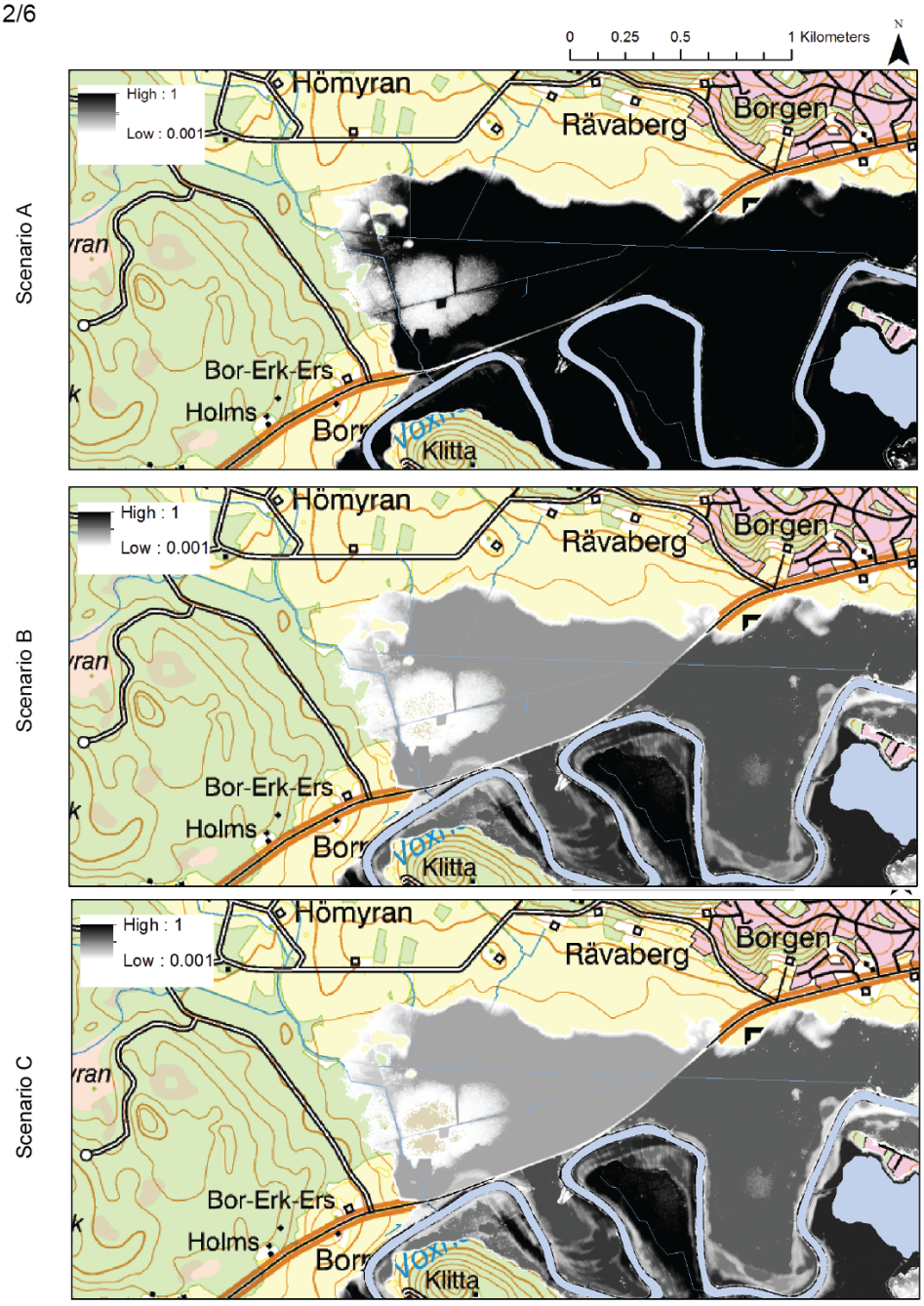
0 0.25 0.5 1 Kilometers
N
Scenario A
Scenario B
Scenario C
High : 1
Low : 0.001
Hömyran
Rävaberg
Borgen
Bor-Erk-Ers
Holms
Klitta

3/6

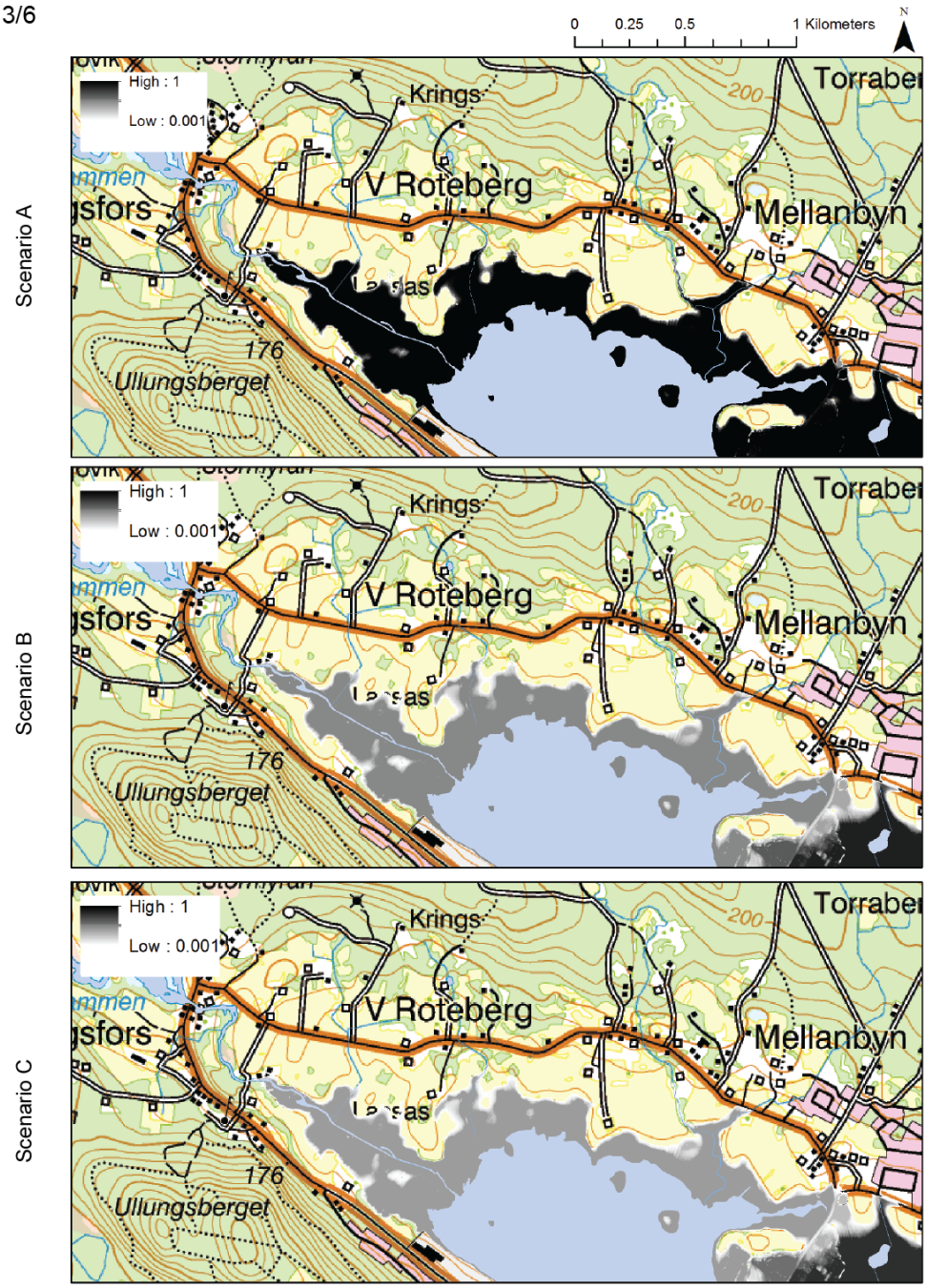
0 0.25 0.5 1 Kilometers
N
Scenario A
Scenario B
Scenario C
High : 1
Low : 0.001
Krings
V Roteberg
Mellanbyn
Torrabe
200
176
Ullungsberget

4/6

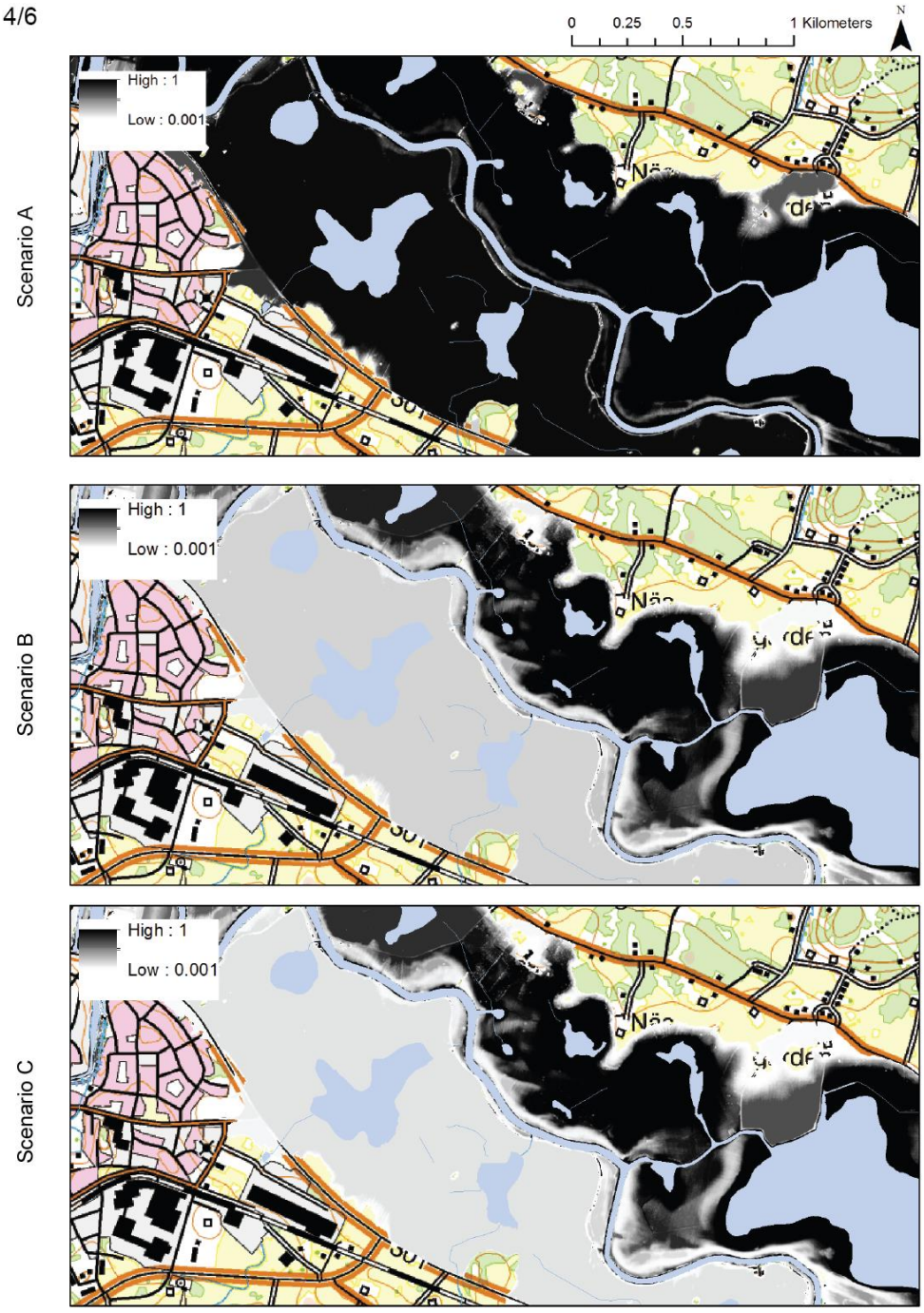
0 0.25 0.5 1 Kilometers
N
Scenario A
Scenario B
Scenario C
High : 1
Low : 0.001

5/6

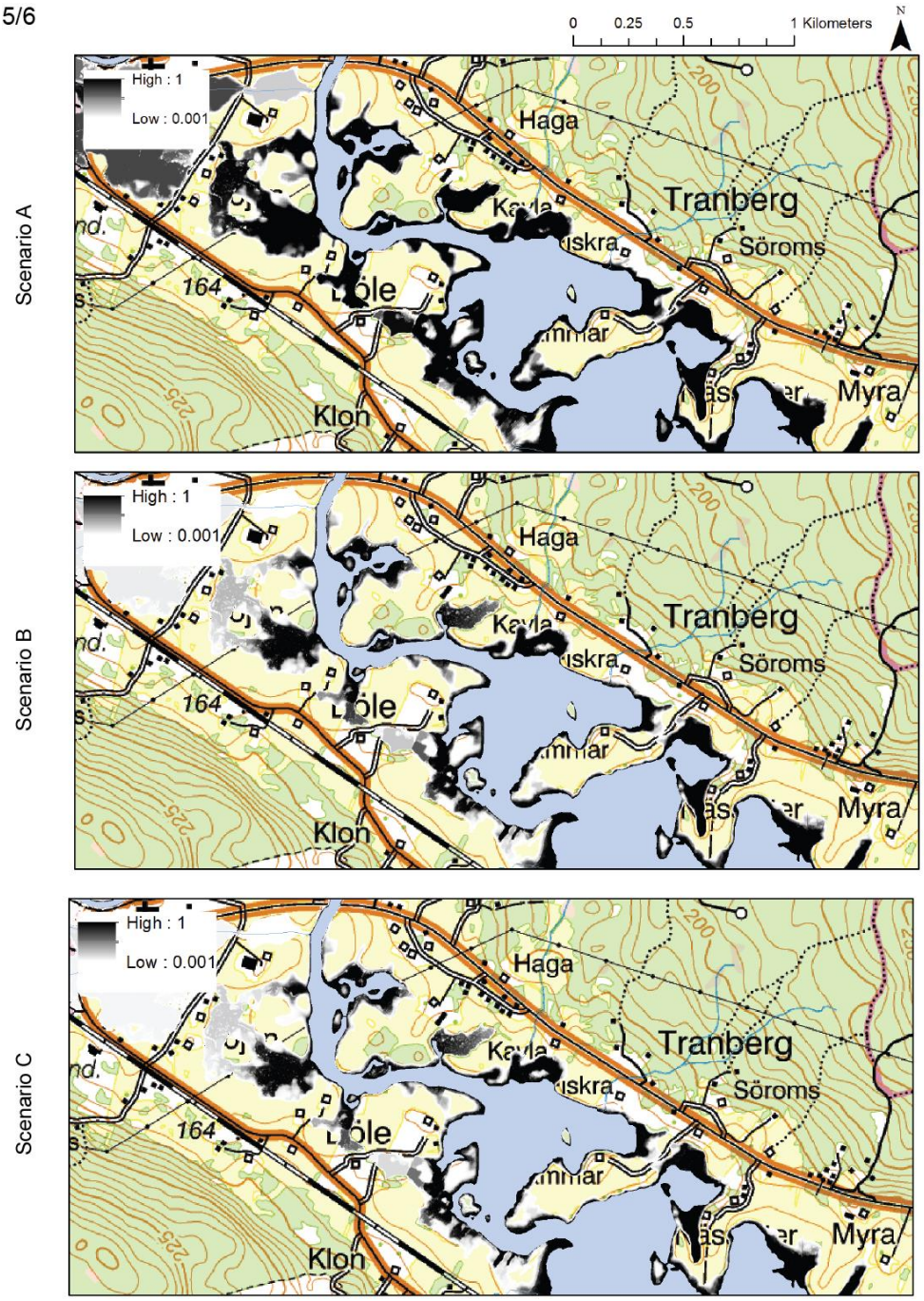
0 0.25 0.5 1 Kilometers
N
Scenario A
Scenario B
Scenario C
High : 1
Low : 0.001
Haga
Tranberg
Söroms
Löle
Klon
Myra
164
200
225

6/6

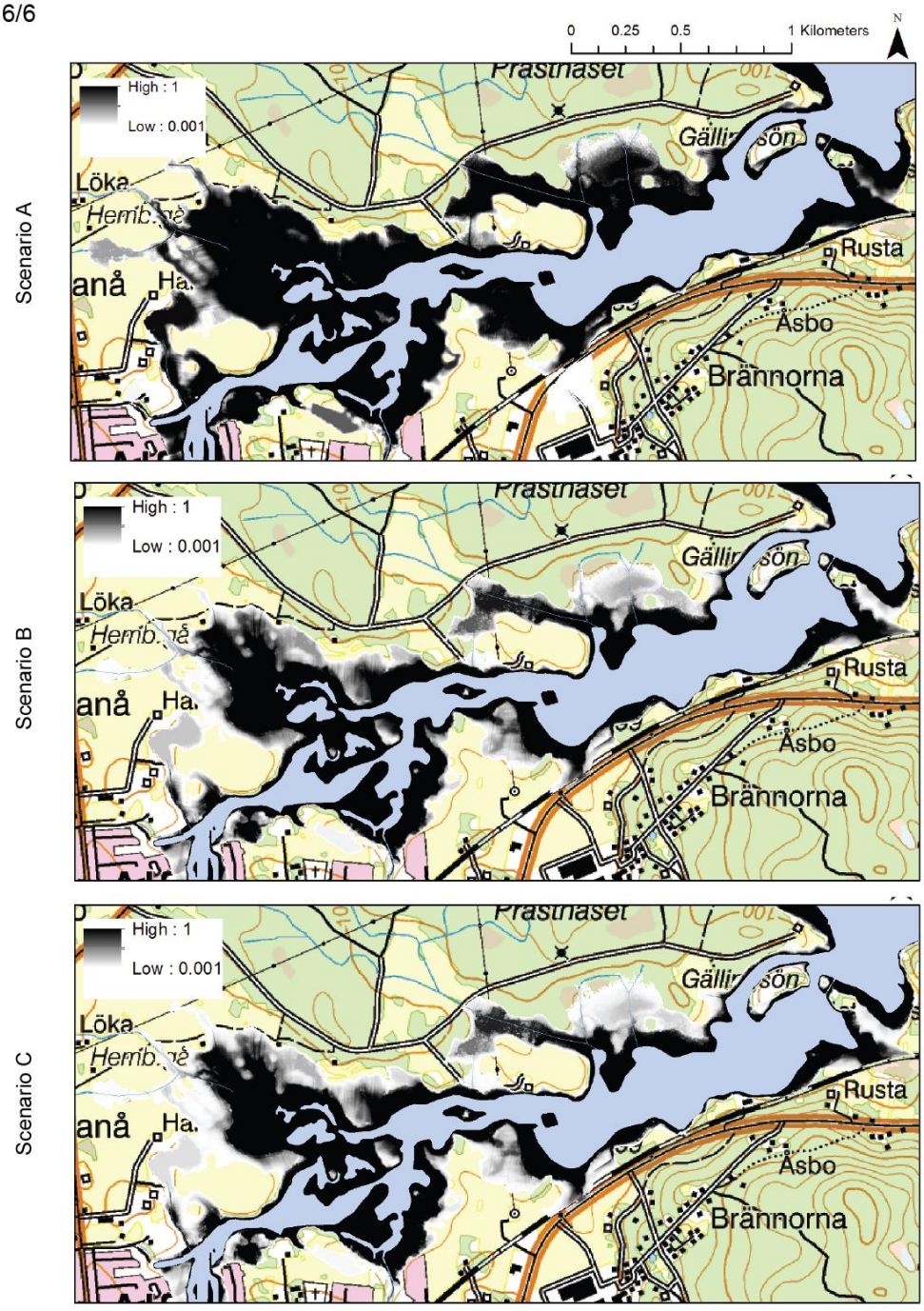
0 0.25 0.5 1 Kilometers
N
Scenario A
Scenario B
Scenario C
High : 1
Low : 0.001
Löka
Rusta
Åsbo
Brännorna